Quantitative Assessment of Human Motion Capabilities with Passive Vision Monitoring

by:

Boniface Mbouzao

A thesis submitted to the

Faculty of Graduate and Postdoctoral Studies

In partial fulfillment of the requirements for the degree of

Masters of Applied Science – Biomedical Engineering

Ottawa-Carleton Institute of Biomedical Engineering

School of Electrical Engineering and Computer Science

Faculty of Engineering

University of Ottawa

Abstract

Rheumatoid Arthritis (RA) is a disease in which the body has "turned on itself", with its immune system attacking mobility. In RA, an immune mechanism attacks and destroys the joints and limits mobility, in some circumstances to the point of needing replacement of joints. The aim of this research is the development of a less costly, widely accessible, passive sensing technology that provides a quantitative assessment of RA and that monitors the therapeutic effectiveness on joint-debilitating diseases.

The proposed solution relies on a quantitative evaluation of human gestures. Such a quantitative assessment supports the comparison between the motion capabilities of a patient and that of a healthy person, using a kinematic model of the human skeleton. Criteria for the classification of severity were established, and tables were generated to classify the levels of severity as a function of the measurements extracted from processed videos of a subject performing predefined movements.

This research project, while contributing a new tool to the process of classification of RA level of severity, opens the way for using widely accessible digital imaging for diagnosing and monitoring the evolution of the illness. Replacing MRI or HRUS with a cheaper and more accessible technology would have a major impact on health care services. From the clinical point of view, the proposed techniques based on digital images processing combined with a monitoring approach based on infrared images that was previously developed may provide a utility of care for patients with RA, as well as an alternative and automated approach for early detection of RA and active inflammation at a critical time.

Acknowledgements

I would like to thank my thesis supervisors, Dr. Pierre Payeur and Dr. Monique Frize, for their guidance and assistance throughout my studies and my research. I would also like to thank the University of Ottawa and all VIVA research laboratory members. Finally, I would like to thank my family and friends for their support and encouragement.

I would like to thank also the Society of Jesus and especially the Jesuits in English Canada who gave me the opportunity and all the support needed to pursue these studies.

Table of contents

Abstract ..... **i**
Acknowledgements ..... **ii**
Table of contents ..... **iii**
List of Figures ..... **viii**
List of Tables ..... **xii**
Acronyms ..... **xiv**
Chapter 1: Introduction 1
1.1 Context 1
1.2 Motivations 2
1.3 Objectives 4
1.4 Structure of the thesis 5
Chapter 2: Literature Review 7
2.1 Introduction 7
2.2 Forms of Arthritis 8
2.2.1 Ankylosing spondylitis 8
2.2.2 Bursitis and tendinitis 9
2.2.3 Gout 9
2.2.4 Pseudo-Gout 10
2.2.5 Reiter's Syndrome 10
2.2.6 Psoriatic arthritis 10
2.2.7 Infectious arthritis 10
2.2.8 Osteoarthritis 10
2.2.9 Juvenile arthritis 11
2.3 Nature of Rheumatoid Arthritis 11
2.4 Clinical symptoms of RA 12
2.5 Human joints affected by Rheumatoid Arthritis 13
2.6 Treatment of RA 14
2.7 Technologies to monitor movement 15

2.7.1 Motion capture 15
2.7.2 Marker Based Systems 16
2.7.3 Markerless Systems 19
2.8 Skeletal Motion Estimation for RA Diagnosis 21
2.9 Literature Review on Motion Estimation 22
2.9.1 Motion Vectors 22
2.9.2 Block Matching for Motion Estimation 23
2.9.2.1 Exhaustive Search (ES) 26
2.9.2.2 The Three-Step Search (TSS) 26
2.9.2.3 New Three-Step Search (NTSS) 27
2.9.2.4 Simple and Efficient Three-Step Search (SESTSS) 27
2.9.2.5 Four-Step Search (4SS) 27
2.9.2.6 Diamond Search (DS) 27
2.10 Selected algorithm: Adaptive Rood Pattern Search (ARPS) 28
2.10.1 Procedure 28
2.10.2 Prediction of motion vector 30
Summary **32**
Chapter 3: Kinematics of Human Hand and Arm 33
3.1 Introduction 33
3.2 Kinematics and motion estimation 35
3.3 Kinematics of the human hand 35
3.3.1 Anatomy of the hand bones 35
3.3.2 Forward kinematics 39
3.3.3 Inverse kinematics 50
3.3.4 General inverse kinematic solution for the thumb 52
3.3.5 Simplified inverse kinematic solution for the thumb 54
3.3.6 General inverse kinematic solution for all fingers except the thumb 58
3.3.7 Simplified inverse kinematic solution for all fingers except the thumb 59
3.4 Kinematics of the human arm 63
3.4.1 Forward kinematics 70
3.4.2 Inverse kinematics 72
Summary **74**

Chapter 4: Methodology and Analysis **76**
4.1 Introduction 76
4.2 Methodology 77
4.2.1 Evaluation Methodology 77
4.2.2 Recruitment of patients and volunteers 79
4.2.3 Ethics approval and protocols 81
4.3 Definition of movements for motion and angle detection 81
4.3.1 Open and close hand quickly 82
4.3.2 Open and close hand slowly 82
4.3.3 Separate and join fingers quickly 83
4.3.4 Separate and join fingers slowly 84
4.3.5 Stretch and bend arms joints quickly 85
4.3.6 Stretch and bend arms joints slowly 85
4.4 First method: Estimation of human hand motion using Sum of Absolute Difference 86
4.4.1 Using SAD for motion estimation in the human hand 88
4.4.2 Mathematical expression of SAD 89
4.4.3 Classification of level of severity based on SAD 90
4.5 Second method: Classification using arm angle estimation 95
4.5.1 Classification based on fingers angles 103
4.5.2 Estimation of the arm's joints using the implemented GUI 105
4.5.3 Comparison of the proposed solution with existing ones 108
4.5.4 Classification based on arm angles 112
4.6 Third method: Using matching blocks for motion estimation 119
4.6.1 Implementation in the GUI 119
4.6.2 Classification based on motion estimation 121
4.7 Infrared based system and See5 classification 127
4.8 Graphical User Interface (GUI) description 129
Summary **130**
Chapter 5: Results and Comparisons **132**
5.1 Introduction 132
5.2 Experimental results based on SAD 133
5.2.1 Estimation of the mobility based on SAD 134

5.2.2 Classification of level of severity of patient according to their SAD results 135
5.2.3 Comparison with See5 Classification and rheumatologist's evaluation 136
5.2.5 Classification of volunteers' experimental results using SAD 137
5.3 Experimental results based on angles of arm joints 138
5.3.1 Classification based on six arm joints 138
5.3.2 Classification according to all arm angle values 139
5.3.3 Comparison with infrared based classification and rheumatologist's evaluation 140
5.3.4 Classification based on wrists angles only 141
5.3.5 Comparison of wrist based classification with rheumatologist's evaluation and See5 classification 142
5.3.6 Classification of the measurements performed on volunteers based on all arms angles and on wrist angles only 143
5.4 Experimental results based on matching blocks for motion estimation 144
5.4.1 Classification based on three categories 144
5.4.2 Comparison with the See5 classification and rheumatologist's evaluation 146
5.4.3 Classification based on six categories 146
5.4.4 Comparison with See5 classification and the rheumatologist's evaluation 148
5.5. Compilation of volunteer results based on six categories 149
5.6 Conclusion 150
Summary **150**
Chapter 6: Conclusions and Future Work 152
6.1 Summary 152
6.2 Contributions 155
6.3 Future work 156
Bibliography **158**
Appendices **170**
Appendix A: Criteria of early diagnosis of Rheumatoid Arthritis 170
Appendix B: Denavit-Hartenberg convention 173
Appendix C (French version) : Protocole de Recherche 175
Appendix C (English version): Research Protocol 177
Appendix D (French version) : Lettre d'information 179
Appendix D (English version): Information Letter 183
Appendix E (French version): Formulaire de consentement 186

Appendix E (English version): Consent Form 190
Appendix F (French version): Affiche 193
AppendixF (English version): Flyer 194
Appendix G: Implementation of SAD using Simulink 195
Implementation of SAD using Simulink 195
Composition of sub-system 196
The System 197
Absolute Difference Image 198
Output of the system 198
Appendix H: Description of Graphical User Interface 200
Appendix I: Microbes and bacteria responsible of RA 208

List of Figures

Fig. 2.1: Illustration of matching block process in a searching window. 25
Fig. 2.2: Illustration of step size and predicted motion vector within a block. 30
Fig. 3.1: Location of the bones of the human hand..... 36
Fig. 3.2: All bones and joints of the human hand. 37
Fig. 3.3: The proposed Degrees of Freedom (DoFs) of the human hand..... 39
Fig. 3.4: The proposed two hand configurations: the thumb and the other fingers. 40
Fig. 3.5: The proposed joint reference frames used to obtain D-H parameters..... 41
Fig. 3.6: Computation of relative movement of two consecutive bones between any two poses of the hand: here between pose 1 and an arbitrary selected pose *i* in the sequence. 42
Fig. 3.7: Proposed kinematic model of the thumb. 43
Fig. 3.8: Proposed kinematic model of all fingers except the thumb. 45
Fig. 3.9: Simplified kinematic model of the thumb. 55
Fig. 3.10: Simplified kinematic model of all fingers except the thumb. 60
Fig. 3.11: Proposed model of human arm structure. 63
Fig. 3.12: Mechanism of human arm skeleton..... 64
Fig. 3.13: Proposed kinematic model of the human arm. 65
Fig. 3.14: Zero position of the arm's joints with movements' capabilities. 67
Fig. 3.15: Minimum bending capabilities used in this research. 68
Fig. 3.16: Simplified kinematics of the human arm. 73
Fig. 4.1: The setup with the uniform background. 78
Fig. 4.2: Camera used for data collection. 79
Fig. 4.3: Open and close hand quickly movement for the right hand. 82
Fig. 4.4: Open and close hand slowly movements for the right hand. 83
Fig. 4.5: Separate and join fingers quickly movement for the right hand. 84
Fig. 4.6: Separate and join fingers slowly movement for the right hand. 84
Fig. 4.7: Stretch and bend arm joints quickly. 85
Fig. 4.8: Stretch and bend arms joints slowly. 86
Fig. 4.9: Result obtained by computing SAD from frame to frame over a sequence of 40 seconds of video..... 87

Fig. 4.10: Representation of SAD computation over two consecutive images. 90
Fig. 4.11: Low level of RA according to volunteers' results and Standard Deviation (SD). 94
Fig. 4.12: Distribution of RA level according to patients' results and SD. 94
Fig. 4.13: Thresholds according to all participants' results and SD. 94
Fig. 4.14: 2D proposed representation of arm with shoulder, elbow and wrist angles. 96
Fig. 4.15: Process of estimation of skeleton pose in an image. 99
Fig. 4.16: Pruned pose skeleton. 99
Fig. 4.17: Transformation from (X1,Y1) to (X2, Y2) as image reference frame. 101
Fig. 4.18 : Coordinates of each points in the reference frame and computation of the distances. 102
Fig. 4.19: Selection of a proper hand picture, here showing thumb and index. 103
Fig. 4.20: User pointing the finger's joints, here thumb and index. 104
Fig. 4.21: Results for finger's joint angles with proposed approach. 105
Fig. 4.22: Sample of a selected image by the user. 106
Fig. 4.23: Selection of the processing area. 106
Fig. 4.24: Selection of the three valid arm's joints 107
Fig. 4.25: Pop ups displaying the joints angle values. 108
Fig. 4.26: Five consecutive frames from two points of view as proposed by B. Rosenhahn *et al.* [37]. 110
Fig. 4.27: MaxTRAQ's results from the contour estimation obtained with our proposed solution. 110
Fig. 4.28: Angles computed with MaxTRAQ software on fingers. 112
Fig. 4.29: Low level of RA according to volunteers' results and SD. 115
Fig. 4.30: Distribution of RA level according to patients' results and SD. 115
Fig. 4.31: Thresholds on arm angles according to all participants' results and SD. 115
Fig. 4.32: Low level of RA according to volunteers' results and SD. 117
Fig. 4.33: Distribution of RA level according to patients' results and SD. 117
Fig. 4.34: Thresholds on wrist angles according to all participants' results and SD. 118
Fig. 4.35: Motion vector magnitude from frame to frame for a volunteer. 120
Fig. 4.36: Graphic of motion vector magnitude from frame to frame 120

Fig. 4.37: Example of a sequence of frames from a video used to compute motion vector magnitude. 121
Fig. 4.38: Low level of RA according to volunteers' motion vector average and SD. 124
Fig. 4.39: Distribution of RA level according to patients' motion vector average and SD. 124
Fig. 4.40: Thresholds according to all participants' results and SD. 124
Fig. 4.41: Low level of RA according to volunteers' motion vector average and SD for classification based on six categories. 125
Fig. 4.42: Distribution of RA level according to patients' motion vector average and SD for classification based on six categories. 125
Fig. 4.43: Thresholds according to all participants' motion vector average and SD for classification based on six categories. 126
Fig. 4.44: A320 Infrared Camera from FLIR Systems (FLIR Systems, 2007) used for See5 classification. 128
Fig. 4.45: Sample infrared images used to obtain temperatures used by See5 classification, image of hands: a) with markers and b) without markers. 129
Fig. 4.46: Graphical User Interface (GUI) of the System. 130
Fig. A. 1: 1987 ACR decision tree for RA classification 172
Fig. G.1: Computational process of SAD using Simulink blocks. 196
Fig. G.2: Video acquisition sub-system. 196
Fig. G.3: Sub-system (motion energy estimation) using SAD and Threshold. 197
Fig. G.4: Complete SAD based motion estimation system. 198
Fig. G.5: Graphical result of SAD based motion estimation through Simulink where X axe represents the time in seconds and Y axe the SAD values. 199
Fig. H.1: First user interface page of the system. 200
Fig. H.2: "Limb" button. 201
Fig. H.3: Number of angles selection. 201
Fig. H.4: "Hand" button. 202
Fig. H.5: Results of finger's joint angles. 203
Fig. H.6: Body part specification. 203
Fig. H.7: "Live Video" button. 204
Fig. H.8: "Motion Estimation" button. 204

Fig. H.9: “Process video” button. 205
Fig. H.10: “Video Frames” button. 206
Fig. H.11: “Exit” button. 206

List of Tables

Table 2.1: Skeleton joints with frequency of the disease in adult RA. 14
Table 3.1: List of all human hand bones per category. 37
Table 3.2: D-H parameters of the thumb. 44
Table 3.3: D-H parameters of all fingers except the thumb 46
Table 3.4: Fingers' joint capabilities, adapted from [63]. 52
Table 3.5: D-H parameters table of the proposed human arm model. 66
Table 3.6: Average healthy person arm's joint capabilities. 67
Table 3.7: Minimum bending capabilities computed in this research. 68
Table 4.1: SAD estimation values of volunteers. 92
Table 4.2: SAD estimation values of patients. 93
Table 4.3: Results from three different systems for the same sequence of images. 111
Table 4.4: Minimum bending arm angles of volunteers. 113
Table 4.5: Minimum bending arm angles of patients. 114
Table 4.6: Wrist bending angles for volunteers. 116
Table 4.7: Wrist bending angles for patients. 117
Table 4.8: Motion vector magnitude estimation results for volunteers 122
Table 4.9: Motion vector magnitude estimation results for patients. 123
Table 4.10: Block matching correspondence with the three categories classification 125
Table 4.11: Block matching correspondence with rheumatologist's classification. 126
Table 5.1: Results of SAD on motions for each patient. 134
Table 5.2: Classification of patients in terms of level of severity according to SAD. 136
Table 5.3: Comparison between SAD based classification, See5 classification, and the rheumatologist's evaluation. 137
Table 5.4: Volunteers classification using SAD results. 138
Table 5.5: Classification based on average minimum bending of the six angles of both arms for each patient from the less to the most affected. 140
Table 5.6: Classification based on all minimum arm bending angle and comparison with rheumatologist's evaluation and See5 classification. 141

Table 5.7: Classification based on minimum bending angles for the wrists only from the least to the most affected. 142
Table 5.8: Classification based on wrist minimum bending angles and comparison with rheumatologist's evaluation and See5 classification. 143
Table 5.9: Classification of volunteers according to average of all arm joints versus wrist joints only 144
Table 5.10: Matching block based motion estimation classification with three categories 145
Table 5.11: Comparison between block matching based motion estimation, See5 classification and rheumatologist's evaluation. 146
Table 5.12: Matching block based motion estimation classification with six categories 148
Table 5.13: Comparison between See5 classification (infrared images), rheumatologist's evaluation and block matching based motion estimation with six categories. 149
Table 5.14: Classification of volunteers using block matching based motion estimation 150
Table I.1: Viruses and bacteria agents in RA. 208

Acronyms

ACR: American College of Rheumatology

ARA: American Rheumatism Association

CIOMS: Council for International Organizations of Medical Sciences

CMC: Carpometacarpal

DIP: Interphalangeal

DMARD: Disease Modifying Anti-Rheumatic Drugs

DoF: Degree of Freedom

GUI: Graphical User Interface

HCI: Human-Computer Interface

HRUS: High Resolution Ultra-Sound

I.D.E.A.S.: Intelligent Decision Aid System

IP: Interphalangeal

MLD: Moving Light Display

MCP: Metacarpophalangeal

MRI: Magnetic Resonance Imaging

NSAID: Non-Steroidal Anti-Inflamatory Drugs

OHREB: Ottawa Hospital Research Ethic Board

PIP: Proximal Interphalangeal

RA: Rheumatoid Arthritis

SAD: Sum of Absolute Differences

SD: Standard Deviation

TMC: Trapeziometacarpal

VIVA: Vision, Imaging, Video and Autonomous Systems

Chapter 1: Introduction

1.1 Context

The development of more accessible approaches to active prevention of a multitude of health problems is desirable. More traceable passive sensing approaches should be made available in all large clinics and hospitals to provide greater access to the population. Early action is important for achieving a less expensive solution for the prevention of the RA disease. The aim of the present research is the development of a less costly and widely accessible technology that will provide a quantitative assessment of rheumatoid arthritis (RA) and help monitor therapy of joint debilitating diseases.

More than two million people (2.5 million in 1997) are affected by RA in the United States, over 300,000 Canadians and 260,000 French are also affected. RA generally occurs between the ages of 20 and 40, although older people and children might also suffer from the disease. More than 90% of patients have chronic inflammation and may get progressively worse over time. Within 10 years of diagnosis, 50% of the patients will suffer severe disability. Early diagnosis and treatment of RA could help to prevent severe disability. The objective of the treatment of RA is to alleviate pain, reduce inflammation, stop or slow joint damage and improve the overall functioning of the body. Current diagnosis relies on qualitative evaluation, including the patient's medical history and physical examination. MRI (Magnetic Resonance Imaging) and HRUS (High Resolution Ultra-Sound) have been used to detect early synovitis. However MRI and HRUS tests are not available to everyone due to their cost and the waiting list is often long to access those tests. A question with which many patients are faced is how to find less expensive technology that will provide a quantitative assessment to diagnose RA.

1.2 Motivations

A research was conducted some years ago in an attempt to measure human movement. The research comprised part of the activities of the Vision, Imaging, Video and Autonomous systems (VIVA) group at the University of Ottawa. The aim of the work was to develop a fully automated system with a set of multi-cameras [1] for musculoskeletal examinations of human upper limbs [2]. The system developed allowed the detection from a video frame of the joints of upper limbs. The research contributed to the use of a markerless computer vision-based system in human motion analysis.

That research, however, did not have as its aim specific medical purposes. Even though Ghazisaeidi [2], in his thesis, admitted the possibility of using his work in evaluating the motion of an arthritic patient, his work was not directed to that specific purpose and remained only a possible extension.

The aim of the present research is to develop a markerless motion estimation of human hands and arms, and to relate it persuasively to the process of diagnosing and monitoring RA. The monitoring of human hand and arm motion is a critical issue in the treatment of RA patients. Defining a safe and easy-to-use method for accurately measuring the motion capabilities of hands and arms could make a significant contribution to the process of diagnosing and monitoring RA.

In the Medical Information Technologies Research Group (MIRG) at Carleton University and the University of Ottawa, researchers made contributions to the diagnosis and monitoring of RA based on infrared images of hand and other joints of the human body which are most affected by the illness [3]. A classification based on the distribution of the body heat around painful areas was proposed. This classification was compared with the conclusions from an expert in rheumatology to measure the efficiency of the classification. The aim of the research was to find a less expensive technology than MRI to diagnose and monitor RA patients more efficiently. The criteria for the distribution of heat over the body and around the painful areas of affected joints

(mostly hands and limbs, knees, toes and ankles) were identified [4] as targets to monitor and diagnose RA. Infrared imaging was selected for the classification of the body heat distribution around the joints.

The present research makes its own contribution to the wider area of movement evaluation for the human hand and arm. Much research was undertaken to evaluate the motion capabilities of the human hand [5], to model the human hand gesture [6], and to estimate the hand pose within a video [7]. Movement evaluation of the human hand has also been used in computer animation and games [8]. This present research, by investigating the quantitative evaluation of human hand motion, could contribute to reinforce the conclusions of previous studies. This study focuses on the quantitative evaluation of human hand motion using a sequence of images, in a manner similar to that found in Lin *et al.* [9], [10], [11], and what Oka *et al.* explored for gesture recognition [12],[13].

The present research also aims at including supplementary criteria in the evaluation, in order to eventually be integrated with the infrared-based diagnostic procedure described above. The combination of both systems can have an impact in determining the level of severity of RA and could help specialists to determine the proper medication for the patient. The best known signs of RA are pain and loss of motion. RA patients suffer from motion restriction. Monitoring motion capabilities therefore represents the main objective of this research, which ultimately aims to contribute to the diagnosis and monitoring of RA.

Several solutions have been developed in computer vision, motion capture, animation and virtual reality technologies to measure and monitor movement. The goal of these approaches was to compare or to measure motion capabilities. Those researches began in the 1970's [14] by gathering information from sensors distributed over the whole body of the subject and by sending the information to a computer. A refinement of the initial approach was achieved when researchers placed optical gel over points on the subject from which they wanted to track the movements. These systems imposed

severe constraints on the subject and made the setup complex. Results were unreliable because of the numerous sources of error involved, including the presence of magnetic fields in the area of the experiment, mutual occlusion between sensors, or difficulty with performing the expected movement. In addition, special training was needed for the personnel to attach and adjust the sensors. In fact, in the first setup, some markers had to be attached to the subject's joints. Their position was then reported to a system that estimated the movement of the subject. To avoid mutual occlusion between markers and sensors, several variations of setups were developed. In recent years, there have been solutions in response to a need for robotics, computer simulation, and medical applications for the estimation of human movement. For that purpose, new requirements were made for greater precision in the measurement of the motions. The introduction of camera networks in motion capture systems resulted from these efforts [15]. A set of several cameras was set up to record the movement from several points of view. The calibration of the cameras was, then, very important for the setup. Some used wearable sensors to sense the motions directly and to send them to a computer to be analyzed [16]. The main purpose in this research on human motion estimation is to be able to quantify and model human motion capabilities. An efficient system able to give an accurate measurement of human motion could be very helpful in medicine. In fact, physicians are looking for an efficient way of measuring motions for diagnosing and monitoring joint and skeleton diseases.

1.3 Objectives

The main objective of this research is to develop a system based on digital images taken from only one point of view to estimate the motion capabilities of human hands and arms. The efficiency of the system will be measured according to its capacity for measuring the motion capabilities of the subject using one digital camera. The system will then be able to estimate the range of the motion of the joints from their full extension to their full flexion. This will be useful in the case of RA where inflammation

of the joints, especially the joints of the hands, knees and toes, imposes restrictions on joint mobility.

The five specific objectives of the present research are:

1) From one point of view, to estimate the motion capabilities of the subject from the measurement of joint articulation angles, as collected by a standard digital color camera;
2) To classify the measurements of motion in order to determine whether the subject is suffering from RA or is considered healthy;
3) In the case of a RA patient, to estimate the level of severity of the illness based on the measurement of the motion capabilities performed on the subject's joints;
4) To establish a table of classification of severity as a function of the results obtained from the motion capabilities of the subject;
5) To correlate the results from the classification table with the rheumatologist's diagnostic and with the results obtained with methods based on infrared images.

1.4 Structure of the thesis

This thesis is structured around six chapters. After this introduction, the second chapter presents a review of literature on the nature of RA and other rheumatic diseases, on the diagnosis and follow-up of the illness, on the technical solutions, and on image processing techniques used in medical diagnosis. The third chapter discusses the kinematics of the human hands and arms. The physical structure of the hands and arms, along with their bend and flexion constraints, are important for diagnosing and monitoring RA. Chapter four presents the three methods proposed and analyzed in the present research for diagnosing and monitoring RA. It also presents the user interface that helps the rheumatologist to apply the methods presented. It discusses, in the section on methodology, the procedure followed for collecting data, the recruitment of patients and volunteers, the ethical protocol, and finally, the confidentiality of data as

required by ethical constraints. In the analytical part of chapter four, the method for processing data in order to obtain relevant results for diagnosing and monitoring RA is discussed. The fifth chapter presents the results, comparing them to other conclusions from previous research and to an expert rheumatologist's evaluation. In that chapter a general conclusion is drawn from relevant results. The final chapter presents specific conclusions, contributions to knowledge, and areas for future investigation.

Chapter 2: Literature Review

2.1 Introduction

The problem of estimating the human arm's movements and its joint angles variations from sequence of images is a domain of research that interests many. The areas of research that deal primarily with this matter are computer vision for industrial applications and medicine for gait analysis or diagnosis. This present research aims at making a contribution to the medical diagnosis of rheumatoid arthritis. In fact, one needs to implement an efficient algorithm to find the angles variations of the human arm joints within a sequence of frames in a video recording. Much engineering research has been implemented to find joint angles, including the use of a multi-camera based system. Instead of a multi-camera approach, this present research proposes, for the purpose of RA diagnosis, a simpler approach that avoids many challenges that the multi-camera system faces. The purpose of this proposed solution is to be able to make the technology accessible to medical staff without the need of training in computer vision.

The use of images for medical purposes is not a new element in the evolution of scientific research. For several decades, images under all forms have helped to diagnose several diseases. The use of images resulting from radiography, computed tomography scanner, infrared and other types of imaging techniques for medical purposes has varied considerably. Most technologies used to obtain images are still expensive and hardly accessible to the majority of the patients. Because of this, researchers are encouraged to find effective solutions which are less expensive and can be made accessible to everyone. For this reason, it is essential to understand RA under its various forms and manifestations.

2.2 Forms of Arthritis

Some people confuse osteoarthritis and rheumatoid arthritis, which, in fact, are two different diseases bearing similar names. Arthritis is a general term used to describe a group of more than 100 different types of rheumatic diseases that attack the joints. Each type of arthritis has different causes and cures [17], [18], [19].

2.2.1 Ankylosing spondylitis

The manifestation of Ankylosing Spondylitis (AS) is lower back pain and stiffness. In addition, the chest hurts when inhaling. General fatigue and loss of weight are also symptoms of AS. In its early stage, AS can be confused with mechanical back pain. The ligaments and tendons that make back movement possible become inflamed. The response of the vertebrae to the resulting inflammation is hardening of the backbone. The first stage of this process is in the lower back, and involves sacroiliac joints (where the lower spine meets the pelvis). Later on, the middle and upper parts of the back are affected. The disease spreads into the buttocks and thighs and even into the chest where it makes deep breathing very painful. The inflammation can also affect the joints of the shoulder, knees or ankles. In approximately twenty percent of patients, the first signs of the disease appear in the shoulders, hips or other joints.

Young men between sixteen and thirty-five years of age are especially vulnerable to the disease, with the disease appearing in one person in 1000 under the age of forty. Some scientists believe that it may have a genetic basis. The disease is found exclusively in those who have the HLA.B27 gene, but this includes only twenty percent of them. Somehow, the gene has to be “switched on”.

Early diagnosis and proper treatment can reduce or prevent deformity. All treatments aim at reducing pain and preventing deformities and also at strengthening the back of the neck.

2.2.2 Bursitis and tendinitis

Bursitis and tendinitis have symptoms similar to those found in the case of Ankylosing Spondylitis. The symptoms of these two diseases are pain and tenderness in the shoulders, elbows, knees or pelvis that radiate into nearby limbs and sometimes cause fever, which usually occurs after a sudden overuse of a joint. The areas around the joints of shoulders, elbows, wrists, fingers, hips, back, knees, ankles and feet pay the price of over enthusiastic usage.

Tendinitis, in particular, is characterized by the inflammation or irritation of a tendon. A tendon may rupture especially when a person takes off quickly or jumps. It appears suddenly, and can stay a day or even weeks before disappearing. Permanent damage or disability is rare. Tendinitis appears generally after the age of thirty.

2.2.3 Gout

Gout is known also as the "rich man's disease", because it was associated with being overweight, overeating, especially of meat, and overindulging in alcoholic drinks. Gout is therefore a metabolic disorder. A poor diet can worsen the disease.

Gout is caused by uric acid waste in the urea (urine), whether over-produced or under-excreted, or both. In short, the person has too much uric acid in his/her body, which can be deposited as acid crystals into joint spaces. Those crystals can usually be found in the "bunion joint" of the big toe, although they can be found in joints of the feet as well as fingers, wrists, elbows and knees. Stiffness follows sometimes with fever and chills.

Gout affects about 2 millions of Americans, of whom eighty percent are males. The risk factors to get the disease include a family history of gout, drinking alcohol, high blood pressure, obesity or quick weight gain. Gout can often be completely controlled with proper treatment, which includes using non-steroidal anti-inflammatory drugs.

2.2.4 Pseudo-Gout

Although the pain and other symptoms are similar to gout symptoms, pseudo-gout is a different disease. Pseudo-gout attacks suddenly by striking the knees joints, the wrists and ankles, causing pain and sometimes destroying cartilage.

2.2.5 Reiter's Syndrome

Reiter's syndrome is known also as reactive arthritis, and its name comes from Dr. Hans Reiter who discovered it in 1916. It is a form of arthritis that affects joints, eyes and urethra. There are three major manifestations of the disease:

- Urogenital tract symptoms: inflammation of the urinary tract;
- Joint symptoms or arthritis: inflammation of the joints (knees, ankles and feet);
- Conjunctivitis: inflammation of the mucous membranes that line the eyes.

2.2.6 Psoriatic arthritis

Psoriatic arthritis is characterized by inflammation of the skin (psoriatic) and joints (arthritis) which is a type of inflammation that usually appears in people with a skin disease called psoriasis. In addition to inflammation of the joints, another symptom is red patches of skin which are covered with silvery-white scales. Psoriatic arthritis can sometimes evolve from small patches of the skin to much larger ones.

2.2.7 Infectious arthritis

Many forms of bacteria, viruses and fungi can cause infectious arthritis. It is generally characterized by loss of the functioning of the joints, by fever and inflammation of one or more joints. Infectious arthritis can be cured in most of the cases if it is diagnosed early enough.

2.2.8 Osteoarthritis

Osteoathristis is a form of arthritis that is characterized by the loss of cartilage in one or many joints. Osteoarthritis occurs with age. It affects the hands, feet, spine and large weight-bearing joints such as hips and knees. Primary osteoarthritis results with

the natural aging of joints. With age, the water content of the cartilage increases and the protein makeup of the cartilage degenerates. Secondary osteoarthritis is caused by another disease or condition. Such conditions can be obesity, repeated trauma or surgery to the joints' structure, abnormal joints at birth (congenital abnormality), gout, diabetes or other hormonal disorder.

2.2.9 Juvenile arthritis

The symptoms of juvenile arthritis include swings up and down in body temperatures on a daily basis, as well as chills, pain or swelling in the toes, knees, ankles, elbows or shoulders. Juvenile arthritis is a general term for various kinds of arthritis that can affect children under the age of sixteen. The most common one is Juvenile Rheumatoid Arthritis (JRA) which appears in three forms: systemic, polyarticular and pauciarticular. The common characteristic is inflammation of the joints which results in stiffness, swelling, pain, warmth and redness. The three forms of the disease can be defined as:

Systemic: fever of more than 103 degrees Fahrenheit which disappears in a few hours. There may be stomach pains and severe anemia.

Polyarticular: this appears in several joints, that is, five or more, and symmetrically affects the same joints on both sides of the body. Sometimes it includes a slight fever and inflammation of the eyes.

Pauciarticular: this affects only a few joints, most often the large ones such as the knee, ankle or elbow. It is usually not symmetrical.

2.3 Nature of Rheumatoid Arthritis

Rheumatoid Arthritis is a disease in which the body has "turned on itself", with the immune system attacking a patient's mobility. In fact, when someone develops an autoimmune problem, instead of protecting the body from the disease, the person's immune system attacks the body's tissues or cells. Thus, RA involves the destruction of the joints by an immune mechanism. The characteristic in its middle period is joint

discomfort and generally deformed joints from the shoulders to the fingers. Unlike in the case of the other diseases of the joints, such as osteoarthritis, destruction of the joints appears rapidly in RA. After a few months or years, a patient of RA can suffer from painfully deformed joints that limit mobility, and may even need replacement of the joints. RA tends to be symmetrical. The fact that RA affects the areas close to the joints leaves a sufferer with extreme fatigue and fever along with skin, lung, blood vessel, and even heart problems.

Many think that RA begins from a virus infection which causes the joint liming in the part that meets the cartilage to become inflamed. The joint liming will then thicken, overgrow, and invade the cartilage and the other joint-supporting tissues and bones. This weakens the entire structure of the joint, and thus becomes painful, making the joint less able to perform its regular function. When the pressure appears, the joint becomes desolate and deformed in addition to being successively swollen, tender and inflamed. The patient has fever, loses weight and develops a general feeling of sickness, soreness, stiffness and aching. Sometimes the tears and salivary glands become involved, and thus mouth and eyes will dry out. More than ninety percent of patients have chronic inflammation and may get progressively worse over time. The objective of the treatment of RA is to alleviate pain, reduce inflammation, stop or slow down joint damage and improve the overall functioning of the body [20].

2.4 Clinical symptoms of RA

Many studies have shown that in the northern hemisphere, the onset of RA is more frequent in winter than in summer. In general, the onset of RA during the winter months, October to March, is twice as frequent as in the rest of the year. The first symptoms, from about fifty five percent up to seventy percent of the patients, are fatigue, malaise or diffuse musculoskeletal pain, while joints become affected later on. Due to the accumulation of oedema fluid within inflamed tissues during sleep, morning stiffness may be among the first symptoms. The noticeable changes that RA brings to the patient are the development of muscular atrophy around affected joints. This is

followed by the decrease in efficiency and strength of joint and this increases pain proportionally. The patient feels this when opening doors and climbing stairs, and when daily work becomes more demanding. The first joints to become involved in early-stage RA are the metacarpophalangeal (MCP) joints, proximal interphalangeal (PIP) joints and the wrist joints [21].

2.5 Human joints affected by Rheumatoid Arthritis

Generally, in the early stages of the disease, some particular joints are more affected than others [22]. For early diagnosis and treatment, it is important to monitor the motion capabilities of those specific joints. For this reason, tracking the motions of some sensitive joints is crucial in the process of diagnosing and monitoring RA. Table 2.1 shows the different joints of the human skeleton and their respective sensitivity in terms of percentage of being affected by RA. One can see that the most affected joints are around the hands and limbs. In fact, as shown in Table 2.1, carpal (eight bones), and metacarpal (five bones) joints are the most affected with more than 66%. They represent the majority of the human hand bones. The rest of the human hand bones are phalanges (only three joints) and are affected for less than 33%. The concentration of all those affected joints makes the hand one of the most visible signs of RA presence. The fact that humerus-ultera and clavicula-scapula joints are affected between 33% and 66% makes the human arm the second most sensitive to RA. This means that monitoring of the joints of the hands and arms can be helpful both to diagnose RA and to follow up on the appropriate treatment according to the level of severity of the illness.

Joints	Frequency of the disease in percentage
• Metatarsal joints	**>66%**
• Patella joints (Femur-Tibia)	
• Carpal joints	
• Metacarpal joints	
• Tarsal joints	**33%- 66%**
• Humerus-Ultera joints	
• Clavicula-Scapula joints	
• Phalange joints (foots and hands)	**<33%**
• Femur-Ischium joints	

Table 2.1: Skeleton joints with frequency of the disease in adult RA.

The various criteria for early diagnosis of RA [23], [24] have been developed by the American Rheumatism Association (ARA). All those criteria to declare a patient affected by RA or not are detailed in appendix A.

2.6 Treatment of RA

As damage to the joints occurs early in RA, and its progress tends to be very fast over the years, therapy should focus on an early and rapid control of inflammation of the joints and upon the prevention of joint destruction. To achieve that goal, the treatment will depend upon the patient and upon the level of severity of the illness. The final goals of the treatment are to achieve the lowest possible level of RA activity and remission of the disease, and if possible, the minimization of damage to the joints and the enhancement of physical functions. As there is no way of eradicating the disease completely, the strategy aims at helping the patient to have a better life without the loss of mobility. For that to happen there are, in addition to medication, social and emotional aspects that should be integrated into the process of treatment. The patient's

family, for example, should be educated about the nature and course of the disease. Alongside this, inflammation must be suppressed and mechanical and structural abnormalities corrected or compensated for by assistive devices. Sometimes, the treatment can involve decision-making on the part of a patient and his/her family about medication, reduction of joint stress, physical and occupational therapy and even surgical intervention. In general, the medications most in use are non-steroidal anti-inflamatory drugs (NSAID), systemic and intra-articular glucocorticoids, methotrexate and leflunnomide. In some cases, antimalarials, sulfasalazine and other DMARDs (Disease-Modifying Anti-Rheumatic Drugs) can be used [19].

2.7 Technologies to monitor movement

In the scientific literature, two major methods were developed to monitor human motion capabilities from a sequence of movements, marker based and markerless respectively. These methods summarize well most of the research performed so far on human movement tracking. Before presenting those two methods, it is important to summarize the notion of motion capture which is the idea behind the development of the technologies for movement monitoring.

2.7.1 Motion capture

Motion capture is the procedure that collects data from a human or a moving object to evaluate its motion. This study started with Etienne-Jules Marey (1830-1904) with his work on chronographic techniques. From his work, it was possible to capture phases of motion in a single photographic plate. In fact, he was the first to correlate motion with ground reaction forces [25]. Eadweard Muybridge, by studying human and animal motion using multiple photographs of objects moving over short periods of time, was able to give a further estimation of motion. He used multiple still cameras to capture rapid motions. He provided many examples of photography of motion capture, such as subjects descending staircases, boxing, children walking or, his most famous, a horse at full gallop [25].

After Eadweard Muybridge, many researchers studied motion capture, and in our days, it became an area that is used for many applications such as three-dimensional reconstruction, computer graphics, computer animation and video games. Segmenting the human body or a part of the body from a sequence of images can help to reconstruct the 3D structure of the image parts, and can be used for analyzing athletic performances or medical diagnosis. In recent times, another application of motion capture is made in security, in which organizations are interested in monitoring human activities with computers along borders, in building lobbies, public facilities, on streets, or in airports. In video conferencing, the possibility of using synthetic human faces as avatars or clones became real by making automatic selections from an original video sequence. Motion capture became very important in the implementation of virtual reality, smart surveillance systems and advanced user-interfaces.

It is possible today with further research on motion capture to track many points at a very high speed with good accuracy and in three dimensions [26]. Those capabilities are far beyond the design used by Marey and Muybridge in their early motion capture research. Yet, the basic limitations of the optical methods, as described in the following sections remain.

2.7.2 Marker Based Systems

The first method used was that of a marker based vision system which was introduced in 1973 by Johansson [14], with his system known as Moving Light Display (MLD), a psychological experiment aimed at monitoring the movements of the skeleton. In order to obtain good results, Johansson attached reflective markers to the joints of the arm such that one could observe the movement of the arm by following the trajectory of the reflective markers on a screen. This helped him estimate the skeletal pose at every moment during the arm's movement. The advantage of the system was that it imposed few limitations on the subject in terms of environmental or temperature constraints during the experiment. The drawback was that a precision error was introduced each time the system was used due to difficulties of tracking light during the movement [26].

A marker based system is therefore considered when the captured sources or sensors are placed on a moving subject whose movement is to be tracked. In this category, there are three classes of motion capture systems depending on how the captured sources and sensors are placed according to D.F.J. Perales [27].

i) *Outside-in* systems where external sensors are placed such that they collect information from the source placed on the subject's body. In general, the signals of those sensors are optical. The accuracy of these systems is well established because of the possibility of using as many sensors as needed to gain more information. In addition, it is easy to change the configuration of sensors just by changing their position on the subject, and then it is possible to obtain approximations to internal skeleton using information from groups of markers. This system requires, however, very costly post-processing work. In addition to this drawback, the optical system cannot capture motion if the markers are occluded for a long period of time. Moreover, such systems operate reliably only when the experiment is performed far from other possible optical sources, such as yellow light and reflective noise. An optical tracking system is composed of three subsystems: the optical imaging system (which can vary from a simple standard digital camera to specialized infrared camera), the mechanical tracking platform (which holds the optical imaging system in which the points of the target can always be tracked), and the tracking computer (which captures the images from the optical imaging system, analyses the images and extracts the target position by controlling the mechanical tracking platform to follow the target). One of the first version of an optical tracking system was implemented in 1997 [28], and, from that time, commercial versions of it became available, such as the ART-Optical tracking system [29]. Another solution comes from the Vicon systems [30] which are a range of products that track motion from 2D video analysis to the high accuracy of 3D digital optical systems. This particular system can be used indoors or outdoors, underwater or in studio and with markers or without.

ii) *Inside-out* systems where the sensors are placed directly on the subject's body and collect information from external sources. This type consists essentially of magnetic tracking system because almost all sources in this type of system are magnetic. The advantage of these systems is the real-time data output which is possible with immediate feedback because the position and orientation data are available without post-processing. In addition, there is no possibility for the sensors to be occluded, and it is possible to track multiple subjects interacting among themselves. In most cases however, the performance of the subject is constrained to the length of the wires, which makes the capture area smaller. Another limitation is the fact that magnetic trackers have a lower sampling rate than optical systems. Due to the sensitivity of magnetic trackers to metallic parts, the presence of any metallic material around the area can result in an unreliable output. In fact, an electromagnetic tracking system measures magnetic fields generated by running an electric current through three coiled wires arranged perpendicular to one another. A sensor measures how the magnetic field generated by each coil, which acts as an electromagnet, affects the two other coils. Then the direction and orientation of the emitter can be determined. This is why any material that can generate electromagnetic fields such as metals or magnets can disturb the system. Many commercial versions of such tracking systems exist, such as the AURORA tracking system [31] and the Polhemus LIBERTY tracking system [32]. A fully wired magnetic unit of XSensMtx [33] available on the market is able to track three DoFs (Degrees of Freedom) and can be combined using Xbus interface for a complete motion tracking system.

iii) *Inside-in* systems where the sensors and sources are placed on the subject's body. Such systems are generally based on wearing gloves, suit, and hat. In this case, the range of capture can be large and electromagnetic suits are less expensive and more portable than other technologies. At the same time, real-time data collection is possible with no sensors occlusion, and the system can monitor many subjects at the same time. The main limitations are generally the low sampling rate, possible constraints due to the

cables, and the fixed configuration of the sensors. These may impose some limitations on the movement. Also, such systems are very cumbersome and are not suitable for applications that require minimal interference to movements. In this category, there are many kinds of electromechanical body suits. On the market, full-body inertial motion capture suits that are available include the XsensMoven [34] and the AnimazooIGS-190 (formerly GypsyGyro-18) [35]. They are both wired systems and the sensors are mounted on a Lycra body-suit using sixteen Mtx units for Moven and eighteen modified InertialCubes [36] for Gypsy.

2.7.3 Markerless Systems

The second method, which is the most recent one, attempts to eliminate the constraints associated with mutual occlusions and with the use of reflective or magnetic markers found in the previous approach. Rosenhahn *et al.* [37] worked from a calibrated multi-camera system in order to measure the skeletal pose of the human arm over a sequence of movements. The purpose of their research was to estimate at each instant the movement of the different angles of the arm joints. In order to overcome some of the drawbacks of marker based systems, a computer vision solution was also developed by Bériault *et al.* [38] which reduces the problem of mutual occlusion with the use of a network of cameras and was able to reconstruct a 3D silhouette of a person performing some movements. In this case, calibration was one of the most important components in the setup, and the system required a large amount of computation to be able to determine exactly the pose of the silhouette at every instant. Eight cameras were required with very precise calibration and with synchronization software between cameras. The 3D model obtained with this system was helpful to estimate the pose of the arm in 3D space.

Markerless systems do not require markers and are based generally on image sequences or video to capture motion. The challenge here is to match information pertaining to spatial features to the one pertaining to temporal changes. A sequence of

2D video can help to compute the optical flow or motion field in the image. Two different types of implementation are possible:

i) Motion estimation without *a priori* shape models: The analysis of motion from a video capture of the moving subject is done without pre-defined models. The input description is based on points, relations or heuristics that can be found between two consecutive frames in the video. Two different types of analysis can be performed from those descriptors. Those types of analysis can either use feature correspondence such as points, lines, 2D contours or blobs to define the motion, or using motion analysis through motion vectors from matching blocks between frames.

ii) Motion estimation with model-based approaches: In this case, it is required to have a model definition of the subject which can vary from a stick to a volumetric model. The motion can then be modeled to define the kinematics. The known model of the subject helps to locate at each instant the tracking region or the body. This approach can be used for 2D, as well as 3D models.

In general, these two types of implementation use the same major steps: feature extraction process, feature correspondence, and high-level processing. The difference between them is the way in which each algorithm establishes the feature correspondence between two consecutive frames of the video. The motion estimation without *a priori* shape model finds correspondence between two consecutive frames upon prediction or estimation of features related to position, velocity, shape, texture, color and blocks. The model-based motion estimation approach matches the real images to a predefined model.

On the market, the InterSense wireless Inertial Cube3 [39] is a markerless solution that relies on a magnetic three DoFs orientation tracker using Kalman filter to estimate the orientation. Another solution using a low bandwidth IEEE 802.15.4 compatible radio, MicroStrain Inertia-Link [40] is available with three DoFs capabilities as well. In 2011, Organic Motion Inc. released a new markerless motion capture system with an upgraded computer vision platform. Its latest software version has many capabilities

including multiple actors tracking, basic prop tracking, no backdrop, larger scanning space and increased accuracy [41].

2.8 Skeletal Motion Estimation for RA Diagnosis

Most of the studies concerned with estimating the pose of the human arm in a sequence of movements were conducted for non-medical reasons. Generally, it was to detect movement [42] or to make a simulation of the human body [43] or for determining the position of the human skeleton [44]. Many papers published in this area focused on the precision and efficiency of the system with which the estimations were made. Very few results were published so far on motion estimation for medical purposes.

The work of Frize *et al.* [45] contributed to the early detection of RA from the distribution of body heat around articulations from a set of infrared images. Analyzing the infrared images of certain parts of the body of a patient, mainly the hands, feet and knees, they were able to establish the level of distribution of heat. Given that patients who suffer from RA exhibit a non-uniform distribution of body heat, the comparison of the distribution of the heat measured from infrared images of a patient's joints, with that obtained from healthy persons, can help to diagnose whether or not the patient is affected. A table of severity of the RA in function of the distribution of body heat was obtained from the conclusions of their research. The classification obtained through infrared imaging was based on three categories: low, medium and high. On the other hand, the physicians' classification typically contains six categories: low to zero, low, low to medium, medium, medium to high and high. If a physician needs to know the exact level of the severity so that he/she can provide specific medication to a patient, this means that, based on the results from infrared imaging only, further examination is needed to properly refine the level of severity of the disease.

An extra aid is then needed in determining the severity of RA. This can be provided by the evaluation of the motion capabilities of the patient. Because patients suffering from RA mostly experience motion problems in joints of the hands and limbs,

monitoring the motion of these parts of their body can be helpful in determining a patient's level of illness.

2.9 Literature Review on Motion Estimation

To monitor motion, many algorithms have been proposed. Some were used for motion estimation based on a set of digital images. Some use motion estimation for video compression in order to facilitate the transmission of complex videos [46] or to more efficiently make live communication transmission in video conferencing [47], or to encode images [48]. Motion estimation can be based on displacement of blocks from frame to frame in a video sequence. Many algorithms have been implemented for that purpose. The main idea is to make the computation of motion more efficient. For that reason, many algorithms were implemented based on matching blocks [49]. There is a wide variation in terms of rapidity and in the amount of computations from one algorithm to another to obtain similar results [50], [51], [52], [53], [54], [55], [56]. The algorithms range from Exhaustive Search (ES) to Adaptive Rood Pattern Search algorithm (ARPS) [57], with two other variations which are the Joint Adaptive Block Matching Search (JABMS) Algorithm [58] and the Enhanced Adaptive Rood Pattern Search Algorithm (EARPS) [59]. Some other algorithms of motion estimation are the block-based gradient descent algorithms [60]. Among these, the most accurate remain the block-matching algorithms. The least costly in terms of computations is the Adaptive Rood Pattern Search algorithm. Between this algorithm and its two other adaptations, there is no significant difference in terms of cost of computation. Those algorithms are presented in the following sub-sections and will be followed by the algorithm selected for this present research.

2.9.1 Motion Vectors

The primary use of motion vectors is to encode videos. The encoding side estimates the motion between the current frame and the previous one, such that it can create a motion-compensated image for the current frame. The motion vectors built

from blocks of the image from the previous frame are transmitted, as well as the difference of the compensated image within the current frame. The encoded image is then sent such that the receiver can decode it in order to have the original video. For this reason, the decoder has to perform the inverse process to recreate a full frame. This process is then also used for motion estimation and compensation. The general idea is that, from frame to frame, there is very little change in the pictures (very little movement). Instead of sending all the frames, it is more efficient to encode the difference between the macro-blocks of two consecutive frames and send this difference map with the reference frame. In order to achieve that, it is necessary to match the blocks from the present frame with the previous ones. When the best match is found, it estimates the motion vector and sends it with the compensated frame. The displacement between blocks is called the motion vector associated with the block.

Within a video, the motion vectors have to be stored such that the motion between one frame and another can be calculated. The motion vectors are stored in two dimensional arrays, and the array size corresponds to the frame size in terms of macro-blocks. The estimation of motion from one frame to another is performed by subtracting the vector of the present frame from the one in the previous frame. The motion vector defines the distance and the direction of the motion, but not the position of the blocks. This is why it is important to keep the reference frame where it can find the initial position of the vector. Then, only the vector with the same reference point can be subtracted from one frame to another.

2.9.2 Block Matching for Motion Estimation

One can use several block-matching algorithms to estimate motion vectors of the human hands and limbs [49]. The main idea in each algorithm is to estimate the motion in the current frame with respect to a previous frame. For the current frame, one creates a motion-compensated image based on blocks from the previous frame. Then the motion vector (module and orientation) from the first frame to the second is transmitted along with the difference between the current frame and the compensated image. The

new image can be used as the reference frame for the subsequent frames. One of the fastest algorithms (one which uses fewer computations) is the one implemented in 2002 known as Adaptive Rood Pattern Search (ARPS). The algorithms for motion estimation that are presented in this section based on block matching include: Exhaustive Search (ES), Three-Step Search (TSS), New Three-Step Search (NTSS), Simple and Efficient Three-Step Search (SESTSS), Four-Step Search (4SS), Diamond Search (DS), and Adaptive Root Pattern Search (ARPS).

The principle of block-matching for motion estimation is that the pattern of an object and its background in a specific frame of video move within the frame to form the next frame. The challenge is then to find the vector of that movement (orientation and module) such that the movement can be estimated. The technique consists in dividing the current frame into a matrix of "macro-blocks", which will be compared to the corresponding blocks and their adjacent neighbours in the previous frame, in order to create the motion vectors which represent the movement of the macro-blocks from their previous position to the current one. When the estimation of the movement of all the macro-blocks in the current frame with respect to the previous one is obtained, the motion estimation in the present frame is formed. For a good search area, it is required to leave some pixels around the macro-block, such that the search activity can move around each pixel of the block and over the side pixels. The number of pixels to leave around a macro-block is called "p", and, in this research, p=7 pixels (Fig. 2.1). The choice of a 16 by 16 pixels block is justified by the need to detect large motions, as well as small ones, as will be described later in the procedure of ARPS algorithm. "p" is known as the search parameter. Larger motion requires a larger "p" value. Also, if the search parameter is larger, then the process of motion estimation becomes more computationally expensive.

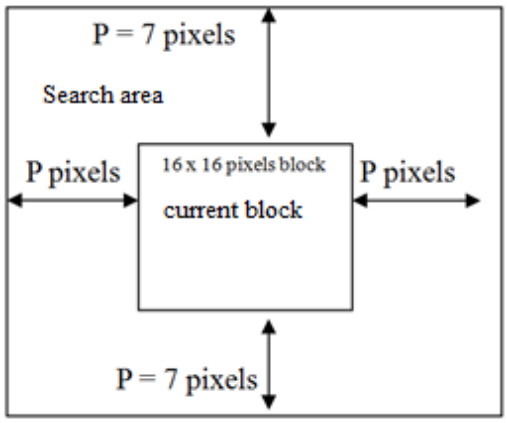

Fig. 2.1: Illustration of matching block process in a searching window.

The performance of each algorithm of matching blocks can be compared in order to choose the most efficient algorithm. The computation of the Mean Absolute Difference (MAD) is used for that purpose.

$$MAD = \frac{1}{N^2}\sum_{i=0}^{N-1}\sum_{j=0}^{N-1}\left|C_{i,j} - R_{i+u,j+v}\right| \tag{2.1}$$

where the size of macro-block is NxN pixels, here 16x16 and (u, v) lies within the search area, $C_{i,j}$is the pixel intensity at the (i, j) position of the current block in the current frame, $R_{i+u,j+v}$is the pixel intensity at (i+u, j+v) in the candidate block. The best match displacement (u, v) is the motion vector which represents the estimate of the displacement in horizontal and vertical directions respectively.

Another performance criterion (least cost match) for the best match is the Mean Squared Error (MSE) defined as:

$$MSE = \frac{1}{N^2}\sum_{i=0}^{N-1}\sum_{j=0}^{N-1}\left(C_{i,j} - R_{i+u,j+v}\right)^2 \tag{2.2}$$

To characterize the quality of the motion compensated image created by using motion vectors and macro blocks from the reference frame, one can compute the Peak-Signal-to-Noise-Ratio (PSNR) defined as:

$$PSNR = 10log_{10}\left[\frac{(Peak\ to\ peak\ value\ of\ original\ data)^2}{MSE}\right] \quad (2.3)$$

2.9.2.1 Exhaustive Search (ES)

This is the most computationally expensive matching block algorithm [51]. It is known also as Full Search and calculates the cost of each possible location of the block in the window. The advantage of this algorithm is that it can find the best possible match and the highest PSNR compared to all other possible algorithms. But, one can define other faster matching block algorithms which have the same PSNR but fewer computations. In addition, enlarging the search window increases the number of computations. For this reason, it is preferable not to use this algorithm for motion estimation based on matching block.

2.9.2.2 The Three-Step Search (TSS)

The three-step search algorithm [51] was the first attempt to reduce the computational cost of ES. It was first implemented in the early 1980s. The main idea is to start by the location at the center of the current block and set a step size. Then for each location it adds or subtracts the step size and search for the least cost match that is found for several iterations. Then the calculated vector is saved. In general, this algorithm reduces the computation factor by nine and uses a uniformly allocated checking pattern for motion detection. It is known, however, for missing small motions, and therefore it is not considered as the best algorithm to choose for motion detection, especially when one needs to detect small movements.

2.9.2.3 New Three-Step Search (NTSS)

This algorithm consists in providing a center-based searching scheme for motion and having provisions for a half-way step to reduce computational cost [50]. In each case, the location that gives the lowest weight is the closest match, and the motion vector is set to that location. Even with this reduction of computations, there is a worst case where the computation becomes very large. This algorithm becomes very computationally expensive when the search window is large. This is a reason to avoid this algorithm over a large search window.

2.9.2.4 Simple and Efficient Three-Step Search (SESTSS)

This is another extension of the Three-Step Search algorithm which is based on the fact that, for a unimodal surface, there are not two minimums in opposite directions. It changes the eight points fixed pattern of TSS, and therefore reduces the amount of computation [51]. Even though this algorithm saves much computation compared to TSS, many did not accept it because the error surfaces are not strictly unimodal, and the PSNR that it achieves is poorer than that of the TSS. Another reason is that by the same period, another algorithm, the Four-Step Search (4SS), was proposed and had lower computational cost compared to TSS. It also reached a better PSNR.

2.9.2.5 Four-Step Search (4SS)

This algorithm, as the New Three-Step Search one, uses center based searching with halfway stop prevision [52]. It has still a best case (seventeen checking points) and a worst case (twenty-seven checking points). For a large window search, it is good to find another algorithm to avoid twenty-seven checking points.

2.9.2.6 Diamond Search (DS)

This algorithm follows the same procedure as the 4SS. The difference is that the square pattern becomes a diamond using two different sizes of pattern. This algorithm has no limit in the number of steps to follow [53]. With this algorithm too, the global

minimum can be found very easily, and the result is that the PSNR is close to reaching an exhaustive search with fewer computations [53], [54], [55], [56].

2.10 Selected algorithm: Adaptive Rood Pattern Search (ARPS)

This algorithm proposed in 2002 by Nie and Ma [57] is still among the fastest and most efficient ones to date. Its main idea is that the general motion in a frame is usually coherent. If a block moves in a particular direction, it can be assumed that the current macro-block moves with a similar motion vector. This algorithm counts on two important steps. The first one is performed at the beginning of the algorithm to find the best starting point for the subsequent refined local search. That is why it is called the initial search. In this, the unnecessary intermediate search that the other algorithms require, and the risk of being trapped into a local minimum matching error, is significantly reduced. In this step, too, an adaptive rood pattern is proposed and the size of the macro-block is dynamically defined based on available motion vector of neighbouring macro-blocks. The second step uses the refined local search to determine the unit size rood pattern. That unit size rood pattern is used until the motion vector is found. To be able to take into account videos with small motion content, a zero-motion prejudgment is incorporated in the algorithm.

This algorithm is two or three times faster than DS, which is the fastest among all the other matching block algorithms for motion estimation. ARPS also achieves a better Signal-to-Noise ratio especially in the case of a sequence with complex or large motions [57].

2.10.1 Procedure

Because only a small number of positions around the search window (16 x 16 pixels macro-block) centre need to be checked, it has a compact space search points. The small size pattern provides the advantage of finding small motion in a video sequence, but tends to get trapped into a local minimum when it tends to find large motions. On the other hand, a large size pattern can easily detect large motions. To

avoid unnecessary computations or search, this algorithm uses different search patterns according to the motion vector behaviour that it estimates.

For the estimation of the motion vector, the idea is that two adjacent blocks belong to the same moving object and have similar motions. Then the motion vector of the current block can be estimated in reference to its neighbouring block motion vector. This algorithm defines also dynamically the pattern size for each macro-block according to the predicted motion vector from its neighbours' motion vectors. It is important to mention that the adaptive rood pattern is used only at the beginning of the algorithm to find the starting point for the local search. If this starting point is found, then a small and fixed pattern size can be sufficient to complete the remaining local search. The same pattern size is kept until the motion vector is completely defined. The matching procedure is performed as illustrated in Fig. 2.2.

ARPS algorithm uses the fact that the general motion within a frame is coherent. If the macro-blocks around the current block move in a particular direction, there is a high probability that this current block will move in the same direction and with a similar motion vector. ARPS algorithm uses the motion vector of the immediate left block of the current block to predict its own motion vector. In Fig.2.2 for example, the predicted motion vector points to (3, -3). This algorithm checks in addition to the location pointed by the predicted motion vector, at rood pattern distributed points shown as stars in Fig. 2.2. Those rood pattern distributed points are at the step distance from (0, 0) coordinate which is the center of the block. The step size is given by:

$S = \text{Max}(|x|, |y|)$ where (x, y) are the x and y coordinates of the predicted motion vector. In the case of Fig. 2.2, the step size is then:

$S = \text{Max}(|3|, |-3|) = 3$

By checking the rood pattern points, ARPS algorithm puts the search always in an area where there is a high probability of having a good matching block. Then the point that has the least weight as defined in eq.(2.1), eq.(2.2) and eq.(2.3) becomes the origin of the subsequent search steps.

The advantage of the ARPS algorithm over other algorithms is that if the motion vector is (0, 0) it does not waste computational time for matching blocks. Furthermore, if the predicted motion vector is far away from the center of the block (0, 0), ARPS also saves on computations by jumping to the area where there is a high possibility of matching the block while other algorithms are matching blocks until they get to that area.

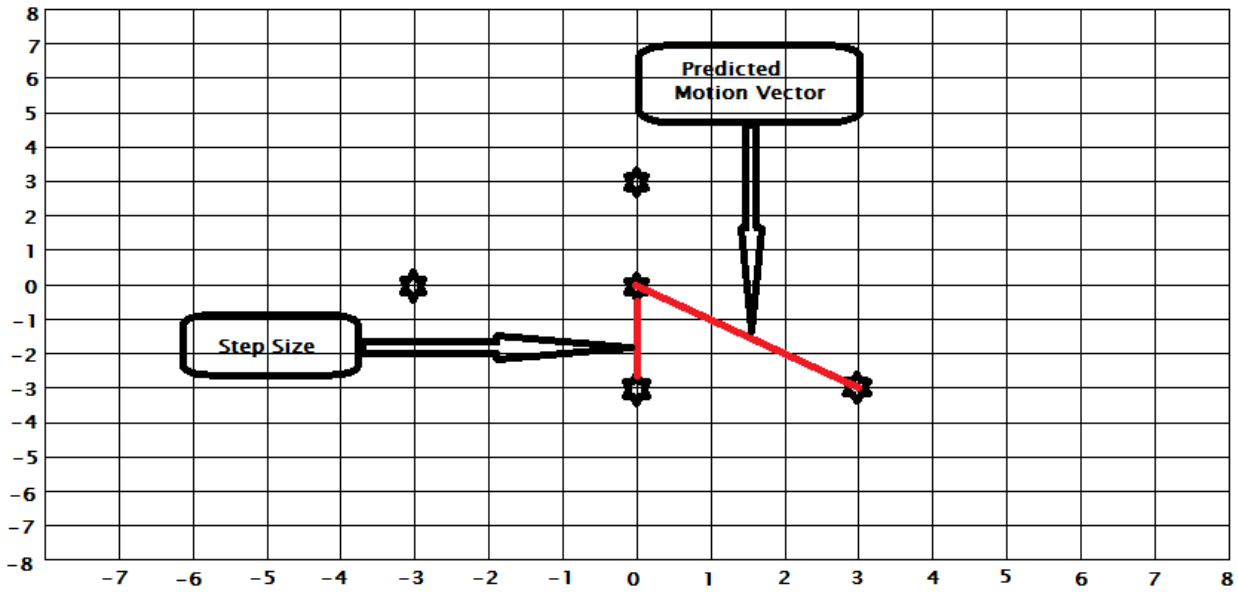

Fig. 2.2: Illustration of step size and predicted motion vector within a block.

To predict the first motion vector, since the first block does not have its neighbour's motion vector, the first step, as described in the procedure, is to use the full search strategy (as in ES algorithm) for the first block until the motion vector is found. Then, the motion vector found can be used for the next block using the prediction of motion vector.

2.10.2 Prediction of motion vector

Two points have to be taken into account, since the choice of the region of support with neighbouring blocks can be taken for predicting the current block matching. To

find the neighbouring block to the current one, it is appropriate to define a motion vector. Four possibilities exist for selecting neighbours:

i) Cover all four neighbouring blocks,
ii) Based on region of support (using international norm such as H.263),
iii) Two directly adjacent blocks,
iv) The block situated at the immediate left to the current block.

The illustration of those four possibilities is shown below:

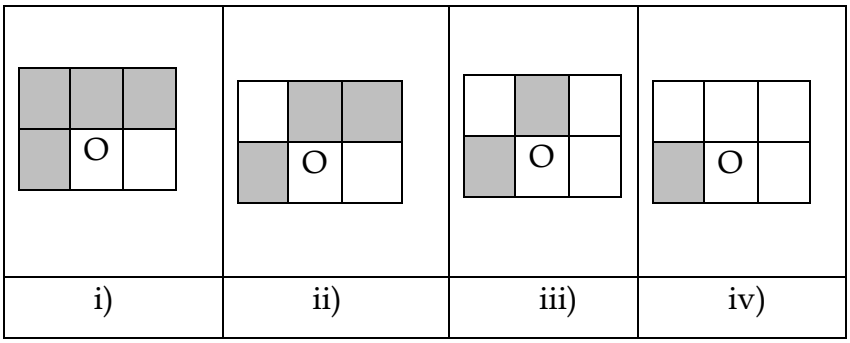

Fig. 2.3: Choosing neighbouring blocks (grey blocks) of a present block (block with circle).

As mentioned previously, the ARPS algorithm version that is used in this present research selects the block situated at the immediate left of the present block (Fig. 2.3 (iv)). Another version of ARPS algorithm was implemented in 2008 by Zhao *et al.* [59], called Enhance Adaptive Rood Pattern Search algorithm (EARPS) for fast Block-matching motion estimation. Another version of this algorithm was presented by Ananthashayana and Pushpa in 2009 called Joint Adaptive Block Matching Search (JABMS) algorithm [58]. These two new versions use the same idea as the one that is used in this research and the gain in terms of computations is not large.

Summary

The purpose of this thesis is to help diagnose and monitor RA. It is then important to distinguish RA from many other joint diseases. An overview of the literature focused, among the more than one hundred different rheumatic diseases, on the ones whose manifestations are closest to those of RA, and presented them. This introduced the specificities of RA in terms of its manifestation and symptoms.

This chapter also summarized the first symptoms and various stages of RA evolution. Finally, the parts of the human skeleton most affected by RA were identified along with the impact on human motion capabilities.

The second part of this chapter discussed the current state of the art on motion capture and motion estimation technologies. Various alternatives were presented with a focus on the quantification of motion capabilities of human gesture. Pose estimation, especially skeleton pose estimation plays an important role in this thesis because of its extensive use in this research. For this reason, the study is extended in the next chapter by an examination of the mechanism of the skeleton movement and of its capabilities with the review of the kinematic model for the parts of the human skeleton that are most affected by RA (i.e. hands and arms).

Chapter 3: Kinematics of Human Hand and Arm

3.1 Introduction

Recently, for medical purposes, more demand has been expressed to have a reliable motion tracking of the human hand. This demand originates, in part, from an increase in research in Human-Computer Interaction (HCI), robotics, ergonomics and bio-mechanics of the hand. The objective is to better trace the hand movement and gesture. Many models exist of the human hand for simulating movements. Such models range from simplified forms with six degrees of freedom (DoFs) or nine DoFs to more complex ones with twenty to twenty six DoFs. Yet the objective here is to develop a model that is as close as possible to the real kinematics of the human hand. Two components are essential for implementing such hand motion monitoring approaches: the tracking and the rendering systems. The latter reproduces and renders what the tracking system measures. For the tracking system, two major methods have been exploited in the literature: glove-based approaches and vision-based approaches.

Glove-based approaches use signals coming from wearing gloves to measure the movement. The advantage of these approaches is that there are fewer errors between the rendered and the real hand motion. However, the main drawback is a multiplication of markers and signals. The problem becomes very complex when the simulated model counts a larger number of DoFs, which consequently leads to a larger number of signals. Because of the multiplication of signals, the possible confusion between those signals, the complexity to wear many sensors, and the variable size of hand from one person to another, glove-based systems are often not appropriate for a functional assessment of the human hand, especially when one wants to evaluate the capacity of bending each articulation individually. In the present research work, the goal is to evaluate the capability of each hand and finger articulation to bend and extend, and to be able to measure, reproduce and compare the hand motion capabilities

of a particular patient to a healthy subject. Another objective in a future work will be to merge thermographic information coming from an infrared camera with the digital images of the hand. In this case, wearing glove would preempt making the thermal information available. Therefore, the glove-based approach does not appear as a suitable alternative.

Vision-based approaches use a camera or a set of cameras to track the hand movement and from there, build on a pre-defined model of the hand to estimate the position and physical configuration of the real hand. For such an implementation, using a set of calibrated cameras rather than a single one could introduce supplementary constraints. The use of a multi-camera system also requires complex calibration and heavier computation before obtaining the estimation of movement. To overcome the multi-camera system drawbacks, Pavlovic *et al.* [60] and Aristidou [61] proposed a vision-based hand tracking method that uses a single camera with a cloth glove. Their systems rely on a custom pattern, and offer the advantage of a lower computational load. The main limitation of their solutions is the fact that they are not as reliable as the glove-based approach described previously in terms of matching accuracy between the rendered hand and the real hand. An ideal solution working only in 2D should rely on a vision-based approach with a single camera (avoiding calibration and heavy computation), while minimizing the risk of matching errors between the rendered hand and the real one such that it is possible to determine with accuracy the minimum bend and maximum extension of each hand and finger articulation taken one after another.

In order to increase the accuracy of a vision-based motion monitoring system such that the error between the real hand and the rendered one remains as small as possible, one strategy consists in relying on a kinematic model of the human hand. The present research work adopts this strategy in order to develop an experimental platform which remains as simple as possible in terms of implementation and operation, given its scope of application in a medical environment, while still providing acceptable accuracy on

the human hand configuration estimation under controlled experimental conditions. The following sections investigate kinematic models of the hand, and extend them to the human arm.

3.2 Kinematics and motion estimation

In the present work, the information extracted from image processing is merged with the knowledge available about the kinematics of the human hand and arm to experimentally determine the angle of each joint over a sequence of movements recorded in a short video. This proves helpful to formally quantify measurements of the hand and arm motion capabilities. In order to merge properly the visually extracted movement information with the kinematic model which defines specific angles for each joint, one needs to know where the hand or arm can reach under a specific configuration. The ultimate goal is to be able to accurately reproduce a sequence of movements from the estimated sequence of joint angles. The inverse kinematic of hand and arm must be defined because this mathematical formulation allows the formal estimation of the angle of each joint for a known configuration of the end effector (here associated with the extremity of a finger, as will be defined in Fig. 3.5) extracted from a given frame in the video sequence. Therefore it is essential to define the forward and the inverse kinematics for the human hand and arm.

3.3 Kinematics of the human hand

To understand properly the human hand kinematics, one must start by examining the anatomy of the skeleton of the human hand.

3.3.1 Anatomy of the hand bones

The human hand skeleton (Fig. 3.1) is composed of several bones. The carpal bones are all different from one another by their shape and their motion capability, and they are attached at their base to the radius and the ulna (Fig. 3.2).

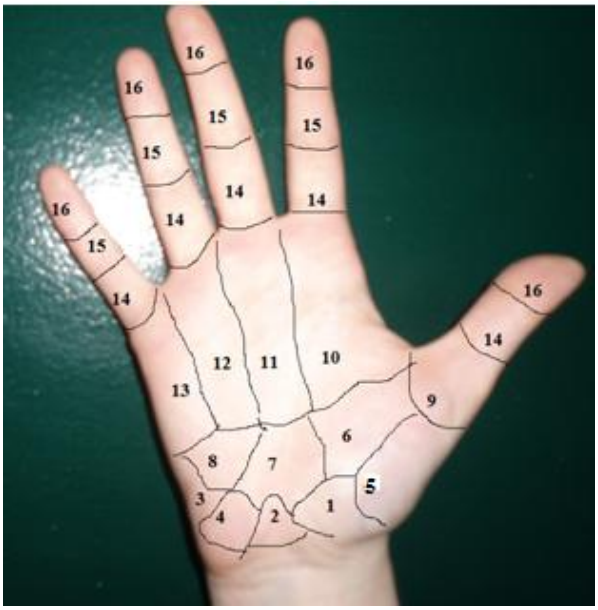

Fig. 3.1: Location of the bones of the human hand.

Label	Bone	Hand part
1	Scaphoid	Carpal bones
2	Lunate	
3	Triquetrum	
4	Pisiform	
5	Trapezium	
6	Trapezoid	
7	Capitate	
8	Hamate	
9	Metacarpal I	Metacarpal bones
10	Metacarpal II	
11	Metacarpal III	
12	Metacarpal IV	
13	Metacarpal V	

14	Proximal phalanx	Phalanges
15	Middle phalanx	
16	Distal phalanx	

Table 3.1: List of all human hand bones per category.

The metacarpal bones are the longest in the human hand's skeleton. The thumb metacarpal makes possible for the thumb to rotate and face the other fingers.

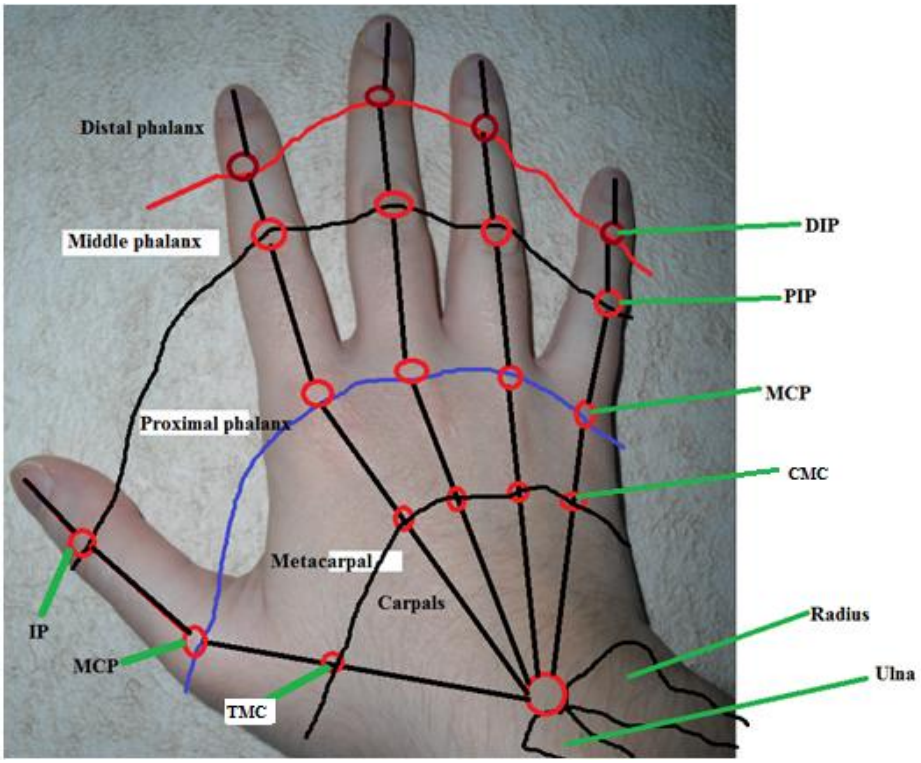

Fig. 3.2: All bones and joints of the human hand.

Each finger has three phalanges (proximal, middle and distal) except for the thumb. The thumb counts only proximal and distal phalanges. The joint between the proximal phalanx and metacarpal bone is called the metacarpophalangeal joint (MCP). The thumb trapeziometacarpal (TMC) possesses two degrees of freedom (DoFs) in

rotation because it is biaxial. The joints between two phalanges for all fingers except the thumb are called the proximal interphalangeal (PIP) and the distal interphalengeal (DIP). For the thumb this articulation is called interphalangeal (IP) followed by the metacarpophalangeal (MCP). The thumb's IP and MCP joints have one DoF each in rotation (Fig. 3.3). The PIP and DIP joints have one DoF each. The MCP has two DoFs for every finger except the thumb, and can rotate around the two latitudinal axes (y and z axes). It is not possible to have a voluntary longitudinal rotation (around x axis) (Fig. 3.5). The joints between the metacarpal and carpal bones are called the carpometacarpal (CMC) for all fingers except the thumb. For the four main fingers, CMC joints have one DoF each. However, the thumb's TMC is called a saddle joint because it looks like a pair of interlocking saddles (Fig. 3.3). The saddle joint is biaxial (two DoFs) as the MCP for the other fingers. Because the thumb is anatomically different from the other fingers, it requires different modeling. For this reason, two different kinematic configurations are defined: one for the thumb and one for all other fingers.

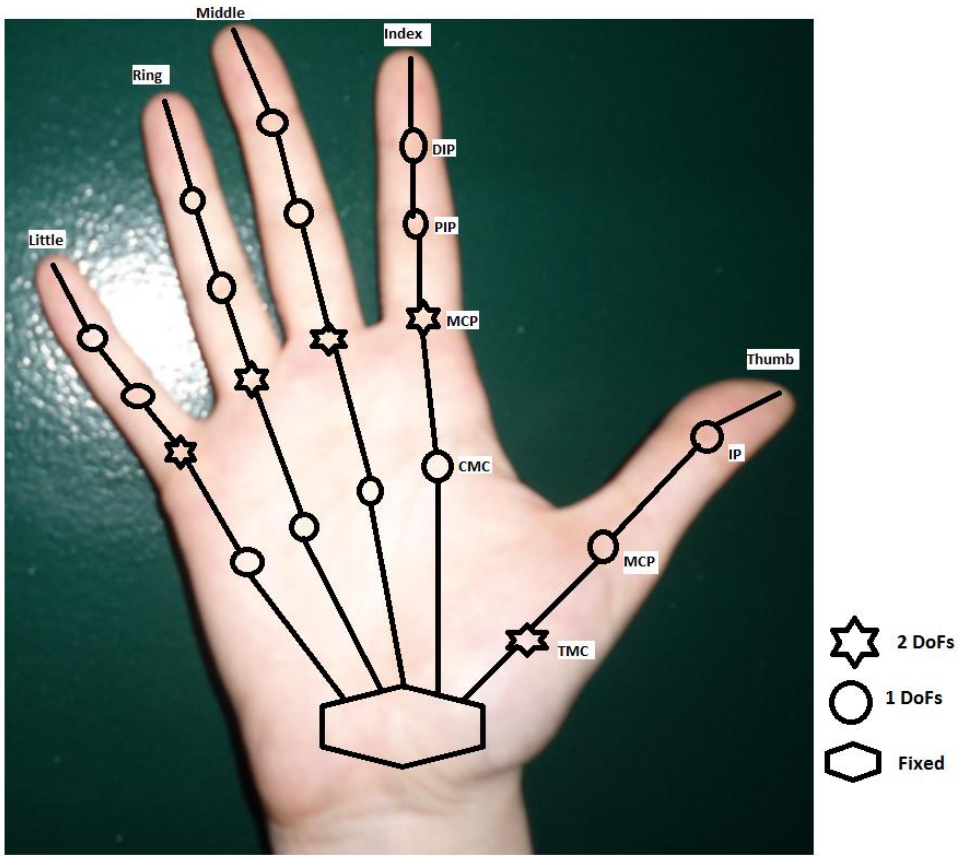

Fig. 3.3: The considered degrees of dreedom (DoFs) on the human hand.

The total number of DoFs of the human hand joints can be computed by adding the number of DoFs of every finger. Overall, there are nineteen different joints with twenty-four DoFs (Fig. 3.3). The wrist joint is not taken into consideration in the kinematic model of the hand used in this work.

3.3.2 Forward kinematics

The forward kinematic model is a set of equations that calculates the position and orientation of an end effector (here defined as the extremity of a given finger in Fig. 3.5) as a function of given joint angles. The set of equations is generated using the Denavit-Hartenberg (D-H) parameters formalism [62] that builds on reference frames assigned to each DoF. The forward kinematics can be used to calculate the pose (position and orientation) of each human hand segment of interest given the set of joint angles. The

problem then consists in defining the end effector point position and orientation in 3D space, which corresponds to the human hand or finger pose, from a set of specified joint angles. The model can also be extended to the human arm, as will be considered in section 3.4.

Given the structure of the hand skeleton, the kinematic model of the hand can adopt two configurations: one for the thumb with three joints and four DoFs, another for the index, middle, ring and little fingers with four joints and five DoFs each. These latter fingers have the MCP modeled with two DoFs, the CMC, PIP and DIP with one DoF each. For the thumb, the trapeziometacarpal (TMC) joint has two DoFs, the MCP and IP have one DoF each.

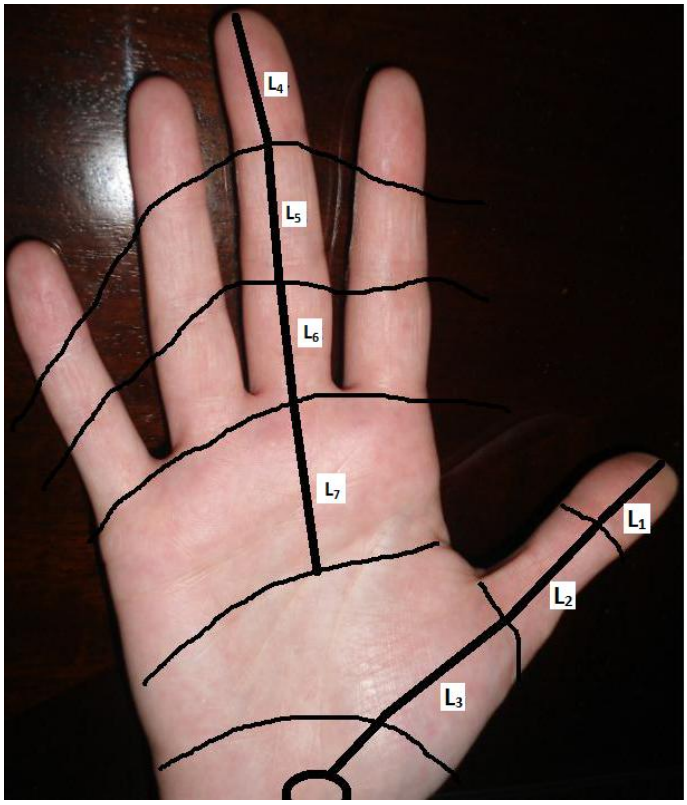

Fig. 3.4: The two hand configurations considered: the thumb and the other fingers.

Given a set of values for each of the joint's angles, the configuration of a finger in 3D space can be computed via the forward kinematic model, assuming that the corresponding length of the bones and their physical assembly at the joints are also defined. From Fig. 3.4 which shows the length of each bone and Fig. 3.5 that defines the axes of the reference frames and the D-H convention rules (Appendix B), the D-H parameters table is established for the thumb (Table 3.2) and for the other fingers (Table 3.3).

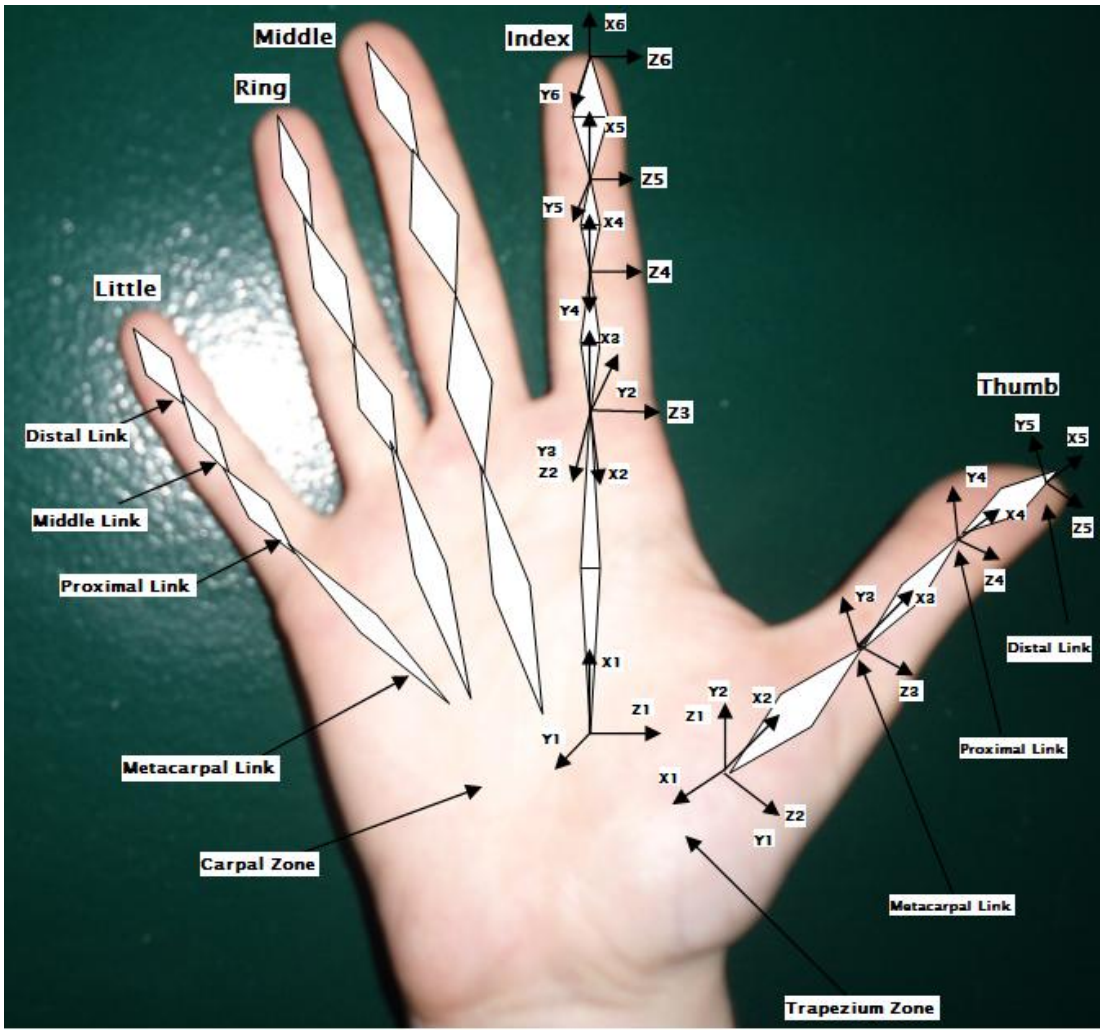

Fig. 3.5: The proposed joint reference frames used to obtain D-H parameters.

From the model representing the mechanism of each finger (Fig. 3.7 for the thumb and Fig. 3.8 for all other fingers) the displacement from a certain location (pose *1*) in the space to any other (pose *i*) is defined according to the global reference frame located on the palm of the hand (Fig. 3.5). The transformation from any pose considered as the reference pose and tagged as pose 1 to another pose *i*= 2, 3, …, extracted from a video sequence of the finger in motion, as illustrated in Fig. 3.6, can be described by D-H transformation matrices (called A_i matrices).

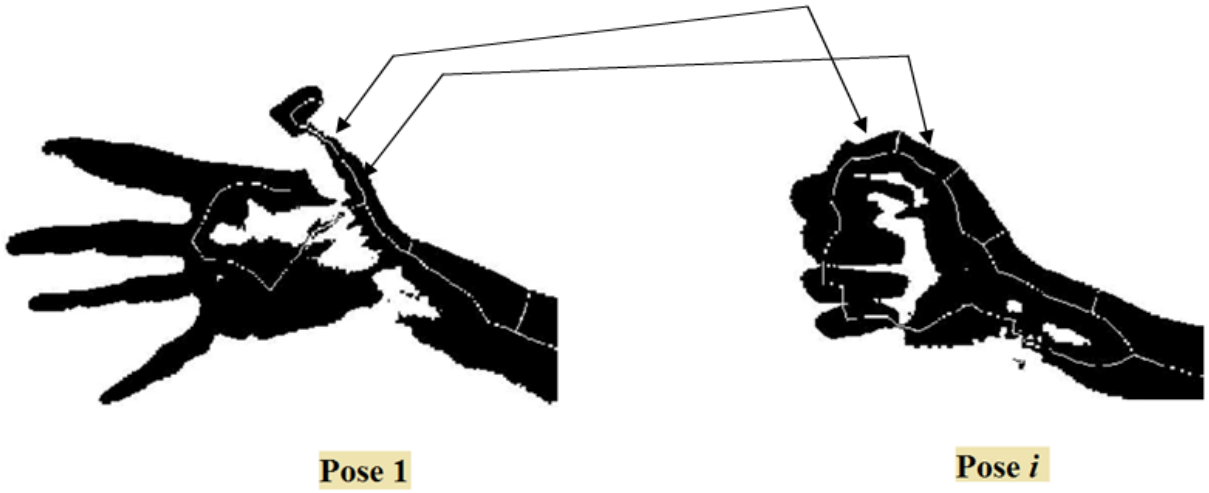

Fig. 3.6: Computation of relative movement of two consecutive bones between any two poses of the hand: here between pose 1 and an arbitrary selected pose *i* in the sequence.

A schematic representation of the kinematic assembly of the thumb is shown in Fig. 3.7. The corresponding kinematic model of the human thumb is built on four degrees of freedom. The four DoFs of the thumb are organized as follows:

i) Two DoFs from the flexion/extension and abduction/adduction of the TMC joint,
ii) One DoF for the MCP joint flexion/extension,
iii) One DoF for the IP joint flexion/extension.

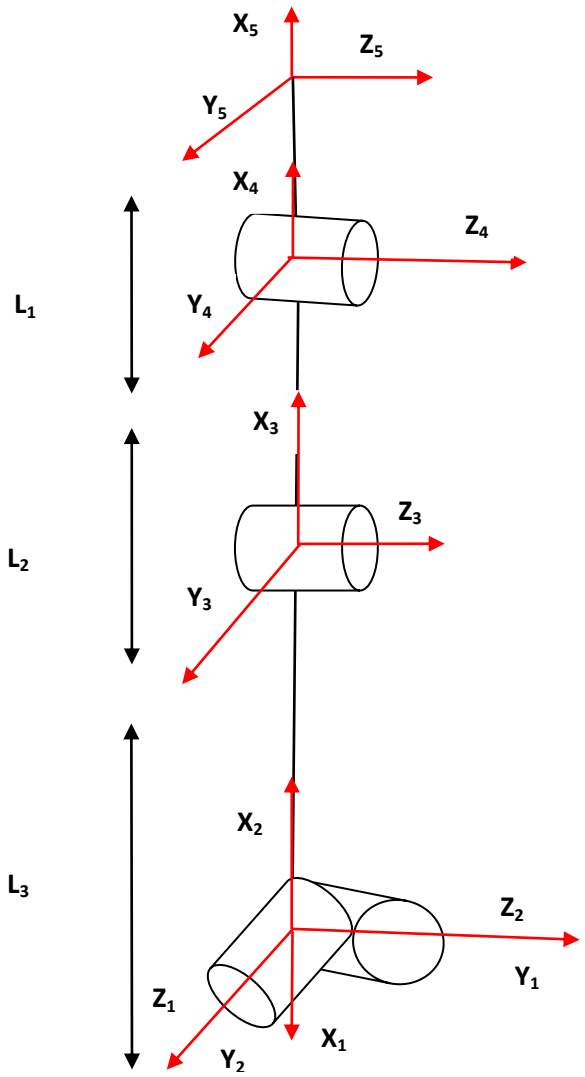

Fig. 3.7: Proposed kinematic model of the thumb.

The forward kinematic describes the Cartesian coordinates and orientation angles of joints variables. The orientation of the end effector is described in Cartesian space by the general transformation equation, eq.(3.7), for the thumb and eq.(3.14) for the other fingers.

The assignment of the coordinate frame is done in accordance to the convention developed by Denavit and Hartenberg (1955) for spatial mechanisms (Appendix B). The

Denavit and Hartenberg's parameters are organized in a table as illustrated for the thumb in Table 3.2. The constant offset of 180 degrees between X_1 and X_2 is not included in this table because it will be subtracted from the computed value of $\theta_{\mathbf{TMC0}}$.

Joints	$\mathbf{d_i}$	$\mathbf{l_i}$	$\boldsymbol{\alpha_i}$	$\boldsymbol{\theta_i}$
1	0	0	$\pi/2$	$\boldsymbol{\theta_{TMC0}}$
2	0	L_3	0	$\boldsymbol{\theta_{TMC1}}$
3	0	L_2	0	$\boldsymbol{\theta_{MCP}}$
4	0	L_1	0	$\boldsymbol{\theta_{IP}}$

Table 3.2: D-H parameters of the thumb.

For all other fingers except the thumb, the kinematic model is slightly modified to take into consideration five DoFs. The DoFs of the other fingers (index, middle, ring and little fingers) are specified as:

i) One DoF from the flexion/extension of the CMC joint,
ii) Two DoFs for the rotation and flexion/extension of the MCP joint,
iii) One DoF from the flexion/extension the PIP joint,
iv) One DoF for flexion/extension of the DIP joint.

The corresponding schematic of the fingers mechanical assembly is shown in Fig. 3.8.

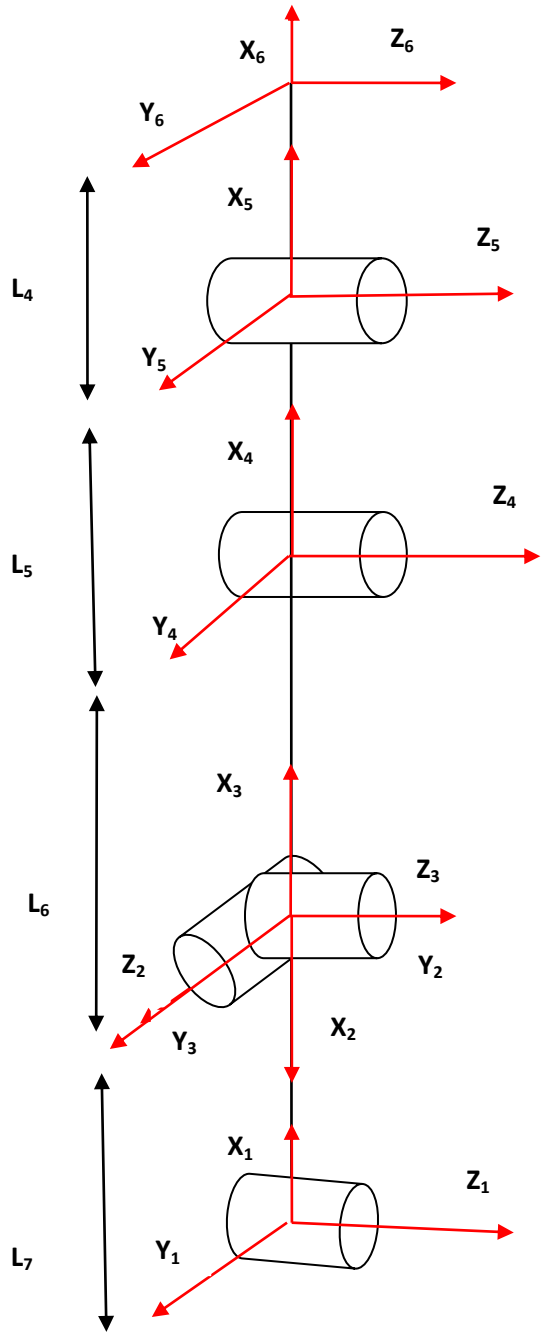

Fig. 3.8: Proposed kinematic model of all fingers except the thumb.

The corresponding D-H parameters table is illustrated by Table 3.3 below. As in the previous table, the constant offsets of 180 degrees between X_1, X_2 and X_2, X_3 are not

included in this table because they will be subtracted from the computed value of θ_{MCP1} and θ_{MCP2}.

Joints	$\mathbf{d_i}$	$\mathbf{l_i}$	$\boldsymbol{\alpha_i}$	$\boldsymbol{\theta_i}$
1	0	L_7	$\pi/2$	$\boldsymbol{\theta_{CMC}}$
2	0	0	$\pi/2$	$\boldsymbol{\theta_{MCP1}}$
3	0	L_6	0	$\boldsymbol{\theta_{MCP2}}$
4	0	L_5	0	$\boldsymbol{\theta_{PIP}}$
5	0	L_4	0	$\boldsymbol{\theta_{DIP}}$

Table 3.3: D-H parameters of all fingers except the thumb.

In the forward kinematic models, A_i matrices are the 3D Euclidean space representation of position and orientation of a rigid member, here associated to any segment of the human hand or limb, defined by a set of D-H parameters. The A_i matrices are 4 x 4 matrices which can be obtained by multiplication of affine transformation matrices. The expression of those matrices results in a combination of the rotations performed by the joints, along with the inherent rotations and translations created by the bones and their anatomical assembly.

For the thumb, applying the set of D-H parameters from Table 3.2 for each of the four DoFs, the A_i matrices become respectively:

$$A_1 = \begin{matrix} cos\theta_{TMC0} & 0 & sin\theta_{TMC0} & 0 \\ sin\theta_{TMC0} & 0 & -cos\theta_{TMC0} & 0 \\ 0 & 1 & 0 & 0 \\ 0 & 0 & 0 & 1 \end{matrix} \quad (3.1)$$

$$A_2 = \begin{matrix} cos\theta_{TMC1} & -sin\theta_{TMC1} & 0 & L_3 cos\theta_{TMC1} \\ sin\theta_{TMC1} & cos\theta_{TMC1} & 0 & L_3 sin\theta_{TMC1} \\ 0 & 0 & 1 & 0 \\ 0 & 0 & 0 & 1 \end{matrix} \quad (3.2)$$

$$A_3 = \begin{matrix} cos\theta_{MCP} & -sin\theta_{MCP} & 0 & L_2 cos\theta_{MCP} \\ sin\theta_{MCP} & cos\theta_{MCP} & 0 & L_2 sin\theta_{MCP} \\ 0 & 0 & 1 & 0 \\ 0 & 0 & 0 & 1 \end{matrix} \quad (3.3)$$

$$A_4 = \begin{matrix} cos\theta_{IP} & -sin\theta_{IP} & 0 & L_1 cos\theta_{IP} \\ sin\theta_{IP} & cos\theta_{IP} & 0 & L_1 sin\theta_{IP} \\ 0 & 0 & 1 & 0 \\ 0 & 0 & 0 & 1 \end{matrix} \quad (3.4)$$

To compute the pose of the end effector, that is the fingertip of the thumb, with respect to the fixed reference frame, R_1, attached to the base of the thumb (Fig. 3.5), one needs to post-multiply the sequence of A_i matrices to obtain the transformation matrix between the base and the fingertip, eq.(3.5).

Multiplying the four A_i matrices, one obtains for the thumb:

$$Q_{fingertip/palm} = \begin{matrix} cos\theta_{TMC0}\, cos\delta & -cos\theta_{TMC0}\, sin\delta & sin\theta_{TMC0} & cos\theta_{TMC0}\ L_1 cos\delta + L_2 cos\beta + L_3 cos\theta_{TMC1} \\ sin\theta_{TMC0} cos\delta & -sin\theta_{TMC0}\, sin\delta & -cos\theta_{TMC0} & sin\theta_{TMC0}\ L_1 cos\delta + L_2 cos\beta + L_3 cos\theta_{TMC1} \\ sin\delta & cos\delta & 0 & L_1 sin\delta + L_2 sin\beta + L_3 sin\theta_{TMC1} \\ 0 & 0 & 0 & 1 \end{matrix} \quad (3.5)$$

where $\delta = \theta_{TMC1}+\theta_{MCP}+\theta_{IP}$, $\beta = \theta_{TMC1} + \theta_{MCP}$ (3.6)

For all other fingers, applying the set of D-H parameters from Table 3.3 for each of the five DoFs, the A_i matrices become respectively:

$$A_1 = \begin{matrix} cos\theta_{CMC} & 0 & sin\theta_{CMC} & L_7 cos\theta_{CMC} \\ sin\theta_{CMC} & 0 & -cos\theta_{CMC} & L_7 sin\theta_{CMC} \\ 0 & 1 & 0 & 0 \\ 0 & 0 & 0 & 1 \end{matrix} \quad (3.7)$$

$$A_2 = \begin{matrix} cos\theta_{MCP1} & 0 & sin\theta_{MCP1} & 0 \\ sin\theta_{MCP1} & 0 & -cos\theta_{MCP1} & 0 \\ 0 & 1 & 0 & 0 \\ 0 & 0 & 0 & 1 \end{matrix} \quad (3.8)$$

$$A_3 = \begin{matrix} cos\theta_{MCP2} & -sin\theta_{MCP2} & 0 & L_6 cos\theta_{MCP2} \\ sin\theta_{MCP2} & cos\theta_{MCP2} & 0 & L_6 sin\theta_{MCP2} \\ 0 & 0 & 1 & 0 \\ 0 & 0 & 0 & 1 \end{matrix} \quad (3.9)$$

$$A_4 = \begin{matrix} cos\theta_{PIP} & -sin\theta_{PIP} & 0 & L_5 cos\theta_{PIP} \\ sin\theta_{PIP} & cos\theta_{PIP} & 0 & L_5 sin\theta_{PIP} \\ 0 & 0 & 1 & 0 \\ 0 & 0 & 0 & 1 \end{matrix} \quad (3.10)$$

$$A_5 = \begin{matrix} cos\theta_{DIP} & -sin\theta_{DIP} & 0 & L_4 cos\theta_{DIP} \\ sin\theta_{DIP} & cos\theta_{DIP} & 0 & L_4 sin\theta_{DIP} \\ 0 & 0 & 1 & 0 \\ 0 & 0 & 0 & 1 \end{matrix} \quad (3.11)$$

Multiplying the five A_i matrices in order (A_1 xA_2 xA_3 xA_4 xA_5), we obtain for all other fingers:

$$Q_{\text{fingertip/palm}} = \begin{matrix} \partial_X & \beta_X & \gamma_X & \rho_X \\ \partial_Y & \beta_Y & \gamma_Y & \rho_Y \\ \partial_Z & \beta_Z & \gamma_Z & \rho_Z \\ 0 & 0 & 0 & 1 \end{matrix} \quad (3.12)$$

where:

$\partial_X = \text{Cos}\theta_{CMC}\text{Cos}\theta_{MCP1}\text{Cos}(\theta_{PIP} + \theta_{DIP} + \theta_{MCP2}) + \text{Sin}\theta_{CMC}\text{Sin}(\theta_{PIP} + \theta_{DIP} + \theta_{MCP2})$ (3.13)

$\partial_Y = \text{Sin}\theta_{CMC}\text{Cos}\theta_{MCP1}\text{Cos}(\theta_{PIP} + \theta_{DIP} + \theta_{MCP2}) - \text{Cos}\theta_{MCP1}\text{Sin}(\theta_{PIP} + \theta_{DIP} + \theta_{MCP2})$ (3.14)

$\partial_Z = \text{Sin}\theta_{MCP1}\text{Cos}(\theta_{PIP} + \theta_{DIP} + \theta_{MCP2})$ (3.15)

$\beta_X = - \text{Cos}\theta_{CMC}\text{Cos}\theta_{MCP1}\text{Sin}(\theta_{PIP} + \theta_{DIP} + \theta_{MCP2}) + \text{Sin}\theta_{CMC}\text{Cos}(\theta_{PIP} + \theta_{DIP} + \theta_{MCP2})$ (3.16)

$\beta_Y = - \text{Sin}\theta_{CMC}\text{Cos}\theta_{MCP1}\text{Sin}(\theta_{PIP} + \theta_{DIP} + \theta_{MCP2}) - \text{Cos}\theta_{CMC}\text{Cos}(\theta_{PIP} + \theta_{DIP} + \theta_{MCP2})$ (3.17)

$\beta_Z = -\text{Sin}\theta_{MCP1}\text{Sin}(\theta_{PIP} + \theta_{DIP} + \theta_{MCP2})$ (3.18)

$\gamma_X = \text{Cos}\theta_{CMC}\text{Sin}\theta_{MCP1}$ (3.19)

$\gamma_Y = -\text{Sin}\theta_{CMC}\text{Sin}\theta_{MCP1}$ (3.20)

$\gamma_Z = - \text{Cos}\theta_{MCP1}$ (3.21)

$\rho_X = \text{Cos}\theta_{CMC}\text{Cos}\theta_{MCP1}[L_4\text{Cos}(\theta_{PIP} + \theta_{DIP} + \theta_{MCP2}) + L_5\text{Cos}(\theta_{MCP2} + \theta_{PIP}) + L_6\text{Cos}\theta_{MCP2}] + \text{Sin}\theta_{MCP1}[L_4\text{Sin}(\theta_{PIP} + \theta_{DIP} + \theta_{MCP2}) + L_5\text{Sin}(\theta_{MCP2} + \theta_{PIP}) + L_6\text{Sin}\theta_{MCP2}] + L_7\text{Cos}\theta_{CMC}$ (3.22)

$\rho_Y = \text{Sin}\theta_{CMC}\text{Cos}\theta_{MCP1}[L_4\text{Cos}(\theta_{PIP} + \theta_{DIP} + \theta_{MCP2}) + L_5\text{Cos}(\theta_{MCP2} + \theta_{PIP}) + L_6\text{Cos}\theta_{MCP2}] - \text{Cos}\theta_{MCP1}[L_4\text{Sin}(\theta_{PIP} + \theta_{DIP} + \theta_{MCP2}) + L_5\text{Sin}(\theta_{MCP2} + \theta_{PIP}) + L_6\text{Sin}\theta_{MCP2}] + L_7\text{Sin}\theta_{CMC}$ (3.23)

$$\rho_Z = \text{Sin}\theta_{MCP1}[L_4\text{Cos}(\theta_{PIP} + \theta_{DIP} + \theta_{MCP2}) + L_5\text{Cos}(\theta_{MCP2} + \theta_{PIP}) + L_6\text{Cos}\theta_{MCP2}] \quad (3.24)$$

3.3.3 Inverse kinematics

Based on the models developed in the previous sections, the inverse kinematics is used to estimate the configuration of fingers at a given time in the video sequence. The main idea is that knowing the end effector's (fingertip) pose, one can determine the corresponding angles to assign on every joint in order for the fingertip to reach that specified pose in the space with respect to the palm. It is, in fact, the inverse situation of the forward kinematics. To perform this calculation, it is required to know the coordinates of the fingertip in 3D space, and then determine the set of angles for every joint to reach this configuration. The coordinates of the measured fingertip pose can be specified under the form of a 3D transformation matrix (in this study the depth information is not used as it is performed in 2D through the use of only one camera) along with the skeletal structure of a given finger. In general, to reach a specific pose in space, there exists more than one set of angles for the joints of the fingers that meet the requirements. Due to the physical configuration of the human hand there are some constraints on each joint articulation. To reach a specific place in the space, some sets of the joint angles will not be admissible because those angles are out of the range of capabilities for some joints. The proper solution can be selected based on the constraints on the finger's joint, as imposed by their capabilities of bending and extending. The constraints are listed in Table 3.4 where for each joint the maximum and minimum angles of bending are defined. Cobos et *al.* [63] performed an important study on inter-finger constraints on movement on each joint of the hand. The final goal is to determine, for a given transformation matrix, $Q_{\text{fingertip/palm}}$, defining the pose of a fingertip, what is the set of values of the joint angles to reach this specific configuration.

Table 3.4 presents in the first column each joint of the hand. The second column lists the range values in degrees for the flexion of each joint, and the third column presents the range of extension of the joints. The last column represents the range values for abduction/adduction for each joint. Where a zero degree value is reported,

that means that the considered joint is not able to perform the considered movement. In fact, all joints are not able to perform flexion, extension and abduction, adduction.

Finger and joint	**Range of flexion (degree)**	**Range of extension (degree)**	**Range of abduction/adduction(degree)**
THUMB			
Trapeziometacarpal ($\boldsymbol{\theta}_{TMC0}$)	50 - 90	0	45 - 60
Trapeziometacarpal ($\boldsymbol{\theta}_{TMC1}$)	50 - 90	15	0
Metacarpophalangeal ($\boldsymbol{\theta}_{MCP}$)	75 - 80	0	0
Interphalangeal ($\boldsymbol{\theta}_{IP}$)	75 - 80	5 -10	0
INDEX			
Carpometacarpal ($\boldsymbol{\theta}_{CMC}$)	5	0	0
Metacarpophalangeal ($\boldsymbol{\theta}_{MCP1}$)	90	30 - 40	60
Metacarpophalangeal ($\boldsymbol{\theta}_{MCP2}$)	60		0 - 60
Proximal interphalangeal ($\boldsymbol{\theta}_{PIP}$)	110	0	0
Distal interphalangeal ($\boldsymbol{\theta}_{DIP}$)	80 - 90	5	0
MIDDLE			
Carpometacarpal ($\boldsymbol{\theta}_{CMC}$)	5	0	0
Metacarpophalangeal ($\boldsymbol{\theta}_{MCP1}$)	90	30 - 40	45
Metacarpophalangeal ($\boldsymbol{\theta}_{MCP2}$)	90	30 - 40	45
Proximal interphalangeal ($\boldsymbol{\theta}_{PIP}$)	110	0	0
Distal interphalangeal ($\boldsymbol{\theta}_{DIP}$)	80 - 90	5	0
RING			
Carpometacarpal ($\boldsymbol{\theta}_{CMC}$)	10	0	0
Metacarpophalangeal ($\boldsymbol{\theta}_{MCP1}$)	90	30 - 40	45
Metacarpophalangeal ($\boldsymbol{\theta}_{MCP2}$)	90	30 - 40	45

Proximal interphalangeal ($\boldsymbol{\theta}_{PIP}$)	120	0	0
Distal interphalangeal ($\boldsymbol{\theta}_{DIP}$)	80 - 90	5	0
LITTLE			
Carpometacarpal ($\boldsymbol{\theta}_{CMC}$)	15	0	0
Metacarpophalangeal ($\boldsymbol{\theta}_{MCP1}$)	90	30 - 40	50
Metacarpophalangeal ($\boldsymbol{\theta}_{MCP2}$)	90	30 - 40	50
Proximal interphalangeal ($\boldsymbol{\theta}_{PIP}$)	135	0	0
Distal interphalangeal ($\boldsymbol{\theta}_{DIP}$)	90	5	0

Table 3.4: Fingers' joint capabilities, adapted from [63].

Respecting those constraints, it is possible to determine a set of joint angles that is adequate for the fingertip to reach a specific pose in the space. The matrix that defines the pose of the fingertip with respect to the palm reference frame, $Q_{fingertip/palm,}$ supports the computation of the joints' angles for a specific finger configuration, and is formulated as follows:

$$Q_{fingertip/palm} = \begin{matrix} X_X & Y_X & Z_X & P_X \\ X_Y & Y_Y & Z_Y & P_Y \\ X_Z & Y_Z & Z_Z & P_Z \\ 0 & 0 & 0 & 1 \end{matrix} \tag{3.25}$$

The matrix, $Q_{fingertip/palm}$, is experimentally estimated from a frame imaging the hand and extracted from a video sequence of the hand movement, as will be detailed in Chapter 4. As there are two different configurations for fingers: the thumb and the other fingers, two general solutions are developed, according to the type of finger.

3.3.4 General inverse kinematic solution for the thumb

The resolution of the inverse kinematic problem involves obtaining the required joints values ($\theta_{TMC0}, \theta_{TMC1}, \theta_{MCP}, \theta_{IP}$) for a given desired end effector (fingertip)

position and orientation. To obtain the general expression of the solution of each angle, we solved the eq.(3.26).

$$\begin{matrix} cos\theta_{TMC0}\,cos\delta & -cos\theta_{TMC0}\,sin\delta & sin\theta_{TMC0} & cos\theta_{TMC0}\;L_1\,cos\delta + L_2\,cos\beta + L_3\,cos\theta_{TMC1} \\ sin\theta_{TMC0}cos\delta & -sin\theta_{TMC0}\,sin\delta & -cos\theta_{TMC0} & sin\theta_{TMC0}\;L_1\,cos\delta + L_2\,cos\beta + L_3\,cos\theta_{TMC1} \\ sin\delta & cos\delta & 0 & L_1\,sin\delta + L_2\,sin\beta + L_3\,sin\theta_{TMC1} \\ 0 & 0 & 0 & 1 \end{matrix} = \begin{matrix} X_X & Y_X & Z_X & P_X \\ X_Y & Y_Y & Z_Y & P_Y \\ X_Z & Y_Z & Z_Z & P_Z \\ 0 & 0 & 0 & 1 \end{matrix} \quad (3.26)$$

where $\begin{matrix} \delta = \theta_{TMC1}+\theta_{MCP}+\theta_{IP} \\ \beta = \theta_{TMC1} + \theta_{MCP} \end{matrix}$ (3.27)

By identification between the two matrices, θ_{TMC0} can be defined as:

$$\theta_{TMC0} = acos(-Z_Y) \quad (3.28)$$

By taking Y_X, X_X, δ can be found as:

$$\delta = \text{atan}(\frac{-Y_X}{X_X}) \quad (3.29)$$

From eq.(3.26) by taking P_X and P_Y a system of two equations with two unknowns is obtained as:

$$\begin{matrix} L_2\,cos\theta_{TMC0}cos\beta + L_3\,cos\theta_{TMC0}cos\theta_{TMC1} = P_X - L_1 cos\delta cos\theta_{TMC0} \\ L_2\,sin\theta_{TMC0}cos\beta + L_3\,sin\theta_{TMC0}cos\theta_{TMC1} = P_Y - L_1 cos\delta sin\theta_{TMC0} \end{matrix} \quad (3.30)$$

Using the first equation of eq. (3.30), $cos\theta_{TMC1}$ is defined as:

$$cos\theta_{TMC1} = \frac{P_X - L_1 cos\delta cos\theta_{TMC0} - L_2\,cos\theta_{TMC0}cos\beta}{L_3\,cos\theta_{TMC0}} \quad (3.31)$$

Putting this value of $cos\theta_{TMC1}$ from eq.(3.31) in the second equation of eq.(3.30), β can be found as:

$$\beta = \text{acos}\left(\frac{P_Y - L_1 cos\delta sin\theta_{TMC0} - tan\theta_{TMC0} P_X + L_1 cos\delta sin\theta_{TMC0}}{L_1 sin\theta_{TMC0} - L_2 sin\theta_{TMC0}} \right) \quad (3.32)$$

As δ is known from eq. (3.29) and β from eq. (3.32), θ_{TMC1} and θ_{IP} can be expressed as:

$$\theta_{IP} = \delta - \beta \quad (3.33)$$

$$\theta_{TMC1} = \text{acos}\left(\frac{P_X - L_1 cos\delta cos\theta_{TMC0} - L_2 cos\theta_{TMC0} cos\beta}{L_3 cos\theta_{TMC0}} \right) \quad (3.34)$$

$$\theta_{MCP} = \beta - \theta_{TMC1} \quad (3.35)$$

Finally the general solution of the inverse kinematic for the thumb is given with equations (3.28), (3.33), (3.34) and (3.35). It can be summarized as:

$$General\ solution\ for\ the\ thumb =$$

$$\theta_{TMC0} = acos\ -Z_Y\ -180 \quad (offset\ mentioned\ in\ section\ 3.3.2)$$

$$\theta_{IP} = \delta - \beta$$

$$\theta_{TMC1} = \text{acos}\left(\frac{P_X - L_1 cos\delta cos\theta_{TMC0} - L_2 cos\theta_{TMC0} cos\beta}{L_3 cos\theta_{TMC0}} \right) \quad (3.36)$$

$$\theta_{MCP} = \beta - \theta_{TMC1}$$

3.3.5 Simplified inverse kinematic solution for the thumb

For this research project as it used a single camera, the depth information is not taken in account. For the inverse kinematic of the fingers, only a set of 3 angles is computed. For the thumb 3 out of 4 angles are found and for the rest of the fingers 3 out of 5 angles are found. In fact, with a 2D image collected from a single camera, one can find all the angles for which the rotation axes are parallel to the principal axis of the camera. Fig. 3.9 and Fig. 3.10 show the set of angles for the thumb and the rest of fingers

that the use of a single camera allows determine. An important factor to highlight in the development of this simplified kinematic model is that the base reference frame for the finger is no longer R_1 but rather R_2 for the thumb, and R_3 for the other fingers. This impacts the relationship that can be achieved and the formulation of the model when compared with eq.(3.5) for the thumb, and eq.(3.12) for the other fingers. However, it does not preempt the estimation of accessible fingers' joint angles as necessary for the application considered on RA monitoring.

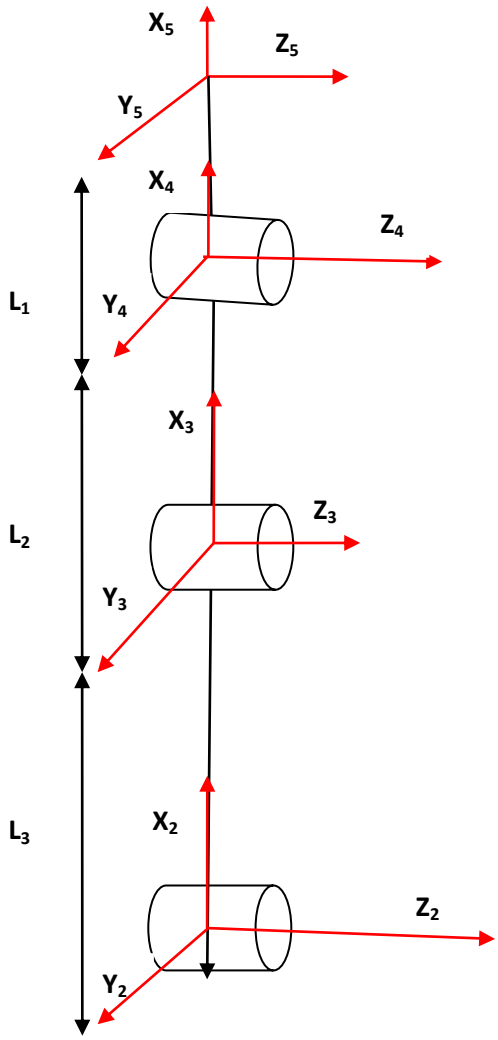

Fig. 3.9: Simplified kinematic model of the thumb.

As 3 angles out of 4 are considered in the implementation, the solution used for the thumb is expressed as:

$$\begin{matrix} \cos(\theta_2+\theta_3+\theta_4) & -\sin(\theta_2+\theta_3+\theta_4) & 0 & L_1\cos(\theta_2+\theta_3+\theta_4)+L_2\cos(\theta_2+\theta_3)+L_3\cos\theta_2 \\ \sin(\theta_2+\theta_3+\theta_4) & \cos(\theta_2+\theta_3+\theta_4) & 0 & L_1\sin(\theta_2+\theta_3+\theta_4)+L_2\sin(\theta_2+\theta_3)+L_3\sin\theta_2 \\ 0 & 0 & 1 & 0 \\ 0 & 0 & 0 & 1 \end{matrix} = \begin{matrix} X_X & Y_X & Z_X & P_X \\ X_Y & Y_Y & Z_Y & P_Y \\ X_Z & Y_Z & Z_Z & P_Z \\ 0 & 0 & 0 & 1 \end{matrix} \quad (3.37)$$

where $$\begin{matrix} \theta_2 = \theta_{TMC1} \\ \theta_3 = \theta_{MCP} \\ \theta_4 = \theta_{IP} \end{matrix} \quad (3.38)$$

$$P_X - L_1 X_X - L_3\cos\theta_2 = L_2\cos(\theta_2+\theta_3) \quad (3.39)$$

$$P_Y - L_1 X_Y - L_3\sin\theta_2 = L_2\sin(\theta_2+\theta_3) \quad (3.40)$$

Let $$\begin{matrix} A = P_X - L_1 X_X \\ B = P_Y - L_1 X_Y \end{matrix} \quad (3.41)$$

Then eq.(3.39) and eq.(3.40) become:

$$(L_2\cos(\theta_2+\theta_3))^2 = (A - L_3\cos\theta_2)^2 \quad (3.42)$$

$$L_2\sin(\theta_2+\theta_3)^2 = (B - L_3\sin\theta_2)^2 \quad (3.43)$$

Developing and adding eq.(3.42) and eq.(3.43):

$$L_2{}^2 = A^2 - 2AL_3\cos\theta_2 - 2BL_3\sin\theta_2 + L_3{}^2 + B^2 \quad (3.44)$$

Organizing eq.(3.44) :

$$A\cos\theta_2 + B\sin\theta_2 = \frac{L_3{}^2 - L_2{}^2 + A^2 + B^2}{2L_3} \quad (3.45)$$

Applying the trigonometric relation:

$$A\cos\theta_x + B\sin\theta_x = \frac{A\cos(\theta_x-\alpha)}{cos\alpha} \quad \text{with } tan\alpha = \frac{B}{A} \tag{3.46}$$

Applying eq.(3.46) to eq.(3.45) :

$$\theta_2 = \text{acos } \frac{(A^2+B^2+{L_3}^2-{L_2}^2)cos\omega}{2AL_3} - \omega \quad \text{with } \omega = \text{atan}(\frac{B}{A}) \tag{3.47}$$

From eq.(3.37):

$$\theta_3 + \theta_4 = \text{atan } \frac{X_Y}{X_X} - \theta_2 \tag{3.48}$$

From eq.(3.39) and eq.(3.40):

$$\begin{aligned} \cos(\theta_2 + \theta_3) &= \frac{A - L_3\cos\theta_2}{L_2} \\ \sin(\theta_2 + \theta_3) &= \frac{B - L_3\sin\theta_2}{L_2} \end{aligned} \tag{3.49}$$

Then:

$$\theta_3 = \text{atan } \frac{B - L_3\sin\theta_2}{A - L_3\cos\theta_2} - \theta_2 \tag{3.50}$$

From eq.(3.48):

$$\theta_4 = \text{atan } \frac{X_Y}{X_X} - \theta_2 - \theta_3 \tag{3.51}$$

The simplified inverse kinematic solution used for the thumb is then:

$$Simplified\ solution\ for\ the\ thumb = \begin{aligned} \theta_{TMC1} &= \text{acos } \frac{(A^2+B^2+{L_3}^2-{L_3}^2)cos\omega}{2AL_3} - \omega \\ \theta_{MCP} &= \text{atan } \frac{B - L_3\sin\theta_2}{A - L_3\cos\theta_2} - \theta_2 \\ \theta_{IP} &= \text{atan } \frac{X_Y}{X_X} - \theta_2 - \theta_3 \end{aligned} \tag{3.52}$$

3.3.6 General inverse kinematic solution for all fingers except the thumb

For the other four fingers, the solution to the inverse kinematic model proceeds in a similar way. However, the resulting expressions for (θ_{CMC},θ_{MCP1}, θ_{MCP2}, θ_{PIP}, θ_{DIP}) are slightly different, and take the following form:

Using the matrix obtained for all other fingers, eq. (3.12), the identification gives:

$$\begin{matrix} \partial_X & \beta_X & \gamma_X & \rho_X \\ \partial_Y & \beta_Y & \gamma_Y & \rho_Y \\ \partial_Z & \beta_Z & \gamma_Z & \rho_Z \\ 0 & 0 & 0 & 1 \end{matrix} = \begin{matrix} X_X & Y_X & Z_X & P_X \\ X_Y & Y_Y & Z_Y & P_Y \\ X_Z & Y_Z & Z_Z & P_Z \\ 0 & 0 & 0 & 1 \end{matrix} \quad (3.53)$$

From identification of Z_x, Z_y, eq. (3.19) and eq.(3.20),θ_{CMC} can be expressed as:

$$\theta_{CMC} = atan(\frac{-Z_y}{Z_x}) \quad (3.54)$$

where $Z_x \neq 0$

Using the value of Z_z and eq. (3.21), θ_{MCP1}can be defined as:

$$\theta_{MCP1} = acos\ -Z_z \quad (3.55)$$

Using eq. (3.15) and eq. (3.18), then:

$$\theta_{DIP} + \theta_{PIP} + \theta_{MCP2} = atan\ \frac{-Y_Z}{X_Z} = w \quad (3.56)$$

From eq.(3.24) $cos\theta_{MCP2}$ can be expressed as:

$$cos\theta_{MCP2} = \frac{P_Z - sin\theta_{MCP1}(L_6 sos\, w + L_5 \cos\ \theta_{PIP} + \theta_{MCP2})}{L_4} \quad (3.57)$$

Using eq. (3.57) in eq. (3.23) $\theta_{MCP2} + \theta_{PIP}$ is:

$$\theta_{MCP2} + \theta_{PIP} = acos\ \frac{P_Z}{L_5 - L_5 cos\theta_{MCP1}}(\frac{P_X + P_Z\, cotan\theta_{MCP14}}{sin\theta_{CMC} cos\theta_{MCP1}} - L_6 cosw - P_Z - L_6 sin\theta_{MCP1} cosw) \quad (3.58)$$

From eq. (3.57) θ_{MCP2} is deducted as:

$$\theta_{MCP2} = \text{acos}(\frac{P_Z - sin\theta_{MCP1}(\ L_6 cos\ w + L_5 \cos\ \theta_{PIP} + \theta_{MCP2}\ )}{L_4}) \tag{3.59}$$

From eq.(3.56) knowing eq.(3.58) θ_{DIP} is:

$$\theta_{DIP} = \ atan\ \frac{-Y_Z}{X_Z}\ - (\theta_{MCP2} + \ \theta_{PIP}) \tag{3.60}$$

Then θ_{PIP} is :

$$\theta_{PIP} = \ atan\ \frac{-Y_Z}{X_Z}\ - (\theta_{MCP2} + \ \theta_{DIP}) \tag{3.61}$$

Finally, the general inverse kinematic solution for all fingers except the thumb is expressed as follows:

$$\begin{gathered} General\ solution\ for\ all\ fingers\ except\ the\ thumb = \\ \theta_{CMC} = atan(\frac{-Z_Y}{Z_X}) \\ \theta_{MCP1} = acos\ -Z_z\ -180 \qquad (offset\ as\ in\ section\ 3.3.2) \\ \theta_{DIP} = atan\ \frac{-Y_Z}{X_Z}\ - (\theta_{MCP2} + \theta_{PIP}) \\ \theta_{MCP2} = \text{acos}\ \frac{P_Z - sin\theta_{MCP1}(\ L_6 cos\ w + L_5 \cos\ \theta_{PIP} + \theta_{MCP2}\ )}{L_4}\ -180 \quad (offset\ as\ in\ section\ 3.3.2) \\ \theta_{PIP} = \ atan\ \frac{-Y_Z}{X_Z}\ - (\theta_{MCP2} + \ \theta_{DIP}) \end{gathered} \tag{3.62}$$

3.3.7 Simplified inverse kinematic solution for all fingers except the thumb

As in this project only one camera is used, the set of 5 angles is reduced to three visible angles. Therefore a simplified version of the inverse kinematic is proposed along with a simplified version of the kinematic model (Fig. 3.10).

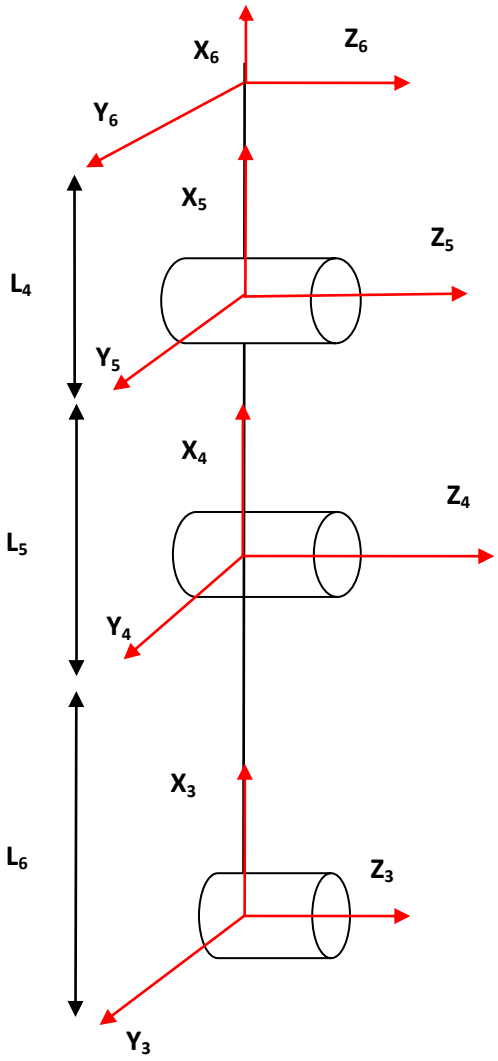

Fig. 3.10: Simplified kinematic model of all fingers except the thumb.

Applying the same principle as for the complete fingers model, the solution for the simplified kinematic model becomes:

$$\begin{matrix}\cos(\theta_3+\theta_4+\theta_5) & -\sin(\theta_3+\theta_4+\theta_5) & 0 & L_4cos(\theta_3+\theta_4+\theta_5)+L_5\cos(\theta_3+\theta_4)+L_6\cos\theta_3 \\ \sin(\theta_3+\theta_4+\theta_5) & \cos(\theta_3+\theta_4+\theta_5) & 0 & L_4sin(\theta_3+\theta_4+\theta_5)+L_5\sin(\theta_3+\theta_4)+L_6\sin\theta_3 \\ 0 & 0 & 1 & 0 \\ 0 & 0 & 0 & 1\end{matrix} = \begin{matrix}X_X & Y_X & Z_X & P_X \\ X_Y & Y_Y & Z_Y & P_Y \\ X_Z & Y_Z & Z_Z & P_Z \\ 0 & 0 & 0 & 1\end{matrix} \quad (3.63)$$

where $$\begin{matrix}\theta_3=\theta_{MCP2} \\ \theta_4=\theta_{PIP} \\ \theta_5=\theta_{DIP}\end{matrix} \quad (3.64)$$

$$P_X - L_4X_X - L_6\cos\theta_3 = L_5\cos(\theta_3+\theta_4) \quad (3.65)$$

$$P_Y - L_4X_Y - L_6\sin\theta_3 = L_5\sin(\theta_3+\theta_4) \quad (3.66)$$

Let $$\begin{matrix}A' = P_X - L_4X_X \\ B' = P_Y - L_4X_Y\end{matrix} \quad (3.67)$$

Then eq.(3.65) and eq.(3.66) become:

$$(L_5\cos(\theta_3+\theta_4))^2 = (A' - L_6\cos\theta_3)^2 \quad (3.68)$$

$$L_5\sin(\theta_3+\theta_4)^2 = (B' - L_6\sin\theta_3)^2 \quad (3.69)$$

Developing and adding eq.(3.68) and eq.(3.69):

$$L_5{}^2 = A'^2 - 2A'L_6\cos\theta_3 - 2B'L_6\sin\theta_3 + L_6{}^2 + B'^2 \quad (3.70)$$

Organizing eq.(3.70) :

$$A'\cos\theta_3 + B'\sin\theta_3 = \frac{L_6{}^2 - L_5{}^2 + A'^2 + B'^2}{2L_6} \quad (3.71)$$

Applying the trigonometric relation:

$$A'\cos\theta_x + B'\sin\theta_x = \frac{A'\cos(\theta_x-\alpha)}{cos\alpha} \quad \text{with } tan\alpha = \frac{B'}{A'} \quad (3.72)$$

Applying eq.(3.72) to eq.(3.71) :

$$\theta_3 = \text{acos}\ \frac{(A\prime^2+B\prime^2+{L_6}^2-{L_5}^2)cos\omega}{2A\prime L_6} - \omega \qquad \text{with } \omega = \text{atan}(\frac{B\prime}{A\prime}) \tag{3.73}$$

From eq.(3.63):

$$\theta_4 + \theta_5 = \text{atan}\ \frac{X_Y}{X_X} - \theta_3 \tag{3.74}$$

From eq.(3.65) and eq.(3.66):

$$\begin{aligned} \cos(\theta_3 + \theta_4) &= \frac{A\prime - L_6\cos\theta_3}{L_5} \\ \sin(\theta_3 + \theta_4) &= \frac{B' - L_6\sin\theta_3}{L_5} \end{aligned} \tag{3.75}$$

Then:

$$\theta_4 = \text{atan}\ \frac{B\prime - L_6\sin\theta_3}{A\prime - L_6\cos\theta_3} - \theta_3 \tag{3.76}$$

From eq.(3.74):

$$\theta_5 = \text{atan}\ \frac{X_Y}{X_X} - \theta_3 - \theta_4 \tag{3.77}$$

The simplified inverse kinematic solution for all fingers except the thumb used in this thesis is then:

$$\begin{aligned} &Simplified\ solution\ for\ all\ fingers\ except\ the\ thumb = \\ \theta_{MCP2} &= \text{acos}\ \frac{(A'^2+B'^2+{L_6}^2-{L_5}^2)cos\omega}{2A'L_6} - \omega \\ \theta_{PIP} &= \text{atan}\ \frac{B'-L_6\sin\theta_2}{A'-L_6\cos\theta_2} - \theta_{MCP2} \\ \theta_{DIP} &= \text{atan}\ \frac{X_Y}{X_X} - \theta_{MCP2} - \theta_{PIP} \end{aligned} \tag{3.78}$$

3.4 Kinematics of the human arm

The kinematic model developed for fingers in the previous sections is revisited and extended to the entire human arm, from shoulder to wrist. This allows the proposed diagnostic system to extend its measurement capability to other joints that are known for being prone to developing RA problems, as reported in section 2.5.

The kinematic model of the human arm is a complex one, and several researchers have proposed various mathematic models. Gams and Lenarcic [64] proposed a definition as a four segments serial mechanism with ten DoFs, involving the shoulder girdle, the upper arm, the forearm and the hand. Because of its high complexity and the large number of DoFs, the kinematic model of the hand was studied separately. Alternatively, Chan *et al.* [65] proposed a simple model with eight DoFs with three segments. The solution that we proposed in this study is based on seven DoFs that capture the more significant motion capabilities of the human arm.

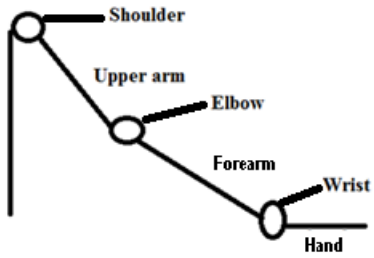

Fig. 3.11: Proposed model of human arm structure.

The proposed model is close to the reality of the human arm with its seven DoFs kinematic chain which is composed of the shoulder girdle, the upper arm, the forearm and the hand (Fig. 3.11). Fig. 3.12 and Fig. 3.13 illustrate the proposed formalism of the human arm model. This model respects all the constraints of the human arm (Table 3.6) and aims to be close to its kinematic structure (Fig. 3.13 and Table 3.5). The numbers 1, 2 and 3 show the different articulations of the arm that are defined in Fig. 3.12 in terms of

their structure. From Fig. 3.13, one can find the number of DoFs of each articulation. The location represented by number 1 is the root of the shoulder as illustrated in Fig. 3.13. Number 1 is also the shoulder joint with 3 DoFs, number 2 is the elbow joint with one DoF and number 3 is the wrist joint with 3 DoFs. The total number of DoFs is 7 for the entire arm as illustrated in Table 3.5.

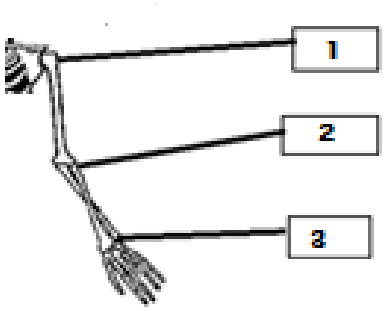

Fig. 3.12: Mechanism of human arm skeleton.

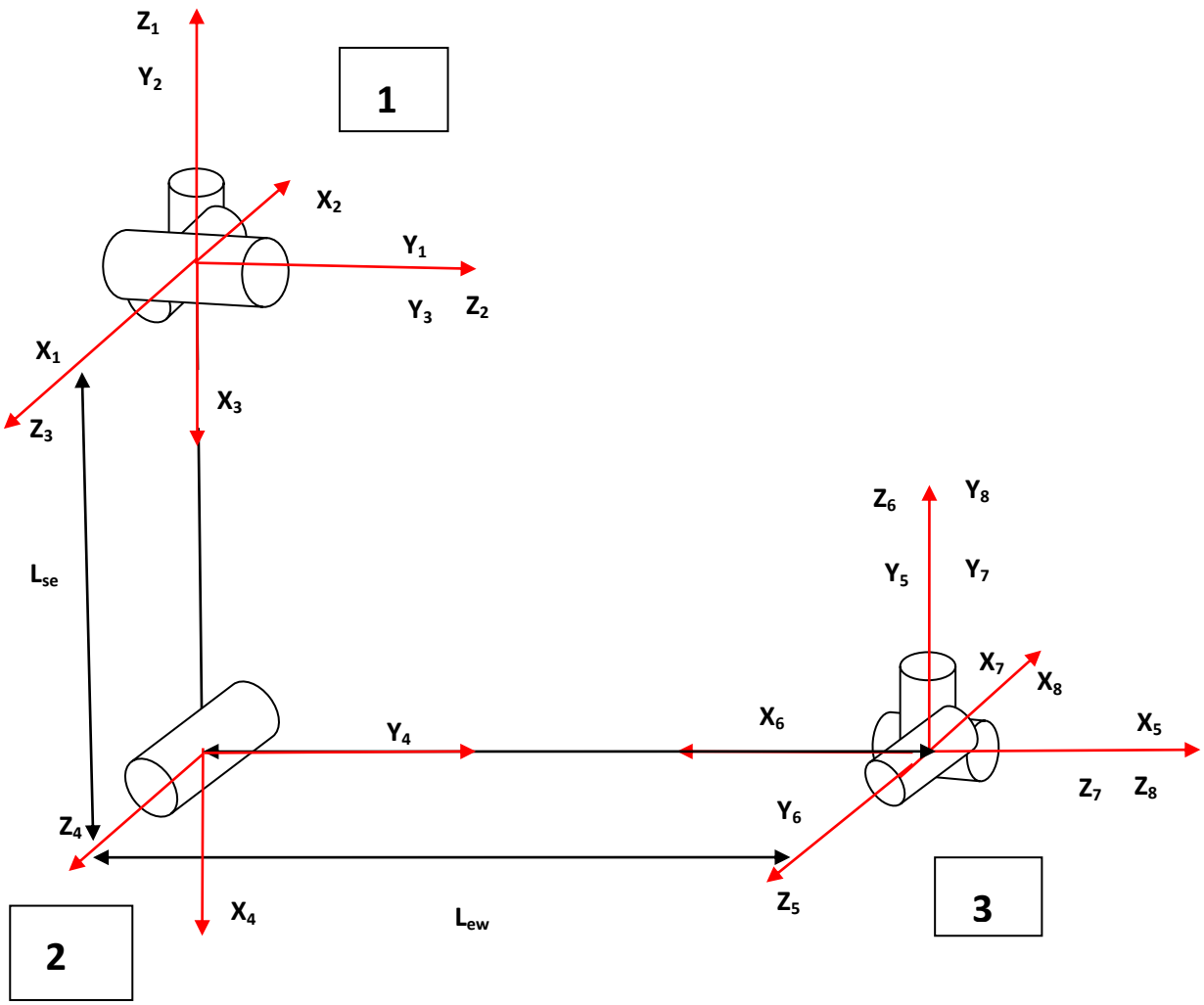

Fig. 3.13: Proposed kinematic model of the human arm.

The reference frame is R_1 attached to the root of the shoulder (Fig. 3.13). As shown in the D-H parameter table (Table 3.5), each θ_i corresponds to a particular angle of one of three articulations of the human arm [66]. The last column of Table 3.5 shows that there are three DoFs for the shoulder, one DoF for the elbow and finally three DoFs for the wrist. Then every θ_i corresponds to each joint of the human arm as follows: θ_1 ($\theta_{shoulder1}$), θ_2 ($\theta_{shoulder2}$), θ_3 ($\theta_{shoulder3}$), θ_4 (θ_{elbow}), θ_5 (θ_{wrist1}), θ_6 (θ_{wrist2}), and θ_7 (θ_{wrist3}).

Joint	$\mathbf{d_i}$	$\mathbf{l_i}$	$\boldsymbol{\alpha_i}$	$\boldsymbol{\theta_i}$	**Correspondence**
1	0	0	$\pi/2$	θ_1	Shoulder1
2	0	0	$\pi/2$	θ_2	Shoulder2
3	0	L_{se}	0	θ_3	Shoulder3
4	0	L_{ew}	0	θ_4	Elbow
5	0	0	$\pi/2$	θ_5	Wrist1
6	0	0	$\pi/2$	θ_6	Wrist2
7	0	0	0	θ_7	Wrist3

Table 3.5: D-H parameters table of the proposed human arm model.

There are some physical constraints of the human arm articulations as shown in Fig. 3.14 and Table 3.6. Those constraints were established after several experiments on volunteers to determine the ranges. These represent the result of the measurement on the 2D image of the arm angles in its minimum bending position for each arm articulation. In Table 3.5, the constant offsets of 90 degrees between X_4, X_5 and -90 degrees between X_2, X_3 and X_6, X_7 are not included in this table because they would be subtracted from the computed values of θ_2, θ_4 and θ_6.

In fact, the angles measured in 2D in this project are the ones for which the rotation axes are parallel to the principal axis of the camera. The set of rotation axes considered here are Z_3 for the shoulder, Z_4 for the elbow, and Z_5 for the wrist. Therefore, the set of the angles of the arm will be simplified to ($\theta_{shoulder}, \theta_{Elbow}, \theta_{Wrist}$) which correspond in Fig. 3.13 and Table 3.5 to ($\theta_3, \theta_4, \theta_5$). Then for the inverse kinematics of the human arm, instead of finding a set of seven angles, the problem is simplified to finding the reduced set of three angles as shown in Fig. 3.14.

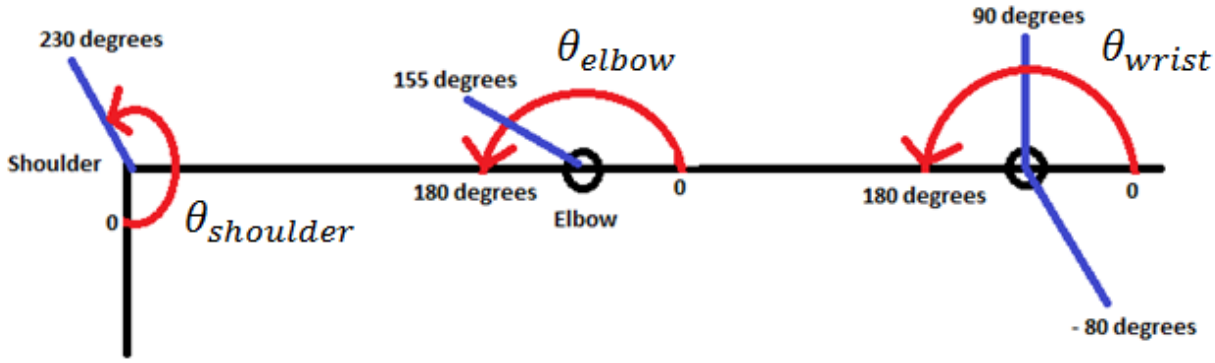

Fig. 3.14: Zero position of the arm's joints with movements' capabilities.

Joint	**Range of bending and extending in degrees**
Shoulder ($\theta_{shoulder}$)	0 to 230
Elbow (θ_{elbow})	0 to 155
Wrist (θ_{Wrist})	- 80 to 90

Table 3.6: Average healthy person arm's joint capabilities.

For this research purpose, one determines the minimum bending capabilities of the subject for those three angles. The kinematics in Fig. 3.13 and Fig. 3.14 give the minimum bending of $\theta_{shoulder}$ ($\theta_{shoulder}$ is smaller when the subject is able to bend properly the shoulder angle). Yet, it is not the case for θ_{Elbow} and θ_{Wrist}. To have the same principle for elbow and wrist angles, one needs to find the minimum bending of those angles as defined in Fig. 3.15. The correspondence between the minimum bending of each angle and their values is defined in Table 3.7.

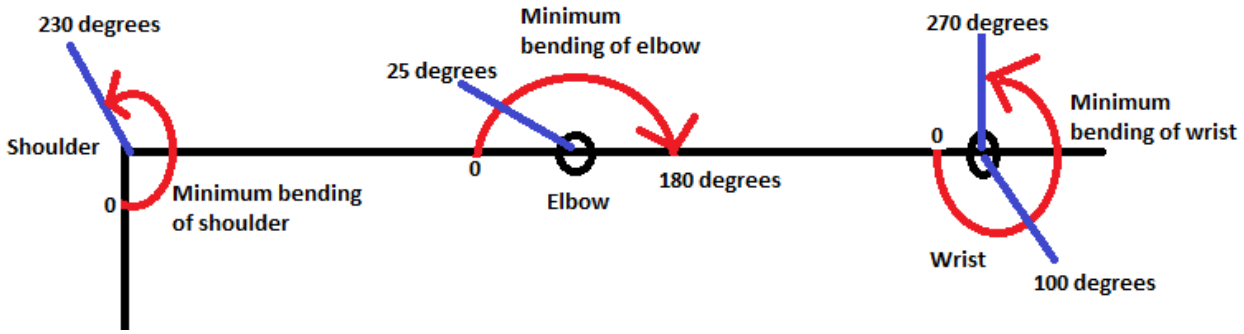

Fig. 3.15: Minimum bending capabilities used in this research.

Angles definition	Correspondence	Range of bending and extending in degrees
Minimum bending of shoulder	$\theta_{shoulder}$	0 to 230
Minimum bending of elbow	$\pi - \theta_{elbow}$	25 to 180
Minimum bending of wrist	$\pi + \theta_{wrist}$	100 to 270

Table 3.7: Minimum bending capabilities computed in this research.

Even though the normal human bending capability of $\theta_{shoulder}$ is between 0 and 230 degrees, in the movement asked to the subject in this research the value expected for this angle will be mostly between 70 and 85 degrees. The reason for this expected high value is link to the kind of the movement asked to the subject. The subject is asked to open widely the arms before performing the bending movements of the three angles starting by the wrist then the elbow and finally the shoulder according to its capabilities. All those angles have to be bent at the same time and they affect each other value. As the RA patient has difficulties to perform extension of triceps and curl/contraction of biceps, bending the elbow articulation will help to measure how the subject is affected. The same principle is applied for the wrist angle by its flexion and

extension. In fact, the muscles that intervene in shoulder bending when the arms are widely opened are the same that are used for bending elbow (biceps and triceps). As the elbow is in its maximum bending (extension of triceps and contraction of biceps) the shoulder angle will not be able to move along the body as expected (contraction of triceps and extension of biceps) [18]. Its value depends on how the subject is able to bend its elbow joint. For this reason, the three angles values are taken in consideration to measure the subject's arms bending capabilities.

The corresponding A_i matrices that embed the D-H parameters defined above (Table 3.5) are defined as:

$$A_1 = \begin{matrix} cos\theta_1 & 0 & sin\theta_1 & 0 \\ sin\theta_1 & 0 & -cos\theta_1 & 0 \\ 0 & 1 & 0 & 0 \\ 0 & 0 & 0 & 1 \end{matrix} \tag{3.79}$$

$$A_2 = \begin{matrix} cos\theta_2 & 0 & sin\theta_2 & 0 \\ sin\theta_2 & 0 & -cos\theta_2 & 0 \\ 0 & 1 & 0 & 0 \\ 0 & 0 & 0 & 1 \end{matrix} \tag{3.80}$$

$$A_3 = \begin{matrix} cos\theta_3 & -sin\theta_3 & 0 & L_{se}cos\theta_3 \\ sin\theta_3 & cos\theta_3 & 0 & L_{se}sin\theta_3 \\ 0 & 0 & 1 & 0 \\ 0 & 0 & 0 & 1 \end{matrix} \tag{3.81}$$

$$A_4 = \begin{matrix} cos\theta_4 & -sin\theta_4 & 0 & L_{ew}cos\theta_4 \\ sin\theta_4 & cos\theta_4 & 0 & L_{ew}sin\theta_4 \\ 0 & 0 & 1 & 0 \\ 0 & 0 & 0 & 1 \end{matrix} \tag{3.82}$$

$$A_5 = \begin{matrix} cos\theta_5 & 0 & sin\theta_5 & 0 \\ sin\theta_5 & 0 & -cos\theta_5 & 0 \\ 0 & 1 & 0 & 0 \\ 0 & 0 & 0 & 1 \end{matrix} \quad (3.83)$$

$$A_6 = \begin{matrix} cos\theta_6 & 0 & sin\theta_6 & 0 \\ sin\theta_6 & 0 & -cos\theta_6 & 0 \\ 0 & 1 & 0 & 0 \\ 0 & 0 & 0 & 1 \end{matrix} \quad (3.84)$$

$$A_7 = \begin{matrix} cos\theta_7 & -sin\theta_7 & 0 & 0 \\ sin\theta_7 & cos\theta_7 & 0 & 0 \\ 0 & 0 & 1 & 0 \\ 0 & 0 & 0 & 1 \end{matrix} \quad (3.85)$$

3.4.1 Forward kinematics

In accordance with the mechanism model presented in Fig. 3.13 that represents the skeleton structure of the human arm, the spatial relationship between the end effector, here associated to the wrist R_8, with respect to the shoulder reference frame R_1, provides the definition for the forward kinematic model of the human arm which is defined as follows:

$$Q_{wrist/shoulder} = A_1 * A_2 * A_3 * A_4 * A_5 * A_6 * A_7 = \begin{matrix} \partial_X & \beta_X & \gamma_X & \rho_X \\ \partial_Y & \beta_Y & \gamma_Y & \rho_Y \\ \partial_Z & \beta_Z & \gamma_Z & \rho_Z \\ 0 & 0 & 0 & 1 \end{matrix} \quad (3.86)$$

where :

$$\partial_X = (cos\theta_5 cos\theta_6 cos\theta_7 + sin\theta_5 sin\theta_7)U_1 + (sin\theta_6 cos\theta_7)V_1 + (sin\theta_5 cos\theta_6 cos\theta_7 - cos\theta_5 sin\theta_7)W_1 \quad (3.87)$$

$$\beta_X = \ cos\theta_5 cos\theta_6 sin\theta_7 - sin\theta_7 sin\theta_5 \ U_1 + \ \ sin\theta_6 sin\theta_7 \ V_1 + \ (sin\theta_5 cos\theta_6 sin\theta_7 + cos\theta_5 cos\theta_7) W_1 \quad (3.88)$$

$$\gamma_X = \ -cos\theta_5 sin\theta_6 \ U_1 + \ cos\theta_6 \ V_1 + (-sin\theta_5 sin\theta_6) W_1 \quad (3.89)$$

with:

$$U_1 = cos\theta_1 cos\theta_2 \cos(\theta_3+\theta_4) + sin\theta_1 \sin(\theta_3+\theta_4) \quad (3.90)$$

$$V_1 = -cos\theta_1 cos\theta_2 \sin(\theta_3 + \theta_4) + \ sin\theta_1 \cos(\theta_3+ \theta_4) \quad (3.91)$$

$$W_1 = \ cos\theta_1 sin\theta_2 \quad (3.92)$$

$$\partial_Y = (cos\theta_5 cos\theta_6 cos\theta_7 + \ sin\theta_5 sin\theta_7) U_2 + \ (sin\theta_6 cos\theta_7) V_2 \ + \ (sin\theta_5 cos\theta_6 cos\theta_7 - cos\theta_5 sin\theta_7) W_2 \quad (3.93)$$

$$\beta_Y = \ cos\theta_5 cos\theta_6 sin\theta_7 - sin\theta_7 sin\theta_5 \ U_2 + \ \ sin\theta_6 sin\theta_7 \ V_2 + \ (sin\theta_5 cos\theta_6 sin\theta_7 + cos\theta_5 cos\theta_7) W_2 \quad (3.94)$$

$$\gamma_Y = \ -cos\theta_5 sin\theta_6 \ U_2 + \ cos\theta_6 \ V_2 + (-sin\theta_5 sin\theta_6) W_2 \quad (3.95)$$

with:

$$U_2 = \ sin\theta_1 cos\theta_2 \cos(\theta_3+\theta_4) - cos\theta_1 \sin(\theta_3+\theta_4) \quad (3.96)$$

$$V_2 = \ -sin\theta_1 cos\theta_2 \sin(\theta_3+\theta_4) - cos\theta_1 \cos(\theta_3+\theta_4) \quad (3.97)$$

$$W_2 = \ sin\theta_1 sin\theta_2 \quad (3.98)$$

$$\partial_Z = (cos\theta_5 cos\theta_6 cos\theta_7 + \ sin\theta_5 sin\theta_7) U_3 + (sin\theta_6 cos\theta_7) V_3 \ + \ (sin\theta_5 cos\theta_6 cos\theta_7 - cos\theta_5 sin\theta_7) W_3 \quad (3.99)$$

$$\beta_Z = \ cos\theta_5 cos\theta_6 sin\theta_7 - sin\theta_7 sin\theta_5 \ U_3 + \ \ sin\theta_6 sin\theta_7 \ V_3 + \ (sin\theta_5 cos\theta_6 sin\theta_7 + cos\theta_5 cos\theta_7) W_3 \quad (3.100)$$

$$\gamma_Z = \ -cos\theta_5 sin\theta_6 \ U_3 + \ cos\theta_6 \ V_3 + (-sin\theta_5 sin\theta_6) W_3 \quad (3.101)$$

with:

$$U_3 = sin\theta_2 \cos(\theta_3+\theta_4) \quad (3.102)$$

$$V_3 = -sin\theta_2 \sin(\theta_3+\theta_4) \quad (3.103)$$

$$W_3 = -cos\theta_2 \quad (3.104)$$

$$\rho_X = L_{ew}\ cos\theta_1 cos\theta_2 \cos(\theta_3+\theta_4) + sin\theta_1 \sin(\theta_3+\theta_4)\ + L_{se}(cos\theta_1 cos\theta_2 cos\theta_3 + cos\theta_3) \quad (3.105)$$

$$\rho_Y = L_{ew}\ sin\theta_1 cos\theta_2 \sin(\theta_3+\theta_4) - cos\theta_1 \sin(\theta_3+\theta_4)\ + L_{se}(sin\theta_1 cos\theta_2 cos\theta_3 - cos\theta_3) \quad (3.106)$$

$$\rho_Z = L_{ew} sin\theta_2 \sin(\theta_3+\theta_4) + L_{se} sin\theta_2 cos\theta_3 \quad (3.107)$$

3.4.2 Inverse kinematics

A solution to the inverse kinematic model that places in evidence the set of seven angles of the joints, given a desired pose for the wrist with respect to the shoulder joints, can be achieved. However, to make the solution easier, and given the decision made earlier to operate from a single view (lateral) of the human arm, the kinematic model as defined in Fig. 3.13 can be simplified as follows (Fig. 3.16):

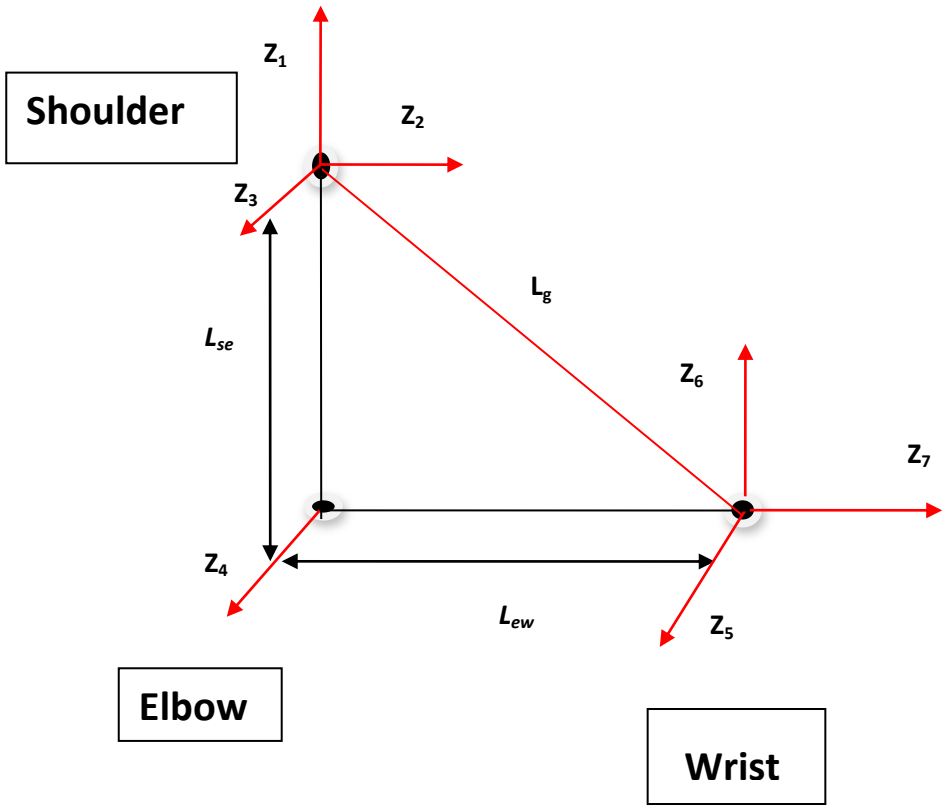

Fig. 3.16: Simplified kinematics of the human arm.

Using the coordinates in the image frame, L_g (the distance between the shoulder and the wrist) can be found using the coordinates of the shoulder point ($x_{shoulder}$, $y_{shoulder}$) and that of the wrist point (x_{wrist}, y_{wrist}) then:

$$L_g = \overline{(x_{shoulder} - x_{wrist})^2 + (y_{shoulder} - y_{wrist})^2}. \quad (3.108)$$

The trigonometric identities provide another way to express L_g:

$$L_g^2 = L_{ew}^2 + L_{se}^2 - 2L_{ew}L_{se}\cos(\pi - \theta_{elbow}) \quad (3.109)$$

Then, $\pi - \theta_{elbow} = acos \ \frac{L_{se}^2 + L_{ew}^2 - L_g^2}{2\, L_{ew} L_{se}}$ (3.110)

The others angles are extracted from the 2D images of the subject arms on their minimum bending. For that, there is no need for finding all the angles of the rotation axes. One can find only the angles for which rotation axes are parallel to the principal axis of the camera. For each subject, three angles are therefore considered: $\theta_{shoulder}$, $\pi - \theta_{elbow}$ and $\pi + \theta_{wrist}$ as explained in the previous sections. The proposed computational process for finding $\pi - \theta_{elbow}$ and $\pi + \theta_{wrist}$ will be detailed in section 4.5 along with the RA classification using arm angle estimation.

When the pose of the arm is extracted by image processing over a frame of a video sequence, the joint angles are computed and one can therefore estimate the motion of the subject from frame to frame. Under the limitation of use of a single 2D view of the arm, the movement is represented as a simplified series of three angular values $\theta_{shoulder}$, $\pi - \theta_{elbow}$, $\pi + \theta_{wrist}$ which can later serve to monitor the movement capabilities of a patient, and eventually determine improvement or degradation of physical condition over the course of a treatment for RA.

All the equations developed in this chapter, that define kinematic models of the human hand and arm, represent a contribution of the present thesis. They were tested and validated by comparing their predicted theoretical values with the image processing results, iteratively, until the estimates from the implemented simplified kinematic model of fingers and arm match the ones obttained from the image processing algorithm.

Summary

One of the objectives of the present research is to quantitatively measure the motion capabilities of the human hand and arm from a sequence of images collected on a subject performing a predefined sequence of movements. The approach adopted here

consists in merging the kinematic information with the image processing stage in order to build a motion capability estimation tool. This chapter introduced the kinematic models of the human hand and arm. Based on these models and on the physical constraints imposed on the rotation of the joints in the human body structure, one can determine the set of angles for the joints when provided with the pose of the fingertips or wrist, and the length measurements of the bones. One of the contributions of this research is the development of a kinematic model of the human hand and arm based on anatomical information. Another contribution is a strategy to merge that anatomical knowledge, represented in the form of kinematic information, with classical image processing techniques to build an efficient quantitative assessment resource for human hand and arm motion capabilities. The next chapter analyses the image processing methodology used for the research and details how kinematics get merged with image processing.

Chapter 4: Methodology and Analysis

4.1 Introduction

To measure the capabilities of bending and extending joints of a patient, this study examines three different methods applied to the arms and hands. The first method uses the Sum of Absolute Difference (SAD) between the video frames recording the gesture of opening and closing the hand on one side, and on the other side, a stretching and bending arm movement. In order to diagnose RA, it is important to be able to determine the capacity of a patient to bend the joints, especially those of the arms and hands. In the second method, the objective is to obtain as efficiently as possible the angles of important joints of the patient's arm from a set of digital images taken in different positions especially in that of bending and extension. Image processing will be used to determine the angles of different joints. From the filtered image and from the definite outline which we obtain, we shall be able to estimate the angle of the joint between two consecutive bones of the skeleton forming an articulation. The estimation of this angle will be compared to the angle of the same joint on a healthy subject. From the comparison, one is able to determine if the angle is smaller than normal. To diagnose RA, a table of comparison of different joints between a patient and a healthy person will be made. A classification according to the severity of RA will also be achieved by comparing the angles of the joints with the results obtained from an expert rheumatologist. The third strategy consists of using the Adaptive Rood Pattern Search algorithm [57] in order to estimate the motion of the patient's hands and arms. From the result of the average range of motion extracted from videos, one can estimate the relative motion capabilities of a patient. From that, it will be possible to estimate the level of severity for each patient case. That level of severity will also be compared to the

one obtained from the rheumatologist's evaluation to measure the efficiency of the method.

4.2 Methodology

To conduct this work, it was necessary to follow a procedure from the data collection to the result phase. The first steps followed the classical methodology for a scientific research involving human subjects, including the ethic approvals, the protocol definition (appendix C), the development of an information letter (appendix D) and of a consent form (appendix E). These documents were released in the two Canadian official languages: French and English. The steps are presented as part of the methodology used for this research.

4.2.1 Evaluation Methodology

Three approaches, each corresponding to a specific method as described in section 4.1, were experimented with for this study: skeletal pose based estimation; arm angles based estimation; and finally, block matching based on motion estimation. Knowing that the first visible signs of RA are perceived in the joints of the hands and limbs for more than sixty-six percent of the cases, as shown in Table 2.1, this study focuses on monitoring some of those joints: hands and arms. To be able to monitor the motion capabilities of the joints of the hands and arms, videos of both the right and left hands were taken with the hand opening and closing, quickly and slowly. From those videos, image processing estimates the level of motion capability of the subject. In the first part, from the processing of those videos, it is possible to judge if the subject shows signs of having of RA or not. In case where signs of RA are found, the second part determines the level of severity of the illness of the patient. A classification can then be made from the processing of the video, and that classification can be compared to the results obtained from the rheumatologist's tests. A table establishes the average of motion capabilities of a healthy subject, which corresponds to a low level of severity of illness in parallel with a specific motion capability of the subject. The video of the arms that is

taken will be used for another classification which will be compared also to the rheumatologist's assessment. It is required during the evaluation that the subject stretches and bends his arms both slowly and as quickly as he can. From the arms videos, the confirmation of the level of severity of the illness of the subject is achieved.

The setup of the test is simple: only a uniform background is required. In the laboratory, a black cloth is chosen as a uniform background to record the videos (Fig. 4.1). The uniform background helps to identify the moving pixels within the video frame and makes it possible to monitor only the movement of the patient.

Fig. 4.1: The setup with the uniform background.

The camera (PointGrey Flea 2 IEEE1394b firewire color camera) used for the data collection, as shown in Fig. 4.2, was set to work with a frame rate estimated at 38 fps. A resolution of 320x240 is used to reduce the computational cost when extracting features (in this study, the skeleton pose estimation). The lens used has a focal length of 3.5 mm so that it can be situated very close (as close as one foot) to the human limb that one is recording (here arm or hand). All the video sequences were recorded for about 40 seconds to ensure the uniformity of the processed videos.

The movements were recorded at the fastest speed that the subject can reach to evaluate the motion capabilities, as described for the first method in section 4.1. The same movements were recorded on their slowest version to facilitate the computation of the second method introduced also in section 4.1 based on angles estimation. The experience demonstrated that when performing a movement slowly, the subject is able to reach closer to the limits of bending and stretching on each articulation than when performing the same movement quickly.

Fig. 4.2: Camera used for data collection.

4.2.2 Recruitment of patients and volunteers

All patients were recruited from the Ottawa General Hospital, where their physician asked them to consider if they would participate in the study. As well, they were informed about the study by a letter of information (appendix D). A consent form (appendix E) was issued to them. They signed the form, and came to the laboratory for tests. The patient participants were already diagnosed with RA and were older than 19 years of age. They all were recruited by Dr. Karsh, rheumatologist at the Ottawa

General Hospital, with the necessary information for the study. Patients from both sexes were interested in participating in the study after receiving all information and the necessary consent forms (appendices D and E) that they signed in the language that they are using as their first language (French or English). Then they voluntarily contacted the student investigator to discuss the test and had the opportunity to ask all their questions concerning the research. The patient was free to set an appointment for the test. Patients signed the consent form before starting the test session. No images of the participants or personal information were shared with Carleton University or the University of Ottawa research team to ensure privacy. The criteria of exclusion from this research were either the patient was diagnosed with joint issues not related to RA, if the patient had recently suffered from any kind of trauma that affected joints, or if the patient had joint sepsis. Patients who agreed to participate in the research did not receive any compensation nor suffer any adverse effect in their quality of care. Overall, 13 patients participated in the study (10 females and 3 males aged between 20 and 55 years old).

The volunteers (considered here as normal subjects) for this study were informed by the same information letter, invited by the flyers (Appendix F) or through one meeting for explanation and the presentation of the research protocol (appendix C). The volunteers also agreed to participate in the study by signing the consent form and coming to the laboratory for the tests. The volunteers were older than 19 years of age and are from the University of Ottawa or Carleton University. None has been diagnosed with RA, or any issues of trauma, and are in good health without any symptoms similar to RA. They received the same forms and information about the research as the patient participants (appendices D and E). They voluntarily agreed to be involved in the research without compensation. The same principle for the privacy of their personal information that was used for the patients is applied to the volunteers. Overall, 10 volunteers participated in the study (6 females and 4 males aged between 20 and 40 years old).

4.2.3 Ethics approval and protocols

As mentioned in the methodology, a consent form, a letter of information and flyers were prepared such that each volunteer and patient involved in this research knew what this research was about and what their rights were.

For this research, the ethics boards of the three institutions involved, that are the Ottawa General Hospital Riverside campus, Carleton University and the University of Ottawa, approved the ethics clearance proposal under the name of "Severity of illness measures in rheumatoid arthritis from multi-spectral imaging". The specialist from the Ottawa General Hospital for this research is Dr. Jacob Karsh, rheumatologist for the Riverside Campus from where the patients were recruited for our tests. From the University of Ottawa and Carleton University, two professors, Pierre Payeur and Monique Frize, and the students were involved in the investigation.

Only videos of hands and arms gestures were taken for this project. There is no way to identify the subject from the videos. The videos have been stored on protected recordable media and on a secure computer. The data from physical tests have been stored in a separate database than those containing the videos of hands. Data are not publicly accessible. Only the researchers involved in the project have direct access to data.

Data (hands and arms videos) will be kept during five years for future reassessment, follow-up and review of the results. All sharing requests will be evaluated carefully. Data, if shared, will remain anonymous and confidential.

4.3 Definition of movements for motion and angle detection

To determine human motion capabilities and joint angles of the most affected joints by RA, we defined a set of movements that the subject needs to perform. Those movements help the proposed system to estimate motion and angles of some specifically selected joints. Six different movements were selected to achieve this goal as described in the following sections.

4.3.1 Open and close hand quickly

This movement allows the observation of the ability of the patient to move all the hand joints, knowing that these joints are the most affected ones by RA. The patient is first asked to perform this movement as quickly as possible, to estimate the maximum motion capacity that can be reached. Through a video sequence of this movement (Fig. 4.3), one can estimate the motion capabilities of the hand joints of the patient. In this video sequence of forty frames, there are 2.5 cycles of open and closed hand. This movement is performed by both, the left and the right hand successively and recorded in two different videos. The total duration of the video sequence recorded, as mentioned above, was forty seconds for each hand. Here one can compute the duration per cycle as:

$$\frac{40\ frames}{38\ frames/second} \times \frac{1}{2.5\ cycles} = 0.421\ second/cycle$$

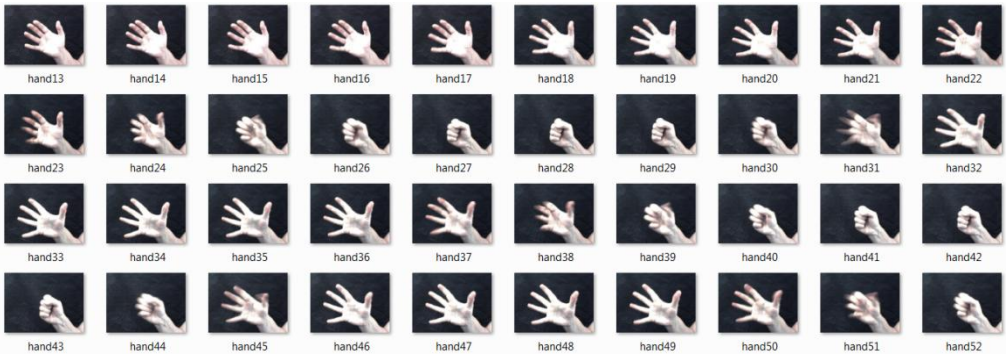

Fig. 4.3: Open and close hand quickly movement for the right hand.

4.3.2 Open and close hand slowly

The patient is asked to open and close the hand slowly, to allow the system to evaluate even the slightest angle. We can see in this case that we have more frames showing similar hand configuration (Fig. 4.4). We have one cycle between frames 143 and 164 which is 22 frames. Then the time per cycle can be calculated as follows:

$$\frac{22\ frames}{38\ frames/second} \times \frac{1}{1\ cycle} = 0.579\ second/cycle$$

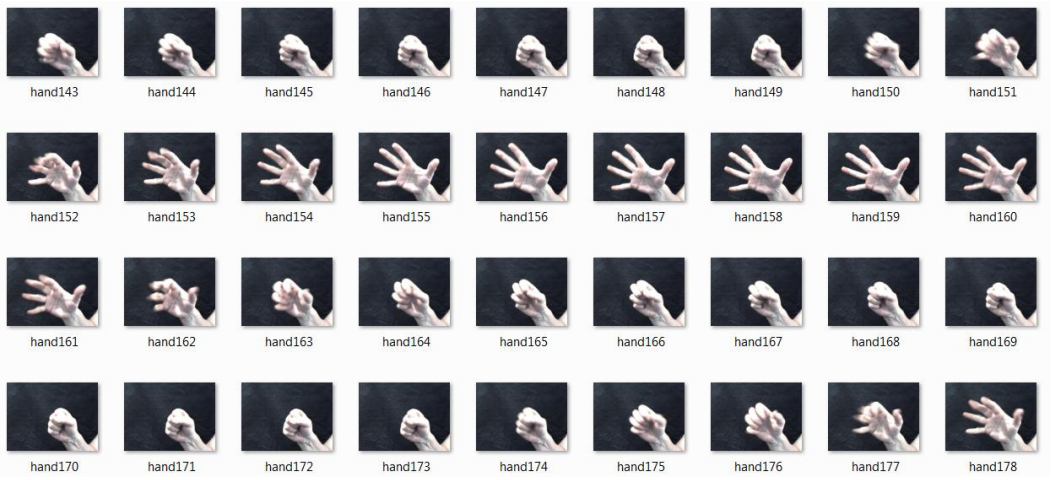

Fig. 4.4: Open and close hand slowly movements for the right hand.

4.3.3 Separate and join fingers quickly

This movement helps to gain a better sense of the motion capabilities of the patient. In fact, it was observed that RA patients have more difficulties with performing this movement. Asking the patient to perform quickly helps to estimate the motion capabilities of his/her hand in horizontal direction as MCPs have two DoFs (Fig. 4.5). Here we can observe 2.5 cycles of separate and join fingers between frames 391 and 417 in 26 frames. The period per cycle is:

$$\frac{26\ frames}{38\ frames/second} \times \frac{1}{2.5\ cycles} = 0.274\ second/cycle$$

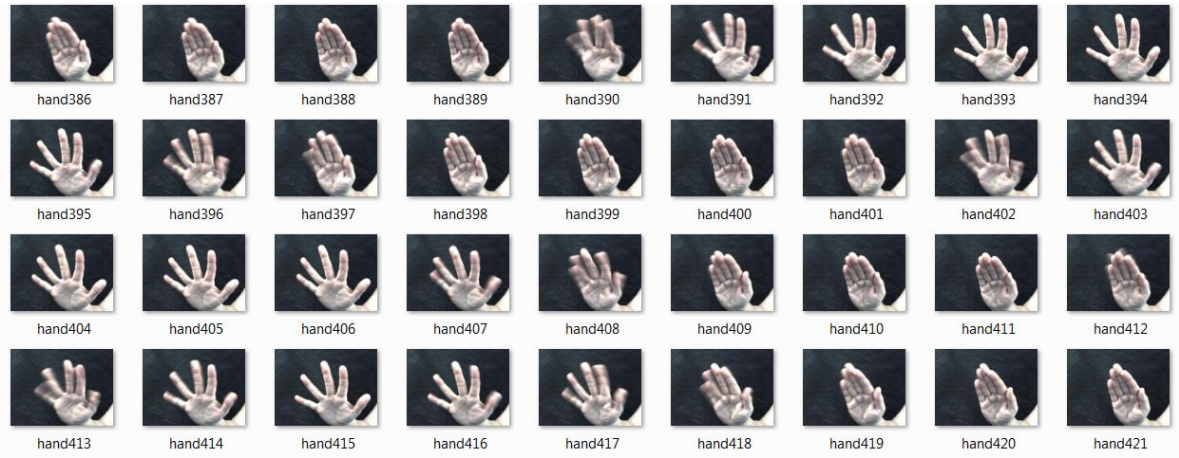

Fig. 4.5: Separate and join fingers quickly movement for the right hand.

4.3.4 Separate and join fingers slowly

This movement is used to provide the system with the possibility of measuring the size of the gap between the fingers. This is to estimate the capability of the patient to separate the fingers. As shown in Fig. 4.6, there are more frames for each part of the movement when compared to the one in Fig. 4.5 where the same movement is performed faster. Here we have one cycle between frame 603 and 635 for thirty-three frames. The period per cycle is:

$$\frac{33\ frames}{38\ frames/second} \times \frac{1}{1\ cycle} = 0.868\ second/cycle$$

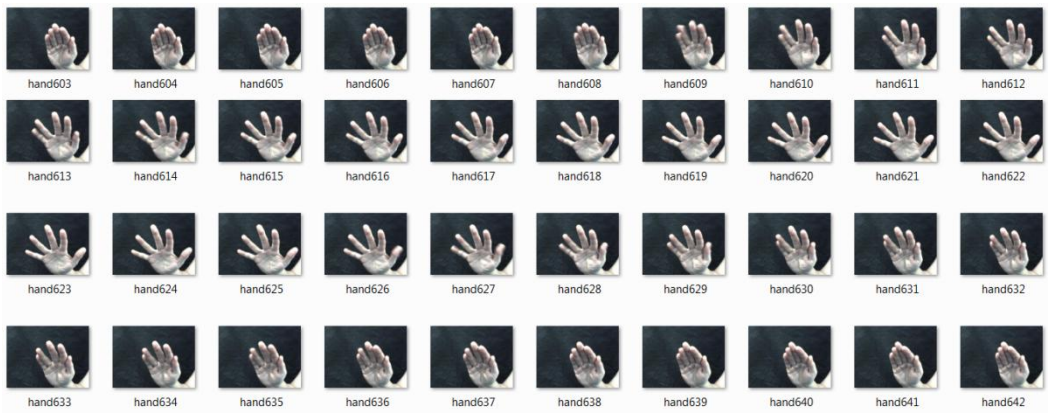

Fig. 4.6: Separate and join fingers slowly movement for the right hand.

4.3.5 Stretch and bend arms joints quickly

The objective of this fifth movement is to be able to quantify the motion capability of the arm joints of the subject. And the consideration of the wrist motion could help in the process of determining the level of severity of the illness. In Fig. 4.7 there is one cycle of movement between frames 35 and 61 for 26 frames.

$$\frac{26\ frames}{38\ frames/second} \times \frac{1}{1\ cycle} = 0.684\ second/cycle$$

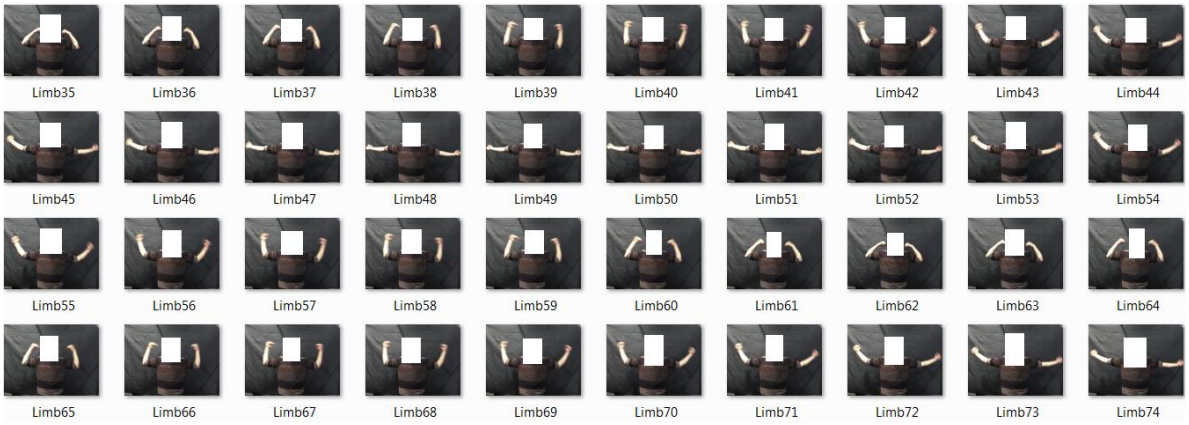

Fig. 4.7: Stretch and bend arm joints quickly.

4.3.6 Stretch and bend arms joints slowly

Slowly performing the bend and stretch movement of the arm also helps the system to better determine the various angles of the arms during the performance. This type of movement better supports the angle based classification of the severity of the illness as explained in section 4.2.1. Here it is one cycle over 30 frames (from frame 305 to 334) and the period per cycle is:

$$\frac{30\ frames}{38\ frames/second} \times \frac{1}{1\ cycle} = 0.790\ second/cycle$$

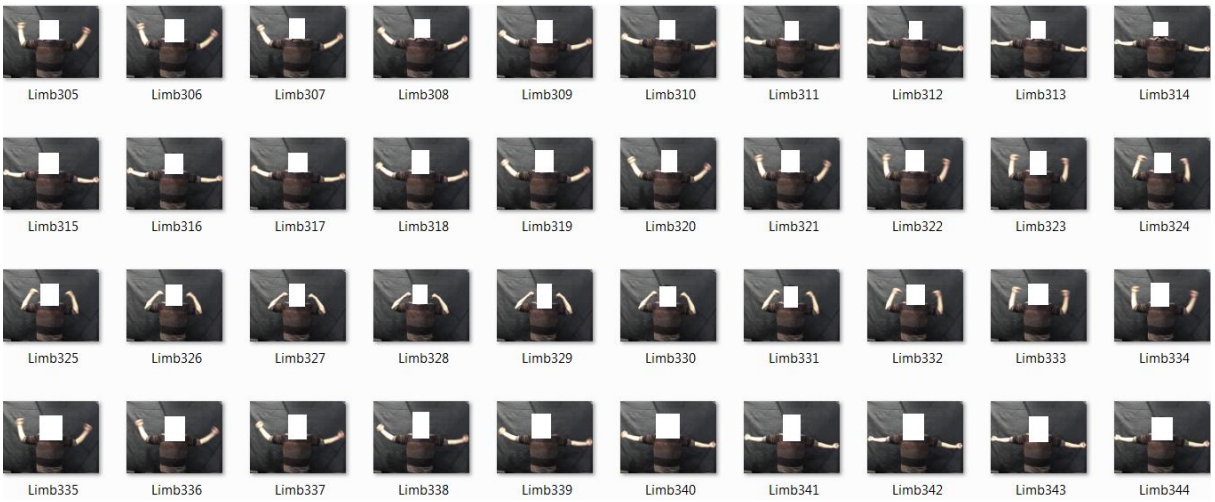

Fig. 4.8: Stretch and bend arms joints slowly.

The three methods used in the research which were introduced in the previous section, will now be defined in details. Each type is an integrated part of the motion estimation procedure that this research uses to determine the illness severity of a RA patient.

4.4 First method: Estimation of human hand motion using Sum of Absolute Difference

The Sum of Absolute Differences (SAD) is a simple algorithm known for finding the correlation between two images, generally in a sequence of images or video frames. It is, in fact, taking the absolute difference between a pixel intensity of the first image and its corresponding pixel intensity in the second image. These differences are added to create a metric of block similarity [67].

The SAD technique can be used for many purposes such as object recognition (comparing two sets of pixels to see if the SAD value is small), motion estimation (used as part of a block matching algorithm) and disparity map estimation for stereo imaging. This is possible through generating a metric based on local uniqueness by computing the distortion within a search window of an image. For each pixel inside the window,

the SAD computes the correlation. Changes in the pixels between two consecutive frames can be identified (Fig. 4.9). This is the reason why SAD is a popular technique for motion detection in video processing. It detects the similarity between two consecutive frames. In fact, greater similarity is achieved when smaller SAD values are obtained [68].

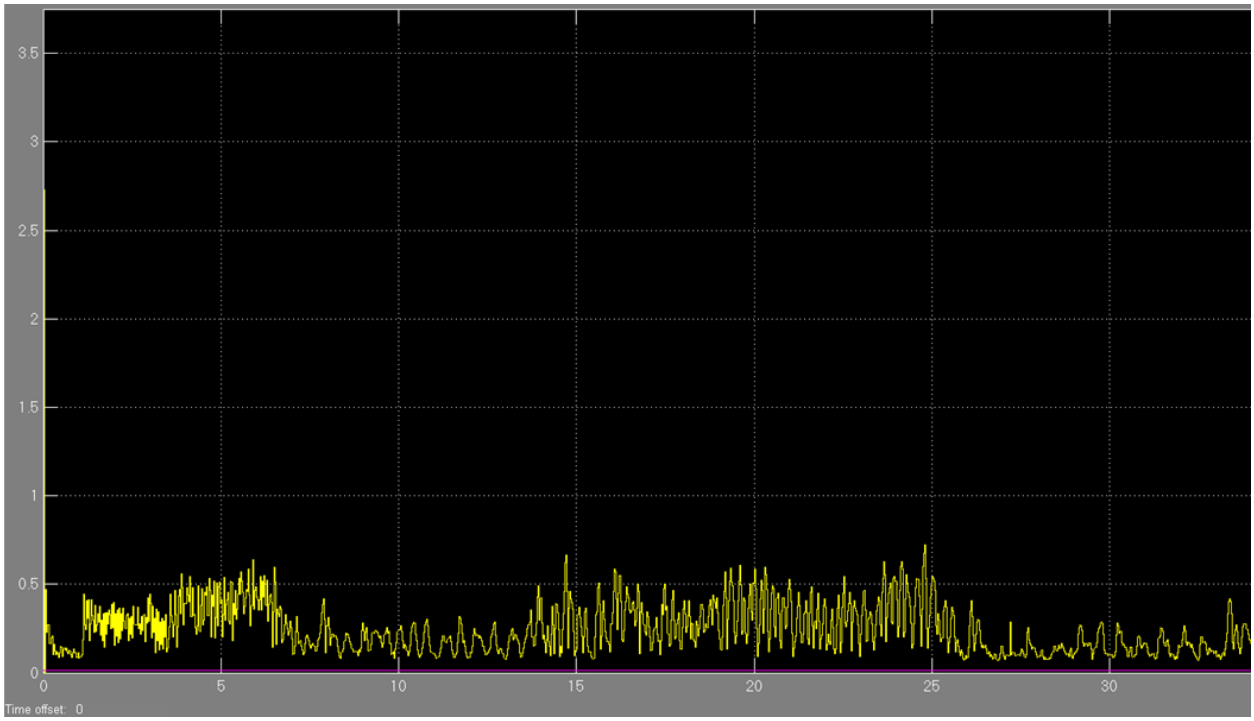

Fig. 4.9: Result obtained by computing SAD from frame to frame over a sequence of 34 seconds of video where the X axis represents the time in seconds and the Y axis represents the SAD value multiplied by $2.9xe^6$.

Fig.4.9 shows the value of SAD from frame to frame over 34 seconds of the video duration. As shown, the results are multiplied by $2.9xe^6$ (Appendix G) to have more significant numbers because the difference from frame to frame is small. The SAD approach provides an estimation of the motion energy that takes place from frame to frame. The relatively small values are compensated by a factor of multiplication of $2.9xe^6$ that is set in the Simulink's block implementation to refine the intermediate

values between the integers (0 and 1 or 254 and 255). The result can be displayed as a function of time. It also can be considered as inter-frame video motion detection because it quantifies the motion variation between two consecutive frames. At the very beginning of the sequence (i.e. at 0 second), there is a large SAD value that should not be considered because the process starts by subtracting the first frame with the hand or limbs from the uniform background, resulting in a meaningless peak in terms of motion estimation.

4.4.1 Using SAD for motion estimation in the human hand

The objective here is to measure the capability of a subject to bend and stretch his/her hand. The SAD method, based on the difference between changing pixels provides an estimation of the displacement of the pixels from one frame to another. In fact, the assumption is that the total intensity of the pixels remains the same from one frame to another, when there is no change in lighting or other conditions that can externally affect the intensity of pixels between successive frames. In such a situation, SAD monitors the motion displacement from one frame to another. This provides an estimation of the motion that has taken place in between two consecutive frames. The drawbacks of this method are that it cannot determine the magnitude of the displacement, the direction of the movement, and remains sensitive to all sources of intensity variations. Also, the displacement of pixels does not always represent the amount of motion. It is then difficult to estimate with SAD the magnitude of the motions of the hands and arms.

SAD is also used for matching block algorithms that match blocks between two frames to find the displacement of the same block from one frame to another. If the SAD value is zero between two blocks from the two frames and they have in addition the same neighboring pixels, then they represent the same block which changes its position from one frame to another. It is possible, then, to estimate the magnitude and the orientation of the movement from the first frame to another. This use of the SAD will be

presented in detail in section 4.6 along with the block matching algorithm used in this research.

4.4.2 Mathematical expression of SAD

SAD is expressed by a mathematical formula that gives the absolute difference between two corresponding pixels from two consecutive frames. Scanning from the first pixel of the two images to the last one and adding the absolute values of their intensity difference gives an expression of the energy in terms of intensity changes between the two frames. The SAD is then expressed as:

$$SAD = \sum_i \sum_j I_k(i,j) - I_{k-1}(i,j) \quad (4.1)$$

where $I_k(i, j)$ represents the intensity of the pixel (i, j) in image k (current frame) and $I_{k-1}(i, j)$ represents the intensity of the same pixel in image k-1 (previous frame).

The operation performed by the computer between two frames is illustrated in Fig. 4.10 and the final computation of SAD value performed during the image processing is defined as follows:

i) Computation of SAD over nxn image between two consecutive frames, let frame k-1 and k represent a pair of successive frames in the sequence. Then, on the first row of the pixels of the frames:

$|I_k(1,1) - I_{K-1}(1,1)| + |I_k(1,2) - I_{K-1}(1,2)| + \ldots\ldots + |I_k(1,n) - I_{K-1}(1,n)| = I_1$

where $I_k(x,y)$ represents the intensity in frame k of the x row and the y column of that row. By computing from row to row one obtains$I_1, I_2, I_3, \ldots\ldots, I_{n-1}, I_n$.

ii) Computation of SAD between a pair of frames by summing overall n rows as :

$SAD = I_1 + I_2 + I_3 + \ldots\ldots + I_{n-1} + I_n$

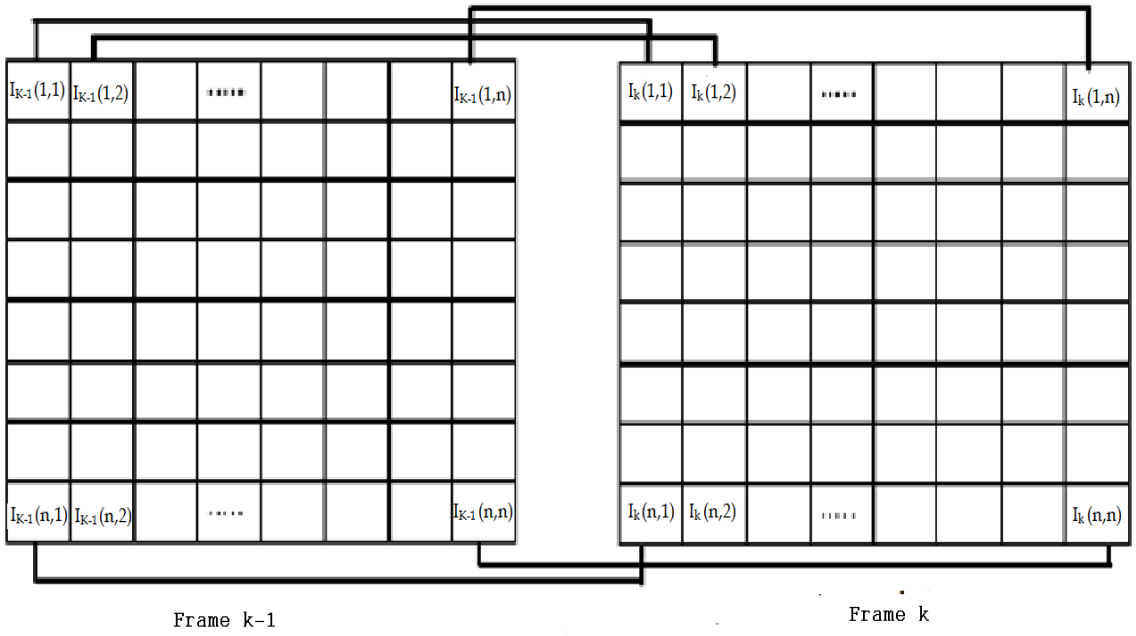

Fig. 4.10: Representation of SAD computation over two consecutive images.

The details of implementation of the SAD method to obtain the result shown in Fig. 4.9 can be found in appendix G. The RGB representation of color images produced by the camera is first converted to a greyscale mapping to be able to express each pixel intensity value within a range of 0 to 255 where 0 represents a black pixel and 255 represents a white pixel. The intermediate values represent the intermediate gray shading between black and white. To obtain significant numbers, SAD values are all multiplied by $2.9xe^{6}$. For more precision it uses the Simulink's block that computes the intermediate values of intensities between the two classical integer values for intensity representation, which , by definition, involves this multiplying factor.

4.4.3 Classification of level of severity based on SAD

The classification of the level of severity of RA based on SAD relies on what we obtained from the processing of volunteers videos. As mentioned in section 4.2.2, the volunteers were considered as a reference for low level of RA. Their results are therefore used to set the threshold for the severity levels. As it can be noticed from the

results of the volunteers in Table 4.1, the average SAD value for all volunteers was 2.9. With this average and looking at the result of all the subjects (Table 4.1 for volunteers, Table 4.2 for patients) we determined three classes of SAD values. We found that we have a series of results with SAD values lower than 3.52. Another series of result are concentrated between 3.53 and 6.02. A last group could be of subjects with a value higher than 6.02 (in our case there is only one patient in such a group). This defines the three levels of severity that could separate one category from another. More elaborate thresholds limits are set considering the average and standard deviation results from both patients' participant and volunteers (Fig. 4.11, Fig. 4.12 and Fig. 4.13).

The assumption is that the greater the difference between the minimum and maximum SAD values, the more severe the level of RA of the patient is considered. This can be explained by the fact that RA patients have difficulties at opening and closing their hands properly. We observed large variations from frame to frame, which we did not observe for healthy subjects. For a healthy subject, the variation from frame to frame should be approximately the same, but as shown here, in Table 4.1, in reality, because of the fatigue process, we obtained some variations.

The way that we are reading results has to be explained. In fact, as said above, the higher the SAD value is, the largest motion happens between one frame and another. But as we are considering the minimum and the maximum values of SAD between two frames to estimate the range of the variation of SAD, one can notice that the larger range does not correspond to the lower level of severity. We are taking into consideration the fact that a RA patient has difficulties to bend and extend properly and progressively the articulations. One can observe from the results that an RA patient has large disproportionalities among some consecutive frames in the sequence of frames. On the other hand, for a healthy subject the difference between two consecutive frames tends to be uniform. This shows the regularity with which a healthy person is able to bend and stretch his/her joints. This irregularity of SAD values from frame to frame for a RA patient, generates differences between the minimum value and the maximum of

SAD as soon as the subject has more difficulty to bend and stretch properly his/her articulations. Consequently when the difference (or range) is larger, it is interpreted on a level of severity that is also higher.

Volunteer ID	**Specification**	**SAD Value (average)**	**Range between average Max. and Min. SAD values**
1	Minimum	0.41	
	Maximum	2.91	2.50
2	Minimum	0.83	
	Maximum	4.58	3.75
3	Minimum	1.87	
	Maximum	3.75	1.87
4	Minimum	0.83	
	Maximum	3.00	2.16
5	Minimum	0.83	
	Maximum	6.19	5.36
6	Minimum	0.83	
	Maximum	3.00	2.16
7	Minimum	0.83	
	Maximum	3.33	2.50
8	Minimum	0.88	
	Maximum	4.51	3.63
9	Minimum	0.83	
	Maximum	3.00	2.16
10	Minimum	0.88	
	Maximum	4.45	3.56
Average			**2.97**
Standard Deviation (SD)			**1.10**

Table 4.1: SAD estimation values of volunteers.

Patient ID	Specification	SAD Value (average)	Range between average Max. and Min. SAD values
14	Minimum	0.309	
	Maximum	3.565	3.25
15	Minimum	0.770	
	Maximum	2.874	2.10
16	Minimum	0.379	
	Maximum	3.231	2.85
17	Minimum	0.716	
	Maximum	6.441	5.72
18	Minimum	0.666	
	Maximum	6.691	6.02
19	Minimum	0.783	
	Maximum	3.758	2.97
20	Minimum	0.666	
	Maximum	3.949	3.28
21	Minimum	0.908	
	Maximum	4.814	3.90
22	Minimum	0.604	
	Maximum	2.468	1.86
23	Minimum	0.702	
	Maximum	4.259	3.55
24	Minimum	0.609	
	Maximum	3.520	2.91
25	Minimum	0.728	
	Maximum	5.218	4.48
26	Minimum	0.650	
	Maximum	3.459	2.80
Average			**3.52**
Standard Deviation (SD)			**1.25**

Table 4.2: SAD estimation values of patients.

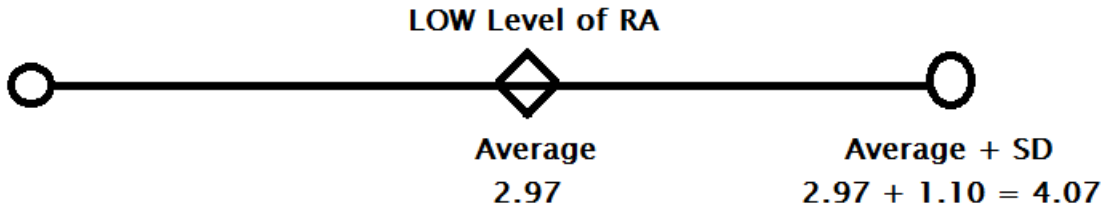

Fig. 4.11: Low level of RA according to volunteers' results and Standard Deviation (SD).

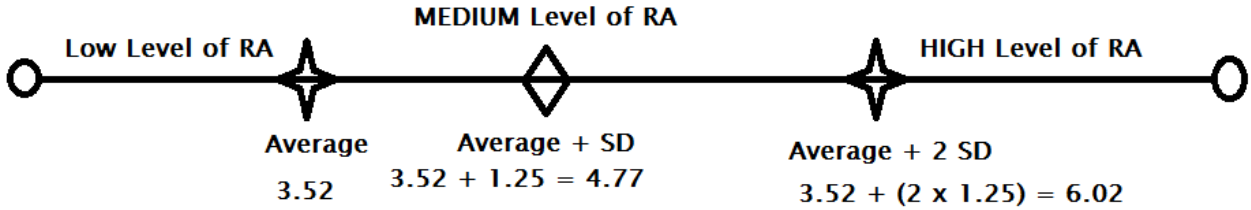

Fig. 4.12: Distribution of RA level according to patients' results and SD.

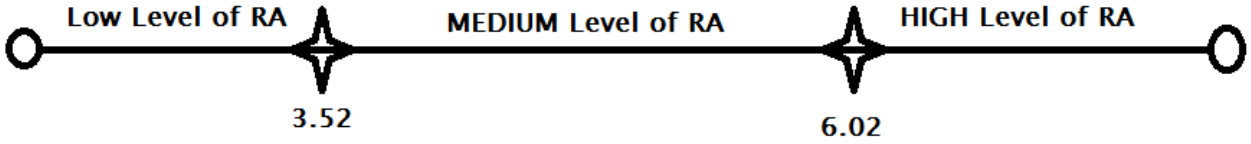

Fig. 4.13: Thresholds according to all participants' results and SD.

In the diagrams of Fig. 4.11, 4.12 and 4.13, the symbols define values as follows:

 Important point (average, average + SD or average + 2 SD) which is not selected as threshold.

 Important point (average, average + SD or average + 2 SD) which is selected as threshold.

 Start and end points.

Using the above results from 10 volunteers and 13 patients, we set three thresholds that we use in this research to classify the level of severity according to the range between maximum and minimum SAD values. The thresholds were set using two

different methods: using the average and standard deviation values respectively for volunteers (Fig. 4.11) and for patients (Fig. 4.12), and then combine them to have the needed thresholds (Fig. 4.13). The two thresholds of 3.52 and 6.02 are taken from the computation of average of patients and volunteers plus the SD as shown in Fig. 4.11, Fig. 4.12 and Fig. 4.13. The levels of severity were then set as follows:

i) Less than 3.52 corresponds to Low level of severity,
ii) Between 3.53 and 6.02 corresponds to Medium level of severity,
iii) From 6.03 and above corresponds to the High level of severity.

By doing such, nearly all the volunteers are classified in the Low level of RA which is the only parameter that we can rely on. In the next chapter we will present all results from patients based on this classification.

4.5 Second method: Classification using arm angle estimation

The second method of classification used in this research is based on simplified arm kinematics and image processing as presented in the previous chapter. The simplified kinematics of the arm helps to make the distinction between a patient and a healthy subject. The image processing part computes the angles of the joint to classify the patient according to the level of severity of the illness. To determine the values of the joints angles, the proposed approach uses the trigonometric relations of a triangle and the kinematic equations for the representation of position and orientation of the arm's bones in Euclidean space. In 2D space, the arm is simplified as a set of three different points (shoulder, elbow and wrist) representing the three main joints as described in section 3.4. But for the sake of measuring the three angles, one needs to add the hand and the chest to the set as shown in Fig. 4.14 below.

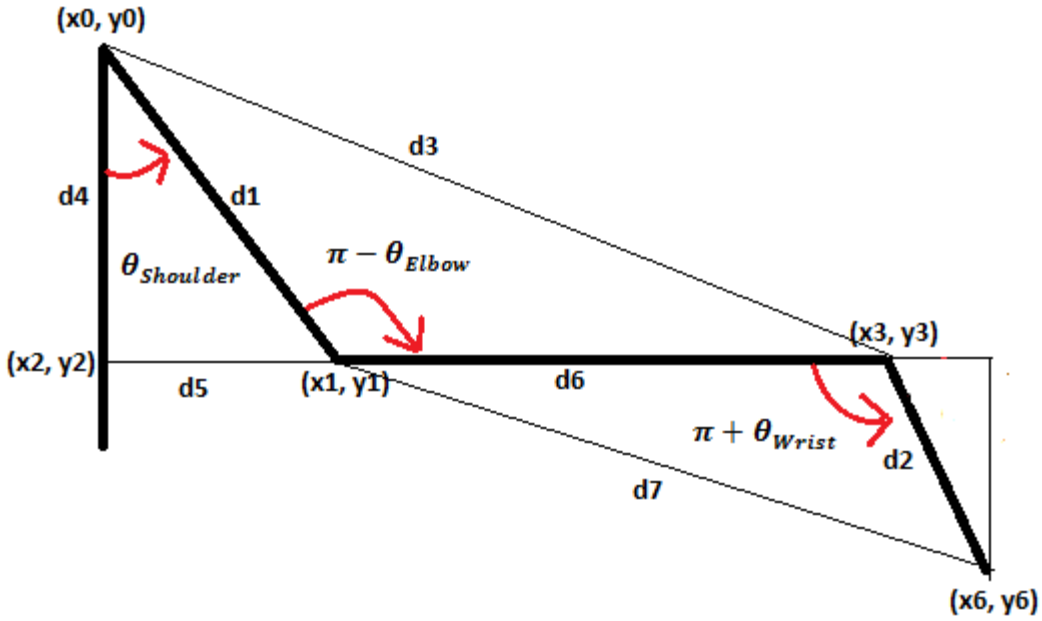

Fig. 4.14: 2D proposed representation of arm with shoulder, elbow and wrist angles.

As specified in Fig. 3.15 and Table 3.7, the wrist angle value that is used in this research is the one shown in Fig. 4.14. The average the minimum bending value of $\pi + \theta_{Wrist}$ for a healthy subject is 100 degrees. Here, smaller the value of $\pi + \theta_{Wrist}$ is, healthier the subject is in terms of RA. The angle $\pi - \theta_{Elbow}$ is computed as shown in Fig. 4.14 and it is the same principle: the smaller the value of this angle is, healthier the subject is in terms of RA. The $\theta_{Shoulder}$ value is imposed to the subject by the values of the two previous angles values. For the experiment, the subject was asked to bend the two first angles (wrist: $\pi + \theta_{Wrist}$ and elbow: $\pi - \theta_{Elbow}$) on their minimum possible bending before considering the third angle (shoulder: $\theta_{Shoulder}$). As the human arm works in chain, the value of $\theta_{Shoulder}$ depends on how the subject is able to bend the two other joints. As the value of $\theta_{Shoulder}$ depends on the value of $\pi - \theta_{Elbow}$, the average of all those three angles was consider in the process of classification based on joint bending capabilities.

$$d1 = |\sqrt{x0 - x1\ ^2 + \ y0 - y1\ ^2}| \quad (4.2)$$

$$d2 = |\sqrt{x3 - x6\ ^2 + \ y3 - y6\ ^2}| \quad (4.3)$$

$$d3 = |\sqrt{x3 - x0\ ^2 + \ y3 - y0\ ^2}| \quad (4.4)$$

$$d4 = |\sqrt{x0 - x2\ ^2 + \ y0 - y2\ ^2}| \quad (4.5)$$

$$d5 = |\sqrt{x2 - x1\ ^2 + \ y2 - y1\ ^2}| \quad (4.6)$$

$$d6 = |\sqrt{x1 - x3\ ^2 + \ y1 - y3\ ^2}| \quad (4.7)$$

$$d7 = |\sqrt{x6 - x1\ ^2 + \ y6 - y1\ ^2}| \quad (4.8)$$

The trigonometry identity is expressed for a triangle as:

$$d5^2 = d1^2 + d4^2 - 2 * d1 * d4 * \cos\theta_{Shoulder} \quad (4.9)$$

$$d3^2 = d1^2 + d6^2 - 2 * d1 * d6 * \cos(\pi - \theta_{Elbow}) \quad (4.10)$$

$$d7^2 = d2^2 + d6^2 - 2 * d6 * d2 * \cos(\pi + \theta_{Wrist}) \quad (4.11)$$

Then we can extract from these equations:

$$\cos\theta_{Shoulder} = \frac{d1^2 + d4^2 - d5^2}{2 * d1 * d4} \quad (4.12)$$

$$\cos(\pi - \theta_{Elbow}) = \frac{d1^2 + d6^2 - d3^2}{2 * d1 * d6} \quad (4.13)$$

$$\cos(\pi + \theta_{Wrist}) = \frac{d6^2 + d2^2 - d7^2}{2 * d6 * d2} \quad (4.14)$$

Finally we have:

$$\theta_{Shoulder} = acos\ \frac{d1^2 + d4^2 - d5^2}{2 * d1 * d4} \quad (4.15)$$

$$\pi - \theta_{Elbow} = acos\ \frac{d1^2 + d6^2 - d3^2}{2 * d1 * d6} \quad (4.16)$$

$$\pi + \theta_{Wrist} = acos \frac{d6^2 + d2^2 - d7^2}{2 * d8 * d2} \quad (4.17)$$

After segmentation of the image of the arm of the subject against the uniform background shown in Fig. 4.1, we get a black and white image of the arm. From that image, the estimation of the arm's skeleton is computed in two steps:

i) Estimate the boundaries of the arm shape and ensure that those boundaries form a closed contour,
ii) Compute the skeleton transform and prune the skeleton.

For the first step, we use the background segmentation technique. After the segmentation of the human arm, the estimation of the skeleton is based on the fact that in 2D the corresponding boundary can be delimited by a distribution of circles with maximal radius such that they all lie within the shape with the circles circumference being tangent to the shape at least at two different locations, as shown in Fig. 4.15. Then, one skeleton point of the shape is the locus of the centre of the circle. Taking all the possible maximum radius circles contained in the shape, we determine the estimation of the skeleton pose.

The second step is performed by using the skeleton transform of the Matlab library which gives the medial axis transform of a shape by finding the radius of each associated largest circle to each point of the estimated skeleton pose. This procedure is used to prune the skeleton. The process of pruning the skeleton is applied after having obtained a closed contour curve of the shape and its corresponding skeleton pose, by removing all the points in the skeleton that are not significant to the shape and considered as "noise". Fig. 4.15 and Fig. 4.16 show the two steps of the process of estimation of the skeleton pose of the human arm.

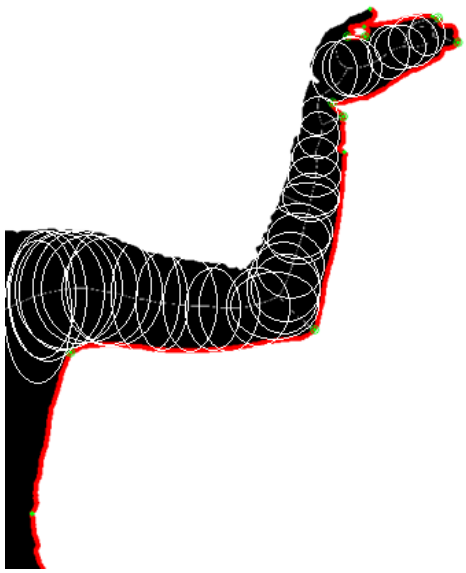

Fig. 4.15: Process of estimation of skeleton pose in an image.

In Fig. 4.15 and Fig. 4.16, the red line around the half contour of the human arm shape is used to find the curves of the shape to estimate the possible location of arm joints. For that, a half contour of the shape is sufficient. The other half will find the same locations from the opposite side.

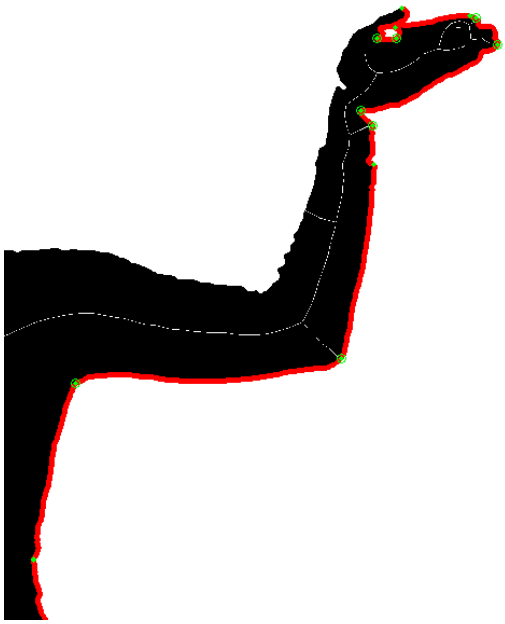

Fig. 4.16: Pruned pose skeleton.

For the estimation of the coordinates of each joint of the arm, Matlab provides the possibility to determine the coordinates of every point in an image using (X1, Y1) as shown in Fig. 4.17. In our case, the Z coordinate is always zero because we are working in 2D images. The coordinate is given to each pixel according to that reference located on the upper left corner of the image (Fig. 4.17). The X axis is from left to right, and the Y axis is from top to bottom. To put the coordinates of the points in the classical form (left bottom corner of the image with X axis from left to right and Y from left bottom to left top as (X2, Y2) reference) (Fig. 4.18), a coordinate transformation is used with the tranformation matrix (Q). Q is the transformation matrix needed to convert coordinates of any point of the images given by Matlab in (X1, Y1) reference to the new set reference (X2, Y2) as shown in Fig. 4.17. The transformation matrix Q is obtained through the set of operations performed to go from the (X1, Y1) frame to the (X2, Y2) frame which is a translation of the height of the image (y is the value of the height of the image), and a 180 degrees rotation around X1. This transformation matrix can be expressed as:

$$\boldsymbol{Q} = \boldsymbol{Q}_{\boldsymbol{T}_{(0,y,0)}} \boldsymbol{Q}_{\boldsymbol{R}_{\boldsymbol{X}(180)}} \tag{4.18}$$

$$\mathbf{Q}= \begin{matrix} \mathbf{1} & \mathbf{0} & \mathbf{0} & \mathbf{0} \\ \mathbf{0} & \mathbf{1} & \mathbf{0} & \boldsymbol{y} \\ \mathbf{0} & \mathbf{0} & \mathbf{1} & \mathbf{0} \\ \mathbf{0} & \mathbf{0} & \mathbf{0} & \mathbf{1} \end{matrix} * \begin{matrix} \mathbf{1} & \mathbf{0} & \mathbf{0} & \mathbf{0} \\ \mathbf{0} & \mathbf{-1} & \mathbf{0} & \mathbf{0} \\ \mathbf{0} & \mathbf{0} & \mathbf{-1} & \mathbf{0} \\ \mathbf{0} & \mathbf{0} & \mathbf{0} & \mathbf{1} \end{matrix}$$

$$\boldsymbol{Q} = \begin{matrix} \mathbf{1} & \mathbf{0} & \mathbf{0} & \mathbf{0} \\ \mathbf{0} & \mathbf{-1} & \mathbf{0} & \boldsymbol{y} \\ \mathbf{0} & \mathbf{0} & \mathbf{-1} & \mathbf{0} \\ \mathbf{0} & \mathbf{0} & \mathbf{0} & \mathbf{1} \end{matrix} \tag{4.19}$$

To convert the coordinates of any joint point with the coordinates (x_i, y_i) in the image frame to (X_i, Y_i) with respect to the reference frame (X2, Y2) the formula is:

$$\begin{matrix} X_i \\ Y_i \\ 0 \\ 1 \end{matrix} = \begin{matrix} 1 & 0 & 0 & 0 \\ 0 & -1 & 0 & y \\ 0 & 0 & -1 & 0 \\ 0 & 0 & 0 & 1 \end{matrix} * \begin{matrix} x_i \\ y_i \\ 0 \\ 1 \end{matrix} \quad (4.20)$$

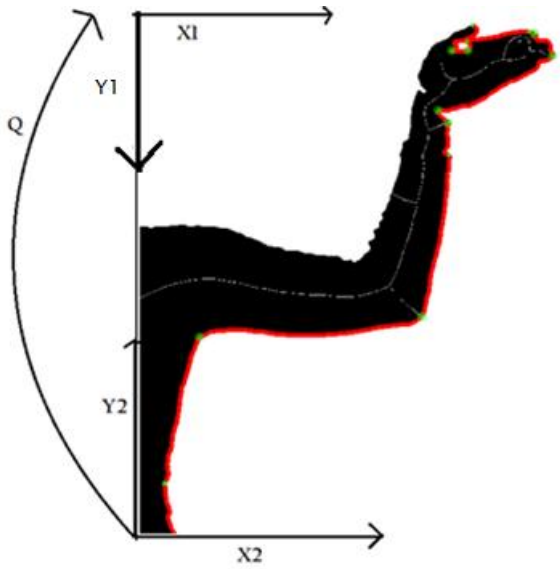

Fig. 4.17: Transformation from (X1,Y1) to (X2, Y2) as image reference frame.

When the coordinates of each articulation are identified in the frame (by the user who points out the intersections which correspond to the articulations), the length of each part of the arm is then computed according to the frame's point of view. Using those lengths, it is possible the find the angles of each articulation. The only important parameters here are the positions of the joints in the Cartesian space (Fig. 4.18).

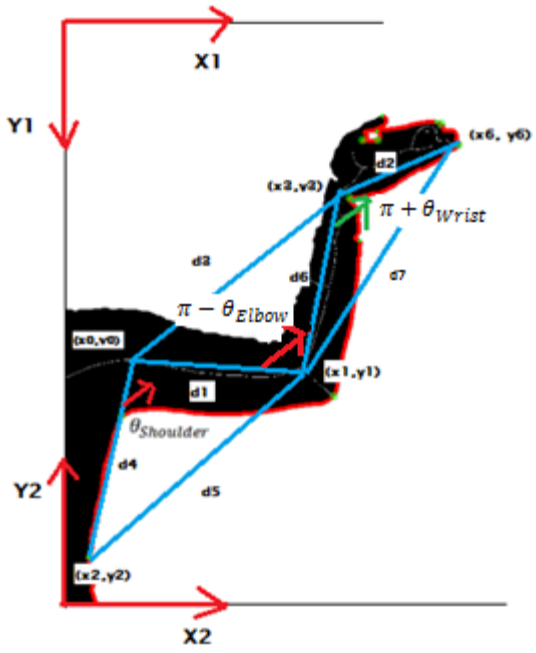

Fig. 4.18 : Coordinates of each points in the reference frame and computation of the distances.

The transformation as described above is used to compute the angle between the forearm and the torso ($\theta_{Shoulder}$) and the angle between the arm and the forearm ($\pi - \theta_{Elbow}$) and the wrist angle ($\pi + \theta_{Wrist}$) (Fig. 4.18).

For this method the classification of the level of severity is based on joints angles along the arm only because for the videos taken from the participants, it was not possible for all of them to estimate finger angles. Some videos were recorded mainly to demonstrate that with the implemented framework, it is also possible to estimate fingers angles (section 4.5.1). The classification is then based primarily on the results of the estimation of the three main joints of the arm (shoulder, elbow and wrist) as shown in Fig. 4.18. A special classification taking into consideration only the wrist bending capability was also performed because our medical specialist pointed it out as one of the most affected joints in case of RA. The previous studies based on infrared images also demonstrated that the wrist was one of the most affected joints [3], [4].

4.5.1 Classification based on fingers angles

The "Hand" button of the implemented GUI (Appendix H) helps the user to extract the three angular values for each finger of the hand using the simplified kinematic model described from sections 3.3.4 to 3.3.7.

To perform these estimations, the system requires an image collected from a proper angle such that the axes of rotation of the three articulations rotation axes are parallel to the principal axis of the camera (Fig. 4.19).

Fig. 4.19: Selection of a proper hand picture, here showing thumb and index.

Then, the user has to point out the intersections of the finger within the image before the process of computation of the three angles starts (Fig. 4.20). Then using the simplified kinematic equations established in section 3.3.5 (for the thumb) and section 3.3.7 (for the all fingers except the thumb) the system estimates the joints angles (Fig. 4.21).

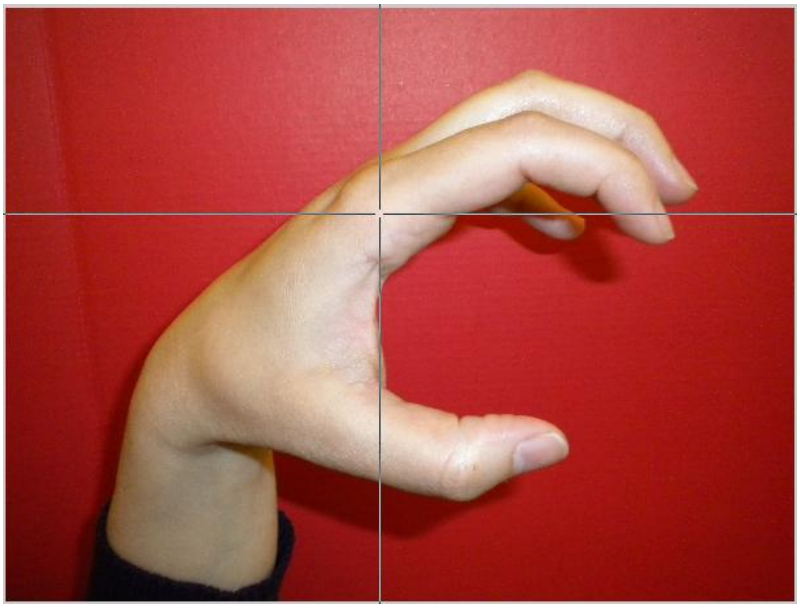

Fig. 4.20: User pointing the finger's joints, here thumb and index.

.

The proposed system provides to the user, through a pop up, the values of the three angles of the chosen finger in an order (Fig. 4.21) which first depicts the angle θ_{TMC1} (for the thumb), θ_{MCP2} (for other fingers) , the second angle is θ_{MCP} (for the thumb), θ_{PIP} (for other fingers) and the third angle is θ_{IP} (for the thumb), θ_{DIP} (for other fingers).

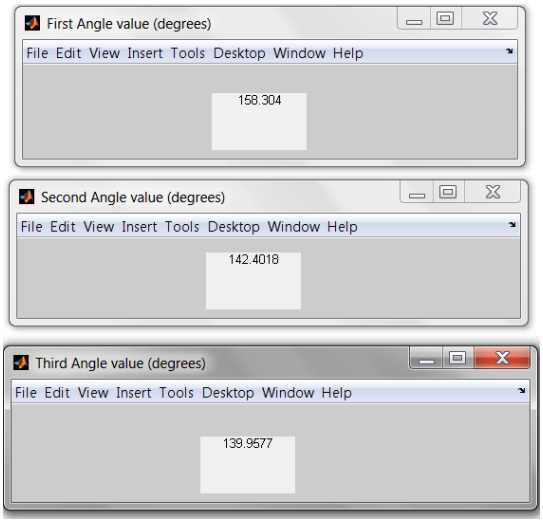

Fig. 4.21: Results for finger's joint angles with proposed approach.

It was not possible to establish in this study a classification based strictly on fingers' angles because in the set of videos that were created for patients and volunteers the frames showing the thumb and other fingers were not in such a position that permitted the system to determine those angles. A special session of picture is needed to provide the angular estimation for each finger in order to set a classification based on those results. However, while the study on the classification of RA level concentrated on the arm's joint angles, the implementation of the proposed system in its actual state is also able to determine fingers' joint angles provided that appropriate video sequences are acquired.

A possible occlusion might happen when considering fingers' angles estimation. To avoid that occlusion one needs to consider one finger at a time. A picture of each finger in its minimum bending angle needs to be taken to have estimation.

4.5.2 Estimation of the arm's joints using the implemented GUI

The "Limb" button of the GUI (appendix H) helps the user process the arm images and obtain the values of the three arm's joint angles.

To determine the arm's joint angles values, the user presses the "Limb" button and chooses the proper image of the subject in the position of a maximum bending of the limb's joints. A sample of the selected image is shown to the user (Fig. 4.22). In this example the subject has not reached his minimum bending, but this case is chosen to make all the interesting points visible in the image, for demonstration purpose. In general, the angles for minimum bending are smaller than the ones depicted here.

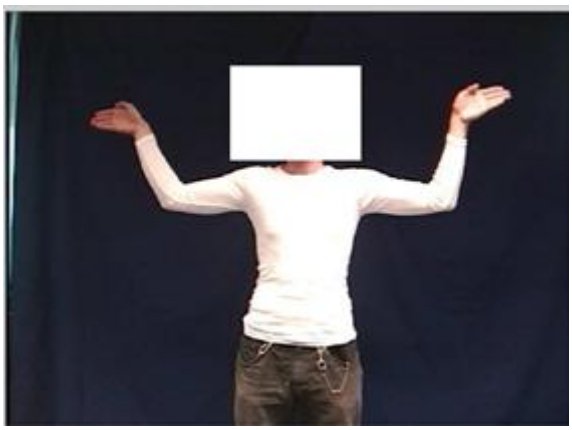

Fig. 4.22: Sample of a selected image by the user.

From the image of the subject with minimum arm joint bending, the user has to select the arm (right or left) over which one wants to evaluate the joint angles. The selection is done by drawing a rectangular area around the selected arm (Fig. 4.23).

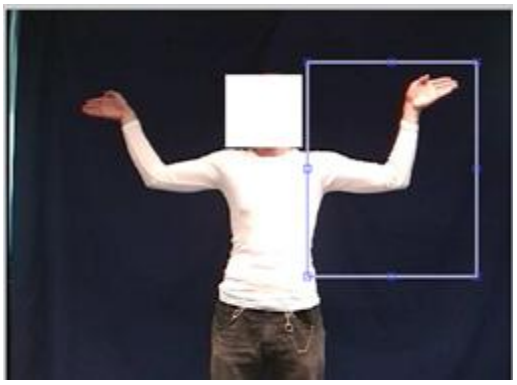

Fig. 4.23: Selection of the processing area.

The system will make an estimation of the skeleton pose using the middle line as explained above for the selected arm. That skeleton pose will be shown to the user who will select the end points of each segment of the limb. In fact, this aims at making sure that the system identified correctly all the joints of the arm (Fig. 4.24). The green dots in the figure are the possible articulations identified by the system. We implemented the system such that, as soon as there is a curve, it is considered as a possible articulation and the angle between the two consecutive lines is computed. To avoid erroneous joints, the user has to select, among the identified possible joints, the ones that the system has to consider as actual joints and compute the angles. The large cross on the image is the cursor line that the user uses to show the articulation cross point. The red line along the half contour of the segmented arm is to identify the curves and mark them as possible joints. To avoid identifying twice the same possible joint, only the half contour of the shape is considered.

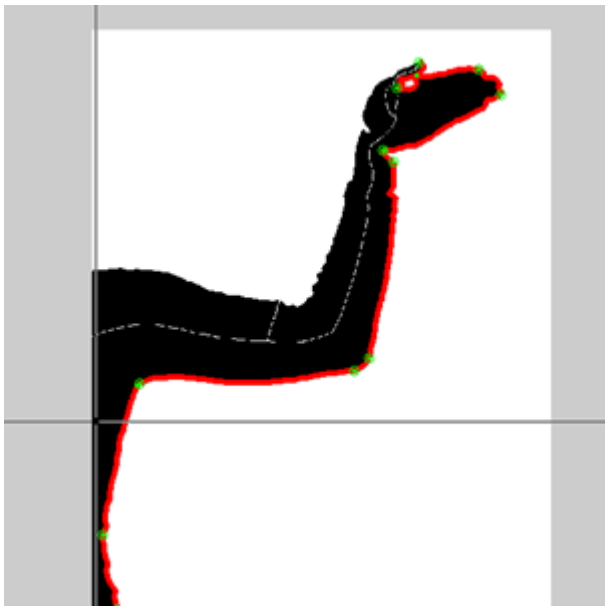

Fig. 4.24: Selection of the three valid arm's joints.

After the user points out the three joints of the limbs, the system provides the value of the three angles that the user wants to measure (shoulder, elbow and wrist).

The system displays the results in angular values to the user (Fig. 4.25) for each articulation. For that, the user has to start by pointing to the shoulder, then to the elbow and finally to the wrist in proper order.

Fig. 4.25: Pop ups displaying the joints angle values.

The values of the three angles are compared to the values of a healthy subject and the patient is classified according to the level of severity monitored by those three angle values. The same process is done for the left and the right arm. Six different angles are then found per subject. The criterion of classification based on volunteers' results is discussed in the section 4.5.4.

4.5.3 Comparison of the proposed solution with existing ones

To verify the validity of the proposed solution we compared it to two different existing solutions: the MaxTRAQ software from Innovision System [69] which is

specialised on tracking joints angles in a video sequence or set of images, and the multi-view tracking system developed by B. Rosenhahn *et al.* [37], [44]. The comparison was made over a sequence of five consecutives images from B. Rosenhahn *et al.'s* samples (multi-view camera system) and the results from their approach were compared to the corresponding angles obtained with MaxTRAQ, and with the proposed solution. The results for the 3 angles (shoulder, elbow, wrist) on the five consecutive images (Fig. 4.26) and the segmented images from the proposed solution combined with the MaxTRAQ tracking (Fig. 4.27) are reported in Table 4.3.

MaxTRAQ is a motion analysis software with a very good performance on the market. It can operate in 2D as well as 3D environment. It has the possibility to operate in auto tracking mode where some markers are already visible. In the video sequence of images, the system follows their trajectory from frame to frame which gives angles between 3 points and distance between 2 points. The other possibility is to operate in manual mode where the user sets points of interest in the first frame of the sequence of images and the system follows those points in the sequence (going frame to frame and finding corresponding points to compute the angles between 3 of them, the distance, the centre of mass, etc). This software is very popular for biomechanical analysis of human and animal movement.

The multi-view system developped by Rosenhahn *et al.* captures the performance of a human or animal from a multiview video sequence. Their system recovers the movement of the skeleton and is able to cover non-rigid temporal deformations of a 3D surface. It can also capture, using skeleton pose and approximate surface skining large scale deformations or fast movements. For human, they were able to determine the 3D pose and the angles of the arm joints from image silhouettes of the torso. Our proposed solution is compared in Table 4.3 to their results obtained from a sample sequence of images shown in Fig. 4.26.

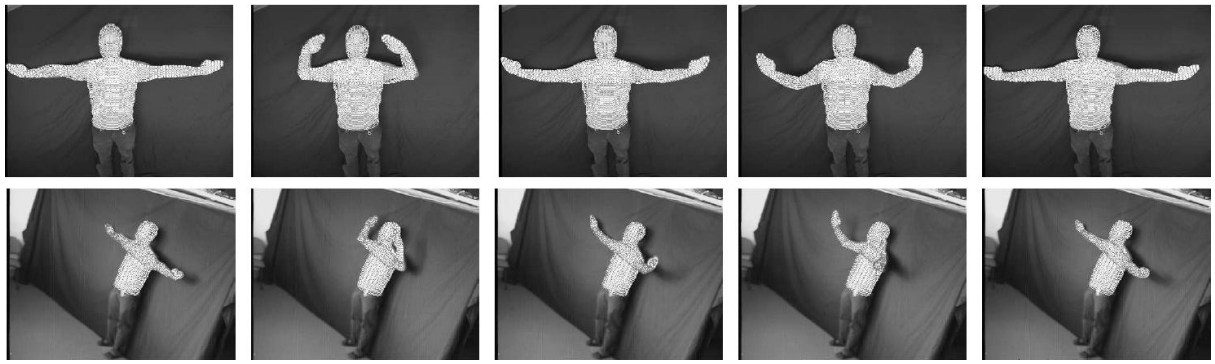

Fig. 4.26: Five consecutive frames from two points of view as proposed by B. Rosenhahn *et al.* [37].

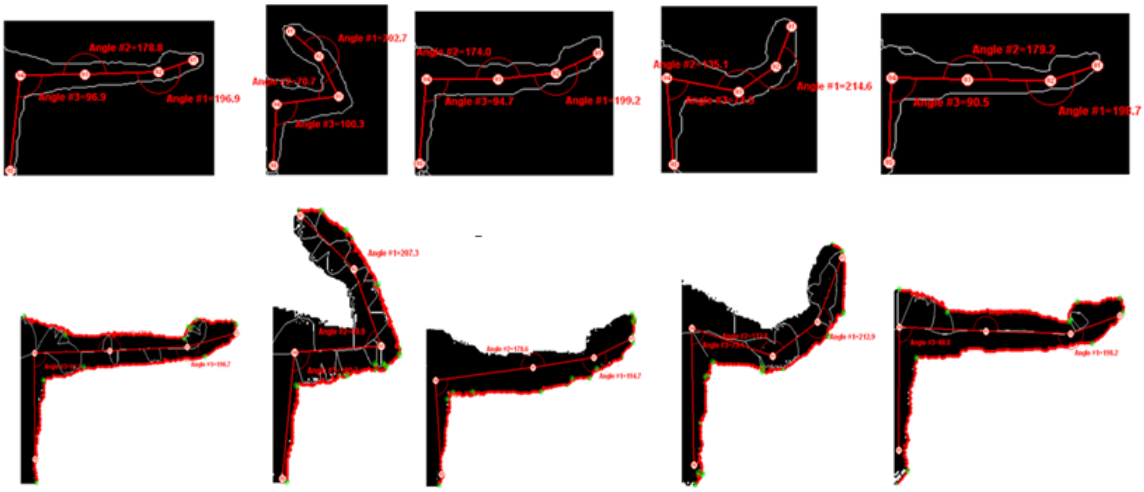

Fig. 4.27: MaxTRAQ's results from the contour estimation obtained with our proposed solution.

Joint	Multi-View camera (degree)	MaxTRAQ estimation (degree)	Proposed solution estimation (degree)	Diff.1* (degree)	Diff.2* (degree)
Wrist	190.5	196.0	190.7	5.5	0.2
	210.0	202.7	207.3	-7.3	-2.7
	190.0	199.2	194.7	9.2	4.7
	200.0	214.6	212.9	14.6	12.9
	190.0	198.7	198.2	8.7	8.2
Elbow	170.0	178.8	170.6	8.8	0.6
	85.0	70.7	70.0	-14.3	-15.0
	185.0	174.0	178.6	-9.0	6.4
	190.0	135.1	182.0	-54.9**	-8.0
	177.0	179.2	179.8	2.2	2.8
Shoulder	95.0	96.9	91.1	1.9	-3.9
	100.0	100.3	100.2	0.3	0.2
	95.0	94.7	96.3	-0.3	1.3
	75.0	74.5	75.4	-0.5	0.4
	100.0	90.5	98.3	-9.5	-1.7

* Diff.1 is the difference between the MaxTRAQ estimation result and the Multiview camera approach and Diff.2 is the difference between the proposed solution result and the Multiview approach . ** Large difference due to a missmatch of the point in MaxTRAQ.

Table 4.3: Results from three different systems for the same sequence of images.

Table 4.3 shows that the proposed solution provides angular estimation in the same order of accuracy than the MaxTRAQ sofware when compared to the multiview system estimation.

The results obtained with the proposed method for fingers' joints were also compared to MaxTRAQ software's results to monitor their accuracy (Fig. 4.28). This comparison also demonstrates that the same order of accuracy is achieved with the proposed implementation and with MaxTRAQ software for fingers angles estimation.

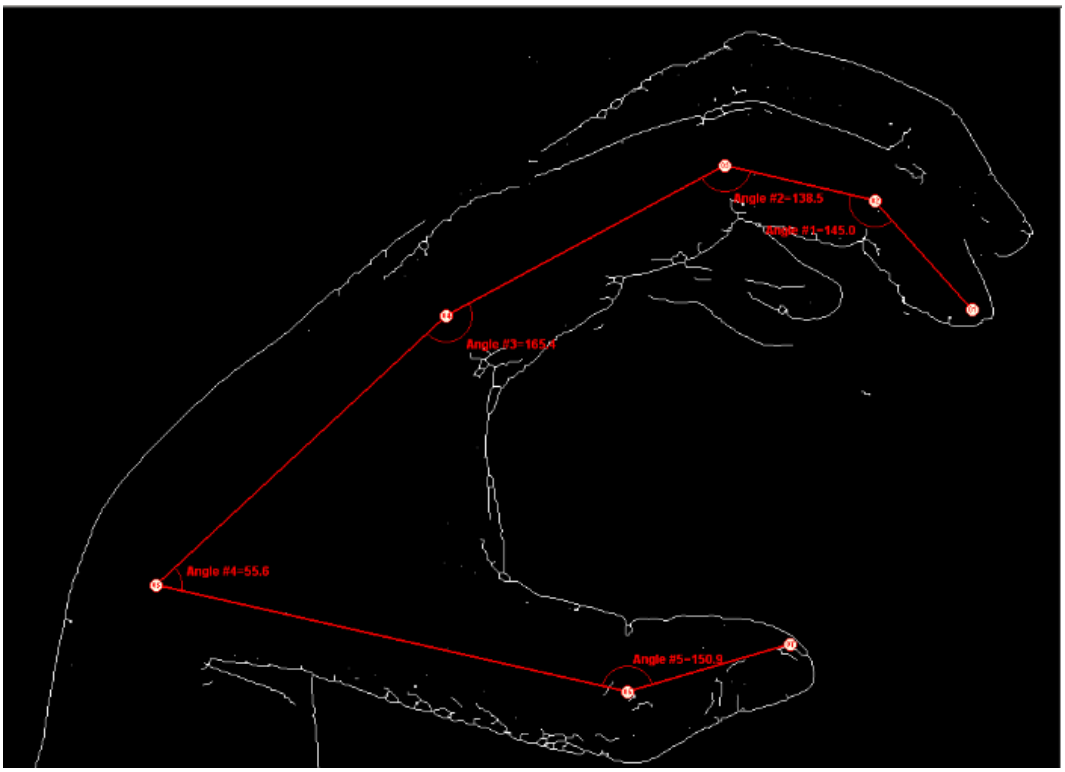

Fig. 4.28: Angles computed with MaxTRAQ software on fingers.

4.5.4 Classification based on arm angles

As for the first classification method presented in section 4.4, specific criteria of classification are determined based on estimation angles obtained with the second method. In the present case, it is not possible for us to set a clear distinction based on six categories for level of RA that the rheumatologist used. As Table 4.4 (for volunteers) and Table 4.5 (for patients) show, the maximum bending results (which actually correspond to minimum bending angles) from volunteers have a general average of 80 degrees. By taking the average over all the articulation angles, it is easier to estimate the severity of the illness, as each patient joint is not affected at the same level. In fact, there can be some significant differences between the left and the right arms. The used of the standard deviation (SD) for the volunteers (Fig. 4.29) and for the patients (Fig. 4.30)

provides clear position of thresholds (Fig. 4.31) for the classification based on arms' joint angles.

Volun-teers ID	**Left shoulder (Degrees)**	**Left elbow $\pi - \theta_{Elbow}$ (Degrees)**	**Left wrist $\pi + \theta_{Wrist}$ (Degrees)**	**Right shoulder (Degrees)**	**Right elbow $\pi - \theta_{Elbow}$ (Degrees)**	**Right Wrist $\pi + \theta_{Wrist}$ (Degrees)**	**Average (Degrees)**
1	59.33	36.81	116.78	83.77	44.78	108.72	75.03
2	77.47	37.80	134.32	78.82	38.41	136.43	83.81
3	76.28	44.94	137.09	87.01	43.23	144.09	88.77
4	93.57	36.41	124.50	77.34	32.30	122.51	81.10
5	87.21	58.03	116.68	85.93	50.52	98.54*	82.81
6	56.62	39.61	107.40	79.02	42.97	110.74	72.72
7	56.70	39.20	113.14	75.17	44.52	110.84	73.26
8	84.67	30.61	101.58	96.55	39.92	111.45	77.46
9	80.53	27.06	141.42	79.72	31.84	127.51	81.34
10	91.30	38.60	132.50	78.64	39.40	126.10	84.42
Average	**76.36**	**38.90**	**122.54**	**82.19**	**49.78**	**119.69**	**80.07**
SD	**14.10**	**8.32**	**13.47**	**6.31**	**5.73**	**14.06**	**5.28**

*For unknown reasons some subjects are able to reach articulation bending positions slide smaller than normal people. In this case volunteer 5 is able to reach 98.54 degrees for the right wrist, which is less than the 100 degrees that is expected from a healthy subject (Table 3.7).

Table 4.4: Minimum bending arm angles of volunteers.

As RA patients have difficulties to bend their arm articulations properly, the higher the average of arm angles is, the higher the level of RA is.

Patient ID	**Left shoulder (Degrees)**	**Left elbow $\pi - \theta_{Elbow}$ (Degrees)**	**Left wrist $\pi + \theta_{Wrist}$ (Degrees)**	**Right shoulder (Degrees)**	**Right elbow $\pi - \theta_{Elbow}$ (Degrees)**	**Right wrist $\pi + \theta_{Wrist}$ (Degrees)**	**Average (Degrees)**
14	71.4	25.7	143.1	64.3	27.3	150.6	80.40
15	80.3	30.5	93.4*	70.8	41.7	42.0*	59.78
16	88.5	44.3	156.4	81.0	48.1	152.4	95.11
17	94.4	30.2	131.6	90.0	41.4	115.7	83.88
18	90.6	30.2	127.8	94.5	41.8	117.3	83.70
19	91.4	47.0	149.3	90.2	48.0	118.3	90.70
20	91.3	43.5	132.7	92.0	39.1	145.2	90.63
21	75.7	33.0	130.9	93.0	31.4	139.8	83.96
22	49.3	30.1	121.9	69.1	24.7*	136.4	71.91
23	84.3	77.3	142.4	81.8	54.2	129.3	94.88
24	96.5	48.3	133.0	92.6	38.7	137.2	91.05
25	89.3	28.8	164.5	82.5	35.2	162.2	93.75
26	95.5	32.0	114.5	100.1	34.5	100.1	79.45
Average	**84.5**	**38.53**	**133.96**	**84.76**	**38.93**	**126.65**	**84.55**
SD	**13.03**	**13.94**	**18.37**	**11.01**	**8.41**	**30.79**	**10.15**

* It can be noticed here that the wrists (right and left) values of patient 15 are lower than expected even from a healthy subject. Same for patient 22 where the right elbow angle is 24.7 degrees which is less than 25 degrees expected from a healthy subject (Table 3.7).

Table 4.5: Minimum bending arm angles of patients.

As we assumed that all volunteers exhibit a low level of RA (because they are all healthy subjects), the average of the angles of their arms plus the standard deviation is used to define the threshold between the low level and the medium level of RA (Fig. 4.29). In this case, the low level threshold is taken from the value obtained by adding the average of volunteers' results with the standard deviation (Fig. 4.29): 80.07 ± 5.28 ≈ 85.35.

The medium level threshold is defined by adding the average value of the results from patients with twice their standard deviation (Table 4.4, Fig. 4.30): 84.55 +20.30 ≈ 104.85.

For a patient whose average level of angles is more than the average plus twice the SD, the level of severity is considered high (Fig. 4.31).

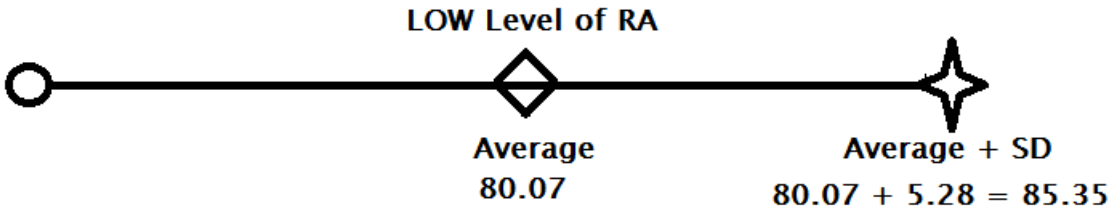

Fig. 4.29: Low level of RA according to volunteers' results and SD.

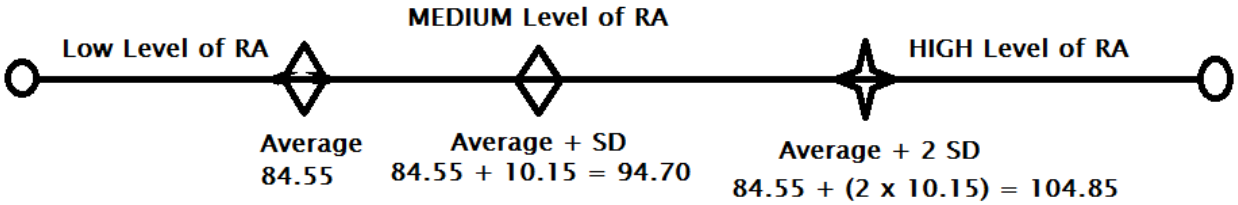

Fig. 4.30: Distribution of RA level according to patients' results and SD.

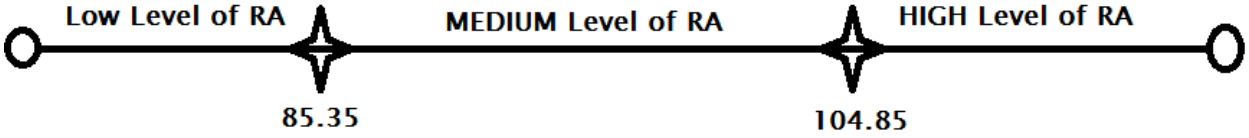

Fig. 4.31: Thresholds on arm angles according to all participants' results and SD.

In the diagrams of Fig. 4.29, 4.30 and 4.31, the symbols define values as follows:

 Important point (average, average + SD or average + 2 SD) which is not selected as threshold.

 Important point (average, average + SD or average + 2 SD) which is selected as threshold.

 Start and end points.

For the classification based on the six angles per subject, three references were identified (Fig. 4.29, Fig. 4.30, Fig. 4.31) to classify in three different categories:

i) The average angle lower than 85.35 degrees shows a low level of RA,
ii) Between 85.36 degrees and 104.85 degrees is a medium level of RA,
iii) More than 104.85 degrees in average shows a high level of RA.

As mentioned previously, the wrist angle is one of the most important for classification based on arm articulations angles. For this reason we also derived a special classification based only on the two wrists angles of each subject. Another motivation to consider a classification based on wrist is that, it is the joint in the kinematic chain of the human hand that is not affected by a previous joint as it is for elbow and shoulder. In the kinematic chain of the human arm, elbow and shoulder depend from each other in terms of their bending capabilities at the same time. This is not the case for the wrist joint that is asked to the participant to bend before bending the two other joints.

Volunteers ID	**Wrist Left $\pi + \theta_{Wrist}$ (degrees)**	**Wrist Right $\pi + \theta_{Wrist}$ (degrees)**	**Average (Degrees)**
1	116.78	108.72	112.75
2	134.32	136.43	135.37
3	137.09	144.09	140.59
4	124.50	122.51	123.50
5	116.68	98.54	107.61
6	107.40	110.74	109.07
7	113.14	110.84	111.99
8	101.58	111.45	106.51
9	141.42	127.51	134.46
10	132.50	126.10	129.30
Average	**122.54**	**119.69**	**121.11**
SD	**13.47**	**14.06**	**13.02**

Table 4.6: Wrist bending angles for volunteers.

Patient ID	Left wrist $\pi + \theta_{Wrist}$ (degrees)	Right wrist $\pi + \theta_{Wrist}$ (degrees)	Average (degrees)
15	93.4	42	67.7
26	114.5	100.1	107.3
18	127.8	117.3	122.55
17	131.6	115.7	123.65
22	121.9	136.4	129.15
19	149.3	118.3	133.8
24	133	137.2	135.1
21	130.9	139.8	135.35
23	142.4	129.3	135.85
20	132.7	145.2	138.95
14	143.1	150.6	146.85
16	156.4	152.4	154.4
25	164.5	162.2	163.35
Average	**133.96**	**126.65**	**130.31**
SD	**18.37**	**30.79**	**23.57**

Table 4.7: Wrist bending angles for patients.

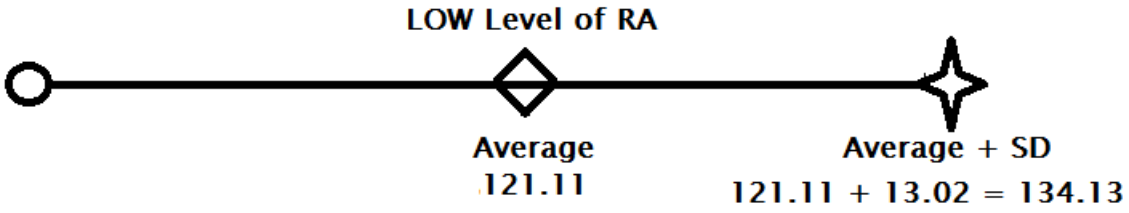

Fig. 4.32: Low level of RA according to volunteers' results and SD.

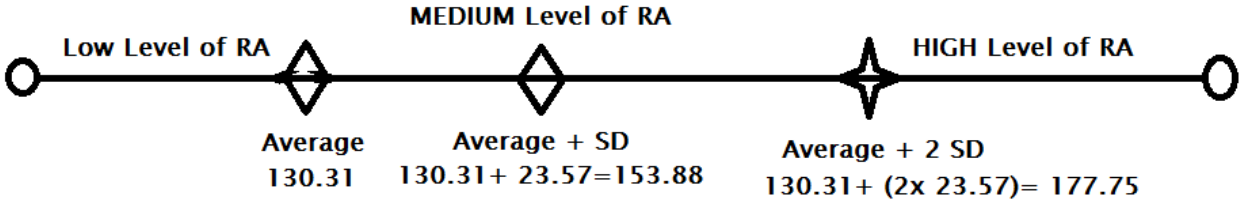

Fig. 4.33: Distribution of RA level according to patients' results and SD.

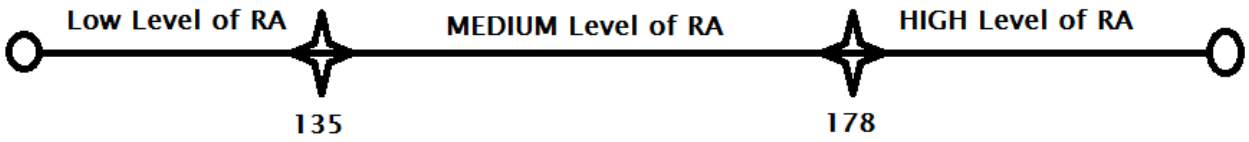

Fig. 4.34: Thresholds on wrist angles according to all participants' results and SD.

In the diagrams of Fig. 4.32, 4.33 and 4.34, the symbols define values as follows:

 Important point (average, average + SD or average + 2 SD) which is not selected as threshold.

 Important point (average, average + SD or average + 2 SD) which is selected as threshold.

 Start and end points.

For the classification based only on wrist angles (Table 4.6 and Fig. 4.32 for volunteers and Table 4.7 and Fig. 4.33 for patients), different criteria on average minimum bending angle (Fig. 4.34) were set as:

i) The average wrist angle lower than 135 degrees shows a low level of RA,
ii) Between 135 and 178 degrees is a medium level of RA,
iii) From 179 and up is a high level of RA.

For the low level threshold we added the average of the volunteers' wrist angles results with their standard deviation (Table 4.6) which gives 135 degrees rounding up $121.11 \pm 13.02 \approx 134.13$.

The medium level threshold was obtained by adding the patient's wrist angles average with their standard deviation (Table 4.7) rounding up $130.31 \pm 2 \times 23.57 \approx 178$.

More than 178 degrees as average of wrist bending angle is considered as a high level of severity.

All the results, classifications achieved and conclusions on this method will be discussed in section 5.3.

4.6 Third method: Using matching blocks for motion estimation

The third approach investigated in this research is based on a matching block algorithm for motion estimation. The SAD as implemented in the first approach is used as a part of the algorithm to find a specific block within a frame to compute its displacement: that is the magnitude of the displacement.

In the case of block matching algorithm, the SAD method is applied to a block of 16x16 pixels to find the right matching block in the second frame. When the SAD value is small between two matching blocks and have the same neighboring pixels, it can be considered as the same block. Then, the algorithm can compute the displacement and orientation of the displacement vector from the first to the second frame. Each algorithm has its own particular implementation in order to obtain the result of motion vector.

For our implementation, we used the ARPS algorithm as described in section 2.10. The implementation is accessible through the GUI of the system.

4.6.1 Implementation in the GUI

The button ”Motion Estimation” of the GUI, described in Appendix H, helps to process the hand or arm video taken from the subject or patient stretching and bending the articulations. The user needs to select the video in which one wants to find the motion vector.

After the selection of the video, the system cuts the video into frames. At the end of this process, the system asks the user to enter the number of frames over which

he/she wants to estimate the motion vector. Generally it is helpful to consider the first 150 frames because the performer has all his strength at the beginning of the exercise and becomes weaker over time. This is to avoid having to compute the motion vector for the whole video and giving the possibility to the user to find the motion vector over a specific part of the video. After the user has specified the number of frames over which he/she wants to estimate the motion vector, the system starts the process, using the ARPS algorithm, for finding the motion vector (the largest motion vector of a block between two consecutive frames is considered as the motion vector between the two frames). At the end of this process, a table of motion vectors, from frame to frame, is saved on the user workspace of the system. One can then open the file as a table (Fig. 4.35) or as a graphic (Fig. 4.36) to see the magnitude of the motion vector in between successive frames. This result is analyzed in section 5.4. In the table of motion vectors magnitude, the largest motion vector magnitude will be taken as the value of the motion capability of the subject.

1	2	3	4	5	6	7	8	9	10	11	12	13	14	15	16	17	18
0	15.1999	12.3372	14.6647	12.0648	23.1694	13.7969	12.0326	16.0594	16.2531	14.0748	16.6902	24.2787	24.0585	13.2679	15.0518	15.8318	16.3069

Fig. 4.35: Motion vector magnitude from frame to frame for volunteer 3.

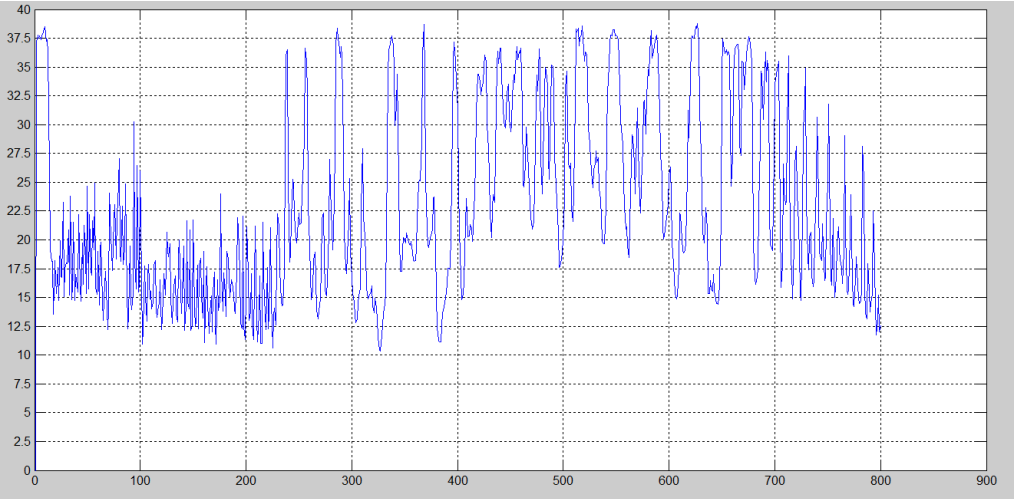

Fig. 4.36: Graphic of motion vector magnitude from frame to frame.

The computation of the magnitude of the motion vector, from frame to frame, comes from the analysis of a sequence of successive frames as shown in Fig. 4.37.

Fig. 4.37: Example of a sequence of frames from a video used to compute motion vector magnitude.

From the motion vector magnitude, the user can estimate the level of severity of RA in the patient. This aspect is explained in section 5.4.

4.6.2 Classification based on motion estimation

The classification based on motion estimation is built according to the result of both the hand and arm motion. The average over the number of frames considered in the sequence, of each of the limbs according to all the results that we had, are similar. For that reason, the classification based on six categories uses the average of hand and arm motion vectors. In this method, the classification is based on the volunteers' results presented in Table 4.8 and on the patients' results presented in Table 4.9. The results are presented in unit of pixels for the magnitude of the motion vector (MV).

For the classification based on motion vector all hand and arm videos were considered. The maximum value (largest magnitude) of motion vector that the subject can reach for the hand is considered as the value of the hand motion vector and it is the

same for the arm motion vector. After processing all videos, one value for the hands motion vector and one value for the arms motion vector are obtained for each participant. For this reason Table 4.9 (for patients) and Table 4.8 (for volunteers) show one value for the hands and another for the arms for each participant. As we are considering average motion vector, the values are always round up to the next number. For example a value between 9.01 up to 10.00 is round up to 10 and so on.

Volunteers ID	**Magnitude of hands MV (pixels)**	**Magnitude of arms MV (pixels)**	**Average magnitude (pixels)**
1	20	23	22
2	20	23	22
3	25	23	24
4	30	15	23
5	23	17	20
6	23	18	22
7	27	18	22
8	23	20	22
9	25	20	23
10	24	22	23
Average	**24**	**20**	**22**
SD	**3.01**	**2.84**	**1.05***

*This value is considered as 2 pixels as there is no decimal in pixels number.

Table 4.8: Motion vector magnitude estimation results for volunteers.

Patient ID	Magnitude of hands MV (pixels)	Magnitude of arms MV (pixels)	Average magnitude (pixels)
14	20	12	16
15	17	17	17
16	18	-	18
17	22	20	21
18	22	23	22.5
19	23	20	22
20	17	17	17
21	23	22	22.5
22	22	20	21
23	10	13	11.5
24	24	20	22
25	13	18	15.5
26	23	20	22
Average	**20**	**19**	**18**
SD	**4.3**	**3.2**	**3.5***

* This value is considered as 4 pixels as there is no decimal in pixels number.

Table 4.9: Motion vector magnitude estimation results for patients.

In this case, we were able to establish two different classifications for the hands and for the arms. The first classification is based on three categories while the second one is based on six categories, in accordance with some of the ranking defined by the rheumatologist. The first classification for the hands and for the arms is defined in Table 4.10 according to the thresholds found using volunteers results (Fig. 4.38), the patients results (Fig. 4.39) and the combination of both (Fig. 4.40) and their standard deviation as it was defined in the previous thresholding process.

The principle here is that the larger the magnitude of the motion vector, the more extensive is the motion capabilities of the subject. As RA reduces the motion capabilities of the patient, the level of the severity of the illness is considered higher when the magnitude of the motion vector is smaller.

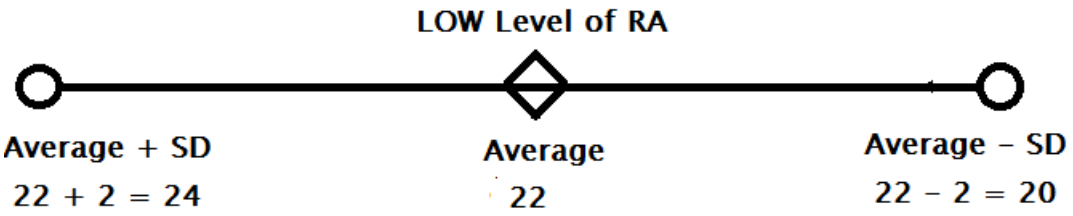

Fig. 4.38: Low level of RA according to volunteers' motion vector average and SD.

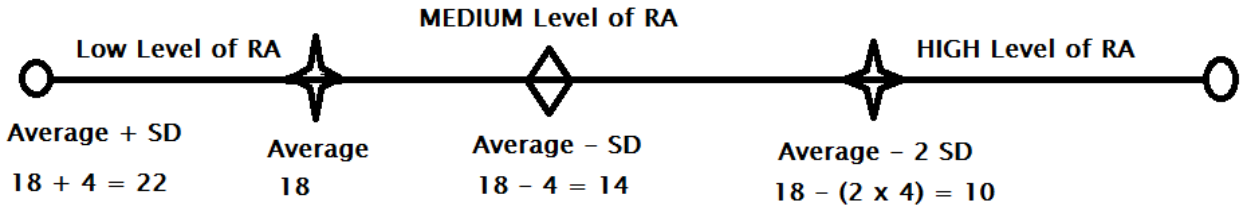

Fig. 4.39: Distribution of RA level according to patients' motion vector average and SD.

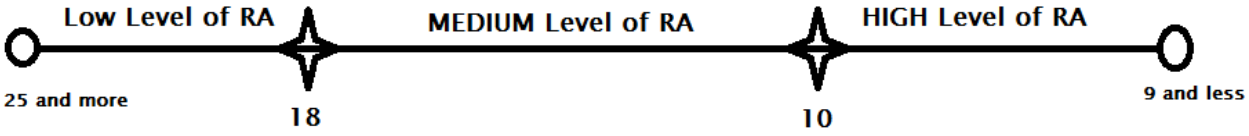

Fig. 4.40: Thresholds according to all participants' results and SD.

In the diagrams of Fig. 4.38, 4.39 and 4.40, the symbols define values as follows:

 Important point (average, average + SD or average + 2 SD) which is not selected as threshold.

 Important point (average, average + SD or average + 2 SD) which is selected as threshold.

 Start and end points.

Level of severity	Average of motion vector magnitude of hands and arms (pixels)
High	< 10
Medium	10-17
Low	18-24
Zero	≥ 25

Table 4.10: Block matching correspondence with the three categories classification.

It was also possible, based on the average of the results and the standard deviation (SD) of volunteers (Fig. 4.38) and patient (Fig. 4.39), to have a classification based on six categories that the rheumatologist used for some patient (Fig. 4.43 and Table 4.11). To achieve those six categories we were able to combine hand and arm results by taking the average of the two results. Table 4.11 defines the six categories based classification that we obtained.

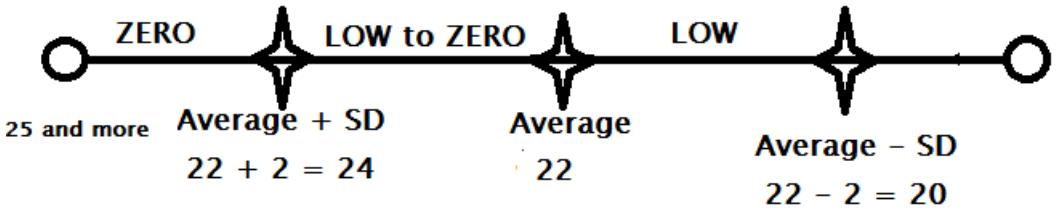

Fig. 4.41: Low level of RA according to volunteers' motion vector average and SD for classification based on six categories.

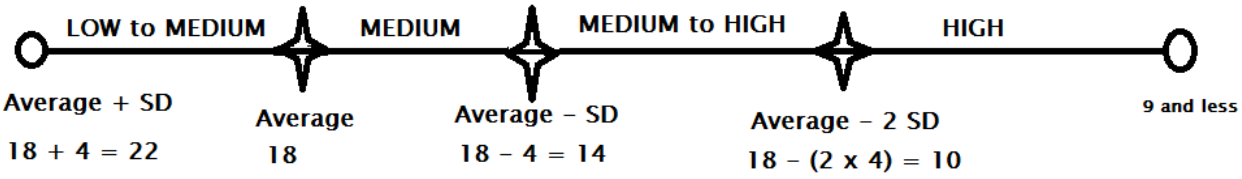

Fig. 4.42: Distribution of RA level according to patients' motion vector average and SD for classification based on six categories.

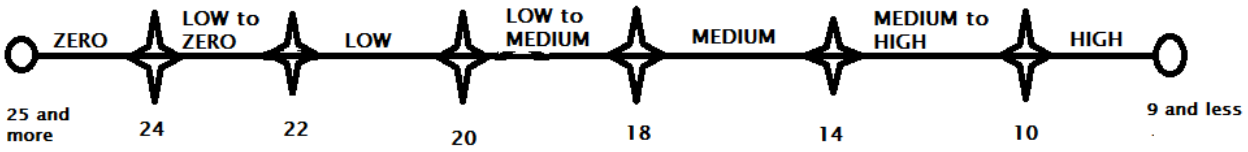

Fig. 4.43: Thresholds according to all participants' motion vector average and SD for classification based on six categories.

In the diagrams of Fig. 4.41, 4.42 and 4.43, the symbols define values as follows:

 Important point (average, average + SD or average + 2 SD) which is not selected as threshold.

 Important point (average, average + SD or average + 2 SD) which is selected as threshold.

 Start and end points.

Level of severity	**Average of motion vector magnitude of hands and arms (pixels)**
High	< 10
Medium to High	10-13
Medium	14-17
Low to Medium	18-19
Low	20-21
Low to Zero	22-24
Zero	≥ 25

Table 4.11: Block matching correspondence with rheumatologist's classification.

To determine the low level threshold as was done for the previous methods, we added the average motion vector magnitude for the volunteers with standard deviation (Table 4.8, Fig. 4.41): 22 ± 2 ≈ between 20 and 24 pixels. We defined the distinction between the low level and the low to zero level by using the standard deviation on the range of low level: 22 -2 ≈ between 20 and 22 pixels.

For the medium level we added the average of the patients' motion vector with the standard deviation (Table 4.9) to determine the range of motion vector magnitude corresponding to the medium level: 18 ± 4 ≈ between 14 and 22 pixels as the low level threshold was set already to 18 pixels. To set the threshold between low to medium and medium, we used the standard deviation as: 18 +2 ≈ 20 pixels (Fig. 4.43) and 18- 4 ≈ 14 pixels (Fig. 4.42). From this we had the low to medium (between 18 and 20 pixels) and medium (between 14 and 18 pixels). For the medium to high we subtracted the standard deviation from the medium threshold: 14 - 4 ≈ 10 and the medium to high is then set between 14 and 10 pixels. The high level is when the motion vector is less than 10 pixels.

A limitation to this method is the influence of the scaling factor on the results. In this study it was avoided by having a solid structure on which the camera was fixed. That avoided the influence of the scaling factor by the fact that all videos were taken from the same distance. To generalize the results of the present research one needs to use the same distance (distance between the camera and the subject: 0.8 m) as it was used to have the same scaling.

4.7 Infrared based system and See5 classification

As mentioned in the first chapter, the results of this research are compared to the results from previous work based on an infrared imaging approach [3], [4]. The previous classification used an infrared camera (Fig. 4.44) to monitor the distribution of temperature over the most affected joints (Fig. 4.45). The results that were obtained from that imaging modality used the See5 classification. In the analysis of the results of this project, in Chapter 5, our classification is compared to the one obtained from See5. For our classification, we used the same patient participants, and the data collection was performed on the same day, at the same location, and at the same time when the infrared images were collected.

Fig. 4.44: A320 Infrared Camera from FLIR Systems (FLIR Systems, 2007) used for See5 classification.

The FLIR A320 Infrared (IR) Camera (Fig.4.44) was used to measure the temperature of joints that was processed by See5 classification. It has an uncooled microbolometer focal plane array of 320 × 240 pixels, acquiring at a refresh rate of 50/60 Hz [3]. The range of operation of this camera is from 7.5 μm to 13 μm in the far IR spectral range of the electromagnetic spectrum. It has a 24 mm germanium lens with an anti-reflective coating that renders a field of view of 25˚x 18.8˚, with a minimum focus distance of 0.3 m. The A320 IR camera has a thermal sensitivity of 0.07 ˚C at 30 ˚C and can measure temperature ranges from -20 ˚C to +120 ˚C. The way that the images were taken enabled the user to view the images live and make manual adjustments to the camera for the best possible images to be captured [4].

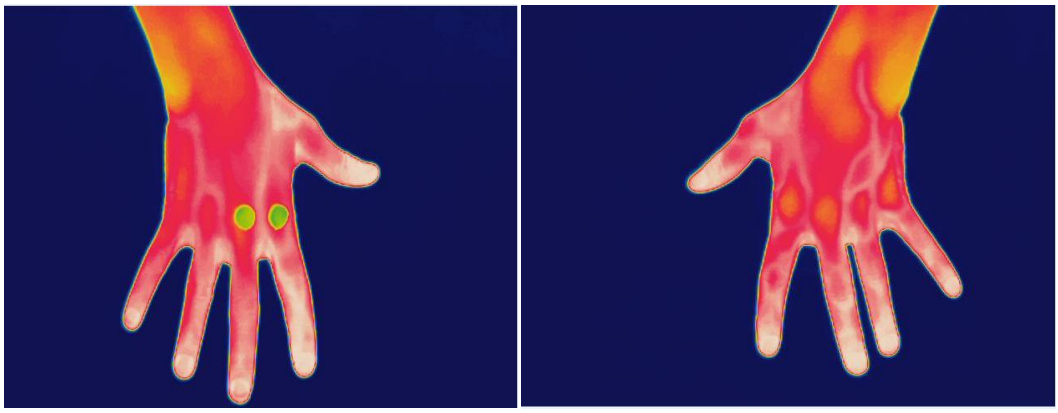

Fig. 4.45: Sample infrared images used to obtain temperatures used by See5 classification, image of hands: a) with markers and b) without markers.

The classification of severity obtained from the IR image modality called See5 classification uses three different levels: low, medium and high. All the patient participants were classified according to those three levels of severity.

4.8 Graphical User Interface (GUI) description

The Human Computer Interaction (HCI) happens through the user interface. For the tests based on the angles estimation method (section 4.5) and the motion vector based method (section 4.6) presented for the current research, a dedicated graphical user-interface was designed where the user can access all implementations and test the motion capabilities of the subject or patient using a recorded video or a sequence of images. The description of the GUI helps to understand the two methods considered. The user interface assists the user to find the results that are needed to assess whether the subject has RA or not and to determine the level of severity of the illness. The main user interface (Fig. 4.46) shows all the options. The user, in fact, is offered two main methods (angles estimation based-method and motion estimation based method) to evaluate the motion capabilities of the subject. Those methods are shown in the user interface as buttons ("Hand" and "Limb" buttons for the angles estimation, and the

"Motion Estimation" button for the motion estimation based method). There are also some extra functions such as "Exit", "Live video" and "Process video" buttons.

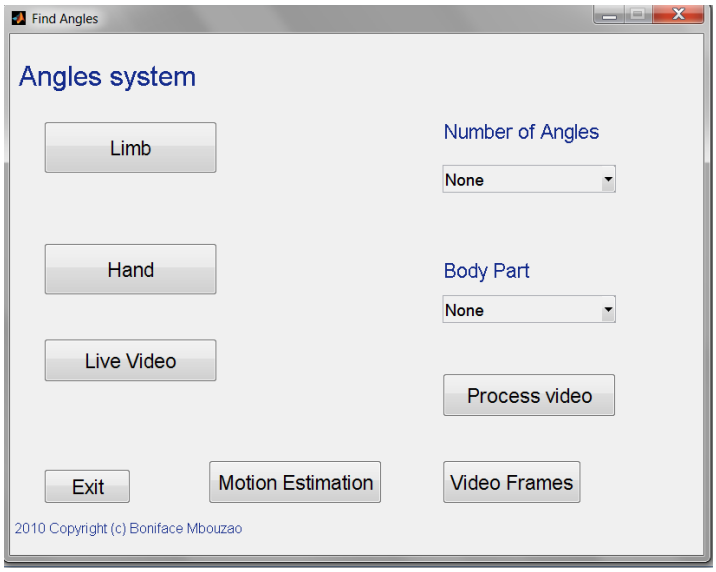

Fig. 4.46: Graphical User Interface (GUI) of the System.

To start the system, the user needs to have all videos of the subject or patient recorded already in AVI format. The camera described in section 4.2.1 is used to record the videos of volunteers and patients. It is one of those videos that the user will choose for the image processing through the Graphical User Interface (GUI). The detailed functionalities associated with each button of the main user interface are further described in Appendix H.

Summary

The present research project needed to develop a methodical approach. This methodology consists, first, in formulating the objectives of the research and second, in recruiting people as volunteers and patient participants to the research. Those two first

steps were possible through the flyers that were posted for volunteers and through our specialist Dr. Jacob Karsh who advertised our research at the Ottawa General Hospital so that patient participants who were willing to participate could contact us. Before that, we obtained the ethical approval from three different ethic boards of the three institutions involved in this research: the Ottawa General Hospital, Carleton University and the University of Ottawa. The third step was to define the type of movement that could help to measure the human capabilities and to implement the tool that can give quantitative evaluation of motion capabilities. In this chapter, the methods and the analysis of the methods were presented. Three different methods have been investigated for this research. The criteria of classification on the relative severity of RA for each method were presented. The presentation and analysis of the results is conducted in the next chapter.

Chapter 5: Results and Comparisons

5.1 Introduction

The results of the experiments presented in this thesis are here analyzed and compared to the results obtained from previous studies, and to the rheumatology specialist's evaluation. The patients who agreed to participate in this investigation were tested on both systems: on the infrared based system and on the system detailed in this thesis that focuses on motion estimation. The fact that the same patients were tested with both systems, on the same day, at the same location, helps to derive a valuable comparison between the results and the efficiency of both examination platforms. The comparison conducted will be in reference to the rheumatologist's evaluation, which is based on his extensive experience and on technologies currently used in medical practice for diagnosing RA. The purpose of these comparisons is not to declare which method is better or which one is the most efficient, but rather to correlate their findings and determine how infrared imaging and vision based motion estimation can be combined to produce an RA diagnostic tool with increased reliability. Another purpose of this comparison is to determine whether or not classification categories similar to those used by rheumatologists can be achieved. This would be helpful for long-term monitoring of RA patients, as the ultimate goal is to transform the proposed instrumentation into a user-friendly tool to help diagnose and monitor the disease. In fact, for the evaluation of the level of illness and to give proper medication to RA patients, one preferably uses the same categories as those typically considered by rheumatologists.

In the context of this research, three different methods using digital image processing are proposed to evaluate the motion capabilities of the RA patients, as detailed in chapter 4. The goal is to classify, according to the estimation of motion capabilities, the level of severity of illness of the subject. The three approaches are:

i) Classification based on Sum of Absolute Difference (SAD);
ii) Classification based on arm angles determination;
iii) Classifications based on motion vector estimation.

In each case, the results are interpreted for the classification of the illness severity. A pattern of general classification, in terms of the results of video processing, is determined for each category of classification. A table showing the classification is presented for each test in this chapter. Those tables show the level of severity of RA as a function of the motion capabilities.

For the tests and experiments, thirteen patients were enrolled, as well as ten volunteers who were never diagnosed with RA. The participants were tested with the proposed motion estimation system, and their images and videos were processed and analyzed. The comparison with the other two conclusions on the severity of RA which are the infrared based classification and that from the rheumatologist's evaluation is performed for each patient. The three methods are examined successively.

5.2 Experimental results based on SAD

Hand movement videos were collected for each patient. The computation of SAD values from frame to frame for each patient and for each type of movement is reported in Table 5.1, with its smallest value on top of each cell and its largest value at the bottom. The computation is performed for each of the eight videos, for each patient. They consist of four videos of two different movements for the left and right hands respectively. This includes open and close hand, slowly and rapidly, and the movement of separating fingers, slowly and rapidly. The results reported in this table are the absolute intensity difference from corresponding pixels between successive frames. Those results give the smallest and largest energy observed from one frame to another for each patient, as described in section 4.4.

Patient ID	Video 1 Open and close rapidly right hand	Video 2 Open and close slowly right hand	Video 3 Separate fingers rapidly right hand	Video 4 Separate fingers slowly right hand	Video 5 Open and close rapidly left hand	Video 6 Open and close slowly left hand	Video 7 Separate fingers rapidly left hand	Video 8 Separate fingers slowly left hand
14	0.125 3.833	---------- ----------	0.708 3.666	0.708 1.666	0.083 4.500	0.041 3.500	0.166 3.625	0.333 4.166
15	1.166 3.750	0.666 3.500	0.833 3.208	0.666 2.500	0.583 3.500	0.625 2.000	1.000 2.833	0.625 1.708
16	0.833 5.000	0.666 4.000	0.083 2.933	0.666 3.333	0.083 3.333	0.208 2.833	0.333 2.416	0.166 2.000
17	0.666 8.166	0.666 6.166	0.800 8.400	0.533 4.000	0.666 6.533	0.533 3.866	1.333 8.933	0.533 5.466
18	1.200 6.666	0.666 5.733	0.666 8.333	0.533 6.333	0.666 8.133	0.533 6.333	0.533 6.533	0.533 5.466
19	0.666 3.333	0.666 2.333	0.666 3.200	0.666 2.666	1.066 6.400	0.666 3.200	1.200 6.000	0.666 2.933
20	0.666 4.666	0.666 2.333	0.666 4.333	0.666 2.333	0.666 4.666	0.666 3.600	0.666 6.000	0.666 3.666
21	0.850 4.350	0.850 3.150	1.250 4.750	0.850 3.000	1.066 6.333	0.533 5.333	1.333 6.533	0.533 5.066
22	0.583 2.000	0.583 2.166	0.583 2.166	0.583 1.916	0.625 3.333	0.625 3.166	0.625 1.708	0.625 3.291
23	0.666 5.866	0.533 2.800	0.800 5.833	0.533 2.533	1.083 4.833	0.583 3.500	0.833 6.000	0.583 2.708
24	0.330 3.000	0.660 2.330	0.660 3.330	0.660 2.500	0.625 5.330	0.660 4.330	0.625 3.500	0.625 3.833
25	1.330 5.000	0.660 3.660	0.660 7.500	0.660 7.000	0.666 5.333	0.625 4.000	0.625 4.416	0.583 4.833
26	0.666 3.333	0.583 2.833	0.625 2.708	0.666 2.533	0.666 5.066	0.666 5.066	0.666 3.066	0.666 3.066

Table 5.1: Results of SAD on motions for each patient.

5.2.1 Estimation of the mobility based on SAD

For each patient, averages of the minimum and maximum SAD values over the eight different movements are computed (Table 4.2). This gives the sense of the average motion in the movement of the hands for each patient. This average includes both hands, left and right, and it is assumed that both hands are affected by RA with the same level of severity, RA disease being generally recognized as symmetrical. Those

average values are used to estimate the motion capabilities of each patient.

The range between average maximum and minimum SAD values that happens in between successive video frames is obtained for each patient, as for volunteers in section 4.4.3, by subtracting the average minimum from the maximum average SAD value. From that subtraction, one obtains the approximate representation of the amount of motion, which is encoded through the average intensity difference that takes place from frame to frame. Those values are reported in Table 5.2 and can be compared between patients. A classification based on those values is achieved as presented in section 4.4. A classification of the level of severity can then be obtained. The classification is based on the fact that for six out of ten volunteers, we obtained the difference between their maximum and minimum SAD values, as being less than 3.52 (Table 4.1). For a healthy person, the level of severity is low to zero according to the rheumatologist classification. Then from one level to another, motion estimation, in terms of intensity changes of image pixels, doubles. For this reason, we established three thresholds to classify the patients in three different categories: low, medium, and high. We refer here to the three categories for RA level used by the previous studies, based on infrared images [3], [4]. This classification shows that less than 3.52 corresponds to a low level of RA. Between 3.53 and 6.02 is medium and over 6.02 is high as explained in section 4.4.3.

5.2.2 Classification of level of severity of patient according to their SAD results

The SAD based classification can be applied to the patients results to obtain the level of severity of each of them as it is shown in Table 5.2. In general, the assumption, as explained above, is that the lower variation from frame to frame, the more mobility capability the patient has. In fact, a healthy subject has the capacity of performing movement with a regular displacement from frame to frame while an RA patient has large differences between displacements from frame to frame because of his/her difficulties to perform uniform movements. This assumption is important for the

classification, but not enough, because it does not work in all cases. There are some mismatches when we see the comparison with other classifications such as the rheumatologist's one, as shown in Table 5.3, and that tends to demonstrate the limitations of this assumption.

Patient ID	Range between maximum and minimum SAD values	Classification Based on SAD
22	1.86	Low
15	2.10	Low
26	2.80	Low
16	2.85	Low
24	2.91	Low
19	2.97	Low
14	3.25	Low
20	3.28	Low
23	3.55	Medium
21	3.90	Medium
25	4.48	Medium
17	5.72	Medium
18	6.02	Medium

Table 5.2: Classification of patients in terms of level of severity according to SAD.

5.2.3 Comparison with See5 Classification and rheumatologist's evaluation

Compared to the See5 classification, the SAD-based classification has more mismatches than with the rheumatologist's evaluation, considered for us as the reference classification (Table 5.3 with mismatches highlighted). For this reason, the SAD method needs to be confirmed by other tools of classification. It cannot be the only reference for an evaluation of the level of severity. This classification based on SAD can provide the user with at best a rough idea about the motion capabilities of the patient, and therefore, only a general idea about the level of severity of the disease. With the

classification based on SAD, the method is not precise enough to use the six categories proposed by the rheumatologist. It can only provide a classification based on three categories, similar to that used by the See5 classification.

Patient ID	See5 Classification	Rheumatologists' evaluation	Classification based on SAD
14	High	Medium	Low
15	Low	Low to Medium	Low
16	Medium	Low to Medium	Low
17	Low	Low	Medium
18	Low	Low to Zero	Medium
19	Low	Low to Zero	Low
20	Medium	Low to Medium	Low
21	Low	Low to Zero	Medium
22	Low	Low	Low
23	High	Medium to High	Medium
24	Low	Low to Zero	Low
25	Medium	Medium	Medium
26	Low	Low to Zero	Low

Table 5.3: Comparison between SAD based classification, See5 classification, and the rheumatologist's evaluation.

5.2.5 Classification of volunteers' experimental results using SAD

As mentioned in the previous chapter, the result of each volunteer should be classified as low level of severity as they all presented no signs of RA. Based on the criteria defined in section 4.4, Table 5.4 shows the level of severity according to the SAD based classification of each volunteer with erroneous classifications highlighted.

Volunteer ID	Range between maximum and minimum SAD values	Classification
1	2.50	Low
2	3.75	Medium
3	1.87	Low
4	2.16	Low
5	5.36	Medium
6	2.16	Low
7	2.50	Low
8	3.63	Medium
9	2.16	Low
10	3.56	Medium

Table 5.4: Volunteers classification using SAD results.

5.3 Experimental results based on angles of arm joints

The classification obtained from the arm minimum bending angles is based on the simplified kinematics of the human arm as defined in Chapter 3. The main idea is that, knowing the motion capabilities of the human skeleton from the kinematic point of view, it is possible to compare the subject's arm motion capabilities to the one expected from a healthy person. The difference between those values can help to estimate the level of severity of RA and achieve a proper classification. The computation of the angles of the skeleton is performed by considering the center of each arm segment as specified in section 4.5.

The values of the three different angles for the right and left arms for each patient are reported in Table 4.5. The shoulder, the elbow and the wrist angles are computed for the right and the left arm individually, and are required for both arms for each patient to support the evaluation.

5.3.1 Classification based on six arm joints

The computation of the average of the six angles for each patient is performed in order to classify the severity of the illness (Table 5.5). The classification is performed here following the same three categories found in the infrared based classification that we use as one of the comparatives. This is because we could not find criteria to classify

the severity of the illness based on the six categories of the rheumatologist, in terms of the arm minimum bending angle average as explained in the previous chapter. From the average of those six angles, we can determine if one can find the pattern of classification based on the assumption that, if the average value of minimum bending angle that the subject can reach is high, then the illness is more severe. We present a classification based on the six arm angles, as well as a classification based on only the most affected joint of the arm (wrist). The two classifications will be compared according to their capability of being closer to the rheumatologist's evaluation.

5.3.2 Classification according to all arm angle values

The classification of severity is first performed according to the average of all the angles of the arms. The threshold of 85.35 degrees as low level is the result of the average of normal arm joints of a healthy subject (Fig. 4.31 and Table 4.4) and the average of volunteers' minimum arm bending angles explained in section 4.5.2. The 104.85 degrees is the estimation average of the minimum bending of arm joints plus twice their standard deviation (section 4.5.4, Fig. 4.30). This classification can be compared to the rheumatologist's evaluation to verify its effectiveness (Table 5.6).

Patient ID	Average of arms joints minimum bending angles (degrees)	Classification based on minimum arm bending angles
15	59.78	Low
22	71.91	Low
26	79.45	Low
14	80.40	Low
18	83.70	Low
17	83.88	Low
21	83.96	Low
20	90.63	Medium
19	90.70	Medium
24	91.05	Medium
25	93.75	Medium
23	94.88	Medium
16	95.11	Medium

Table 5.5: Classification based on average minimum bending of the six angles of both arms for each patient from the less to the most affected.

5.3.3 Comparison with infrared based classification and rheumatologist's evaluation

Comparing the classification obtained from the average of minimum arm bending angles to the rheumatologist's evaluation, three mismatches are noticed (highlighted in Table 5.6). One can also observe that the classification based on the average of all minimum arm joints bending angles is less close to the specialist's evaluation than the See5 classification. It is performing better (three mismatches) than the SAD based classification (five mismatches), but on different patients (Table 5.3 and Table 5.6). This performance can be explained by the fact that from the six joints that get measured in the simplified model of the human arm, only two (the two wrist angles) are the most affected by RA in more than 66% of cases of RA patients, as discussed in section 2.5. The other joints are affected between 33% and 66% of cases of RA patients as shown in Table 2.1. The classification obtained by considering all arm angles cannot be taken alone for a RA diagnosis process. It rather privileges a classification based on the most affected joints as the one proposed for wrists only in section 4.5.4.

PATIENT ID	See5 Classification	Rheumatologists' Evaluation	Classification based on minimum arm bending angles
14	High	Medium	Low
15	Low	Low to Medium	Low
16	Medium	Low to Medium	Medium
17	Low	Low	Low
18	Low	Low to Zero	Low
19	Low	Low to Zero	Medium
20	Medium	Low to Medium	Medium
21	Low	Low to Zero	Low
22	Low	Low	Low
23	High	Medium to High	Medium
24	Low	Low to Zero	Medium
25	Medium	Medium	Medium
26	Low	Low to Zero	Low

Table 5.6: Classification based on all minimum arm bending angle and comparison with rheumatologist's evaluation and See5 classification.

5.3.4 Classification based on wrists angles only

The wrist is known as one of the most affected joints of the arm for a RA patient. It is, then important to consider the two wrist joints of the arms separately. It this case, one needs to take the average angle of only the two wrists of the arms of each patient. A classification can be achieved based on this average. When we take the average angle of the two wrists of each patient, a new classification criterion can be considered. Again the larger the average minimum bending angle is, the higher the severity of the illness is. The thresholds are set based on the average value of wrist angles of volunteers discussed in section 4.5.4.

With this classification, a new table of classifications can be developed (Table 5.7). There are important changes in this new classification compared to the previous one that was based on the average minimum bending angles for all arm joint angles (Table 5.6).

Patient ID	Left wrist angle (degree)	Right wrist angle (degree)	Average (degree)	Classification based on wrists angles
15	93.4	42	67.7	Low
26	114.5	100.1	107.3	Low
18	127.8	117.3	122.55	Low
17	131.6	115.7	123.65	Low
22	121.9	136.4	129.15	Low
19	149.3	118.3	133.8	Low
24	133	137.2	135.1	Medium
21	130.9	139.8	135.35	Medium
23	142.4	129.3	135.85	Medium
20	132.7	145.2	138.95	Medium
14	143.1	150.6	146.85	Medium
16	156.4	152.4	154.4	Medium
25	164.5	162.2	163.35	Medium

Table 5.7: Classification based on minimum bending angles for the wrists only from the least to the most affected.

5.3.5 Comparison of wrist based classification with rheumatologist's evaluation and See5 classification

Compared to the rheumatologist's evaluation, this classification, based on the average of wrist angles, is one of the best matches that we can obtain by using the classification based on three categories. With fewer mismatches, this classification is as good as See5 classification, which has one mismatch when compared with the rheumatologist's evaluation. This confirms the fact that the angles of the wrists are the most reliable joints for performing RA evaluation. The only challenge in this classification is the fact that it is based on three categories while the rheumatologist's evaluation is based on six categories. This classification finds the level of severity, but it is not always as detailed as the rheumatologist's appreciation to fully monitor the illness. According to the rheumatologist's evaluation, the classification based on wrist angles gives better results (Table 5.9). The best solution could then be to find a classification that could provide extra refinements, such that the classifier can further

help to treat the patient. To obtain such results, further developments are proposed using a more formal scheme for motion estimation in section 5.4.

PATIENT ID	See5 Classification	Rheumatologists' Evaluation	Classification based on wrists angles
14	High	Medium	Medium
15	Low	Low to Medium	Low
16	Medium	Low to Medium	Medium
17	Low	Low	Low
18	Low	Low to Zero	Low
19	Low	Low to Zero	Low
20	Medium	Low to Medium	Medium
21	Low	Low to Zero	Medium
22	Low	Low	Low
23	High	Medium to High	Medium
24	Low	Low to Zero	Medium
25	Medium	Medium	Medium
26	Low	Low to Zero	Low

Table 5.8: Classification based on wrist minimum bending angles and comparison with rheumatologist's evaluation and See5 classification.

5.3.6 Classification of the measurements performed on volunteers based on all arms angles and on wrist angles only

We can also estimate the level of severity of volunteers based on the two criteria of classification used in the previous section. In theory we should have for every volunteer a low level of RA. As Table 5.9 shows, the wrist only based classification is performing as well as classification with all arm angles. In fact, the wrist based classification places almost all volunteers except two (same volunteers as all angles based classification) in the low level of RA category, which is what we are expecting. This gives another confirmation of the previous studies that showed that wrist is one of the joints that is reliable for RA level evaluation.

Volunteer ID	All angles average (degree)	Wrists angles Average (degree)	Classification based on all angles	Classification based on wrists angles
1	75.03	112.75	Low	Low
2	83.81	135.37	Medium	Medium
3	88.77	140.59	Medium	Medium
4	81.10	123.50	Low	Low
5	82.81	107.61	Low	Low
6	72.72	109.07	Low	Low
7	73.26	111.99	Low	Low
8	77.46	106.51	Low	Low
9	81.34	134.46	Low	Low
10	84.42	129.30	Low	Low

Table 5.9: Classification of volunteers according to average of all arm joints versus wrist joints only.

5.4 Experimental results based on matching blocks for motion estimation

To achieve better results, based on the same categories that are used by the rheumatologist, a classification based on image processing is investigated. By finding the magnitude of motion vectors, one can classify the patient mobility capabilities. For this experimental evaluation, we had two different classifications: a first one based on the three categories defined by the See5 classification, and a second one based on the six categories used by the rheumatologist.

5.4.1 Classification based on three categories

The infrared based classification (See5) uses three levels of severity, which are low, medium and high. In those terms, the level of severity of the infrared image based classification can help to know in which range of severity the patient is. Eventually, the rheumatologist might need further examination to determine the corresponding level of severity of the disease. Using the methods proposed in the previous chapter, the examination platform can determine, in function of the mobility capabilities, the level of severity according to the infrared based classification. Table 5.10 shows the block matching based motion estimation results corresponding to each level of severity

categories. The level of severity estimation is performed for the hand movement videos and for the arm videos. Both of them give proper results when compared to the rheumatologist evaluation. The level of severity is measured in terms of the maximum magnitude of the motion vector obtained during the processing of the patient videos. The threshold of 25 pixels, as a magnitude of motion between successive frames, is obtained from the volunteers' videos processing, and the intermediate thresholds are obtained as described in section 4.6.

The magnitude of motion vector from the processing of hand (hand opened and closed, slowly and quickly) and arms (arm joints bent slowly and quickly) are computed by taking the average value of the motion vectors of the hands and arms (Table 5.10). The results on the arms are taken into account because they involve the wrist angles that are among the most affected joints in RA, along with all the hand joints, as shown in chapter 2. The motion vector involving those parts of the human body can give a better sense of the motion capabilities of the patient.

Patient ID	**Magnitude of hand MV (pixels)**	**Magnitude of arm MV (pixels)**	**Average magnitude (pixels)**	**Classification (3 categories)**
14	20	12	16	Medium
15	17	17	17	Medium
16	18	-	18	Low
17	22	20	21	Low
18	22	23	22.5	Low
19	23	20	22	Low
20	17	17	17	Medium
21	23	22	22.5	Low
22	22	20	21	Low
23	10	13	11.5	Medium
24	24	20	22	Low
25	13	18	15.5	Medium
26	23	20	22	Low

Table 5.10: Matching block based motion estimation classification with three categories.

5.4.2 Comparison with the See5 classification and rheumatologist's evaluation

The classification that one can find from this method is better than the one obtained from the previous one regarding its similarity with the rheumatologist evaluation and See5 classification. There is no important mismatch between this classification and the rheumatologist's evaluation (Table 5.11) when only three categories are considered. This result is, then, in the same order of accuracy as what was obtained from See5 classification. In fact, with See5 classification, patient 14 is detected as having a high level of severity while the rheumatologist's evaluation and the matching block based motion estimation estimate it as medium. As the goal of the classification is to have as many details as possible on the level of severity, the matching block based motion estimation can be further refined, in the following section, in order to provide more detailed estimates.

Patient ID	**See5 Classification**	**Rheumatologists' Evaluation**	**Motion Estimation based classification (3 categories)**
14	High	Medium	Medium
15	Low	Low to Medium	Medium
16	Medium	Low to Medium	Low
17	Low	Low	Low
18	Low	Low to Zero	Low
19	Low	Low to Zero	Low
20	Medium	Low to Medium	Medium
21	Low	Low to Zero	Low
22	Low	Low	Low
23	High	Medium to High	Medium
24	Low	Low to Zero	Low
25	Medium	Medium	Medium
26	Low	Low to Zero	Low

Table 5.11: Comparison between block matching based motion estimation, See5 classification and rheumatologist's evaluation.

5.4.3 Classification based on six categories

For treatment purposes, the rheumatologist's classification of the level of severity of RA is used as the reference. This classification has six categories. In fact, the aim is to

match as much as possible the rheumatologist categories. With the previous approaches investigated in this research, it was not possible to achieve a classification based on six categories and to fully match them with the rheumatologist's conclusions. The motion estimation based on matching blocks classification enables us to make a classification based on the six categories used by the rheumatologist. By defining the same separations that we achieved in the three categories based classification to obtain the intermediate thresholds, we determined the necessary thresholds for the six categories based classification, as detailed in section 4.6.2. With this extension, the present research could then match well with the rheumatologist's classification. The six different levels of classification of the rheumatologist are low to zero, low, low to medium, medium, medium to high and high. In this research, an extra level of zero was added to be able to classify some exceptional results that could be reached by volunteers. In general, a healthy subject should be classified as low to zero, in terms of level of RA, but that same level can also be reached by an RA patient at the beginning of the illness. A new specification based on the six categories set up by the rheumatologist would be desirable (Table 4.11) in terms of the average magnitude of the motion vectors in the hands and arms. The level of severity is then determined according to the six categories related to the magnitude of the motion vectors of arms and hands. The seventh category is an exceptional one rarely reached by a subject. Thus, it is not counted among the categories.

The results are presented, following the rheumatologist's classification pattern in Table 5.13.

Patient ID	Magnitude of hand MV(pixels)	Magnitude of arm MV(pixels)	Average magnitude (pixels)	Classification (6 categories)
14	20	12	16	Medium
15	17	17	17	Medium
16	18	-	18	Low to Medium
17	22	20	21	Low
18	22	23	22.5	Low to Zero
19	23	20	22	Low to Zero
20	17	17	17	Medium
21	23	22	22.5	Low to Zero
22	22	20	21	Low
23	10	13	11.5	Medium to High
24	24	20	22	Low to Zero
25	13	18	15.5	Medium
26	23	20	22	Low to Zero

Table 5.12: Matching block based motion estimation classification with six categories.

5.4.4 Comparison with See5 classification and the rheumatologist's evaluation

When we compared the latest classification, based on the six categories, to the See5 classification and the rheumatologist's evaluation, this classification is a very good match with that of the rheumatologist (Table 5.13). This means that the classification based on the average magnitude of motion vector for the hands and arms performs the best, when compared to the other two approaches developed in this thesis, to evaluate the level of severity of RA. This method also reduces the risk for some possible errors by the fact that the computations are all performed by an automated system. For the computation of motion vectors, there is no user interaction required, unlike with the two former methods.

Patient ID	See5 Classification	Rheumatologists' Evaluation	Motion Estimation based classification (6 categories)
14	High	Medium	Medium
15	Low	Low to Medium	Medium
16	Medium	Low to Medium	Low to Medium
17	Low	Low	Low
18	Low	Low to Zero	Low to Zero
19	Low	Low to Zero	Low to Zero
20	Medium	Low to Medium	Medium
21	Low	Low to Zero	Low to Zero
22	Low	Low	Low
23	High	Medium to High	Medium to High
24	Low	Low to Zero	Low to Zero
25	Medium	Medium	Medium
26	Low	Low to Zero	Low to Zero

Table 5.13: Comparison between See5 classification (infrared images), rheumatologist's evaluation and block matching based motion estimation with six categories.

5.5. Compilation of volunteer results based on six categories

For this study, ten volunteers were recruited. They underwent the same tests as the patients. The goal was to make sure that this system would mark the difference between patients and volunteers. The level of severity for the volunteers is expected to be low to zero, or at least low.

Using the block matching based motion estimation on the ten volunteers; the results obtained confirmed our hypothesis that healthy persons should have a level of severity from low to zero (Table 5.14). In fact, the result from volunteers shows that the proposed approach is reliable.

Volunteer ID	Magnitude of hand MV(pixels)	Magnitude of arm MV(pixels)	Average magnitude (pixels)	Classification (6 categories)
1	20	23	22	Low to Zero
2	20	23	22	Low to Zero
3	25	23	24	Low to Zero
4	30	15	23	Low to Zero
5	23	17	20	Low
6	23	18	22	Low to Zero
7	27	18	22	Low to zero
8	23	20	22	Low to zero
9	25	20	23	Low to zero
10	24	22	23	Low to zero

Table 5.14: Classification of volunteers using block matching based motion estimation.

5.6 Conclusion

From three proposed modes of classification, the SAD based classification monitors the amount of motion that the subject is generating during movements. The advantage of this method is to measure the displacement performed during the movement. The arm angle based classification provides significant results with three levels of severity. The wrist angle based classification generates more reliable results. It reaches the same classifications as those defined by the rheumatologist, but based on three categories. The motion vector based classification achieves the same results with three categories. Finally, the results that best match the rheumatologist's evaluation are those from the motion vector based classification expanded to six categories. These results are almost identical to the ones that the rheumatologist reported for each patient.

Summary

In this chapter, the experimental results on 10 healthy volunteers and 13 patients suffering from different levels of RA were analyzed, and the results were compared with the classifications provided by the rheumatologist's evaluation. Three main classifications were identified through the experimental results of the various tests. The

SAD based, the angles based and the motion estimation based classifications were all compared to the See5 classification, based on an alternative infrared imaging technology analysis, and to the rheumatologist's evaluation. The analysis of those results shows that the first two classifications (SAD and angles based) are similar in terms of their performance to the ones obtained from the previous study based on infrared images (See5 classification). The results obtained from the motion estimation technique were able to extend from the three levels of severity detected by the previous study to six levels of severity used by the rheumatologist. This extension made the results obtained from motion estimation based classification the closest ones to the rheumatologist's evaluation. It is then fair to believe that motion based monitoring of RA combined with the infrared based classification previously developed would make it possible for a rheumatologist to use the results of such a multi-modal examination system as an early diagnostic platform while relying on more elaborate HRUS or MRI examinations when necessary. The impact of this work and the contributions that this research makes to facilitate access to diagnosis and monitoring processes of RA form the subject matter of the last chapter.

Chapter 6: Conclusions and Future Work

6.1 Summary

The process of diagnosing and monitoring joint-debilitating diseases, such as RA and other rheumatic diseases, some of which were presented in chapter 2 of this thesis, remains an issue in medical research. Many solutions have been proposed to detect those diseases at an early stage. The difficulties related to most of the current solutions are the accessibility of the technologies and the cost of the examinations and tests (MRI or HRUS). This situation motivates researchers to find new solutions which can become more widely accessible and affordable in hospitals and clinics for the benefit of a larger part of the population.

Our proposed solution aims to rely on a quantitative evaluation of human gestures. In fact, a quantitative assessment can help to compare the motion capabilities of a patient with a healthy person's capabilities. Such a comparison could be performed via a kinematic model of the human skeleton. This comparison can help determine whether the subject suffers from RA or not, and if so, at what level. This procedure is possible only if the kinematic model of the human skeleton is developed properly, especially for joints that are the most affected by RA. The latter have been identified in the literature review of chapter 2 as: the wrist joint, the hand joints, the knee and the toes (metatarsal joints). The kinematics of those specific human joints, especially the arm, wrist and hand joints, are useful for the assessment of human motion capabilities. For this purpose, in chapter 3 of this thesis, we proposed the study of kinematic model of human arms and hands which are among the most affected joints by RA as mentioned above. Yet, the kinematic model of the human arm and hand is complex and for the diagnosing and monitoring process of RA, one needs only to assess specifically the most affected joints. For this reason, we proposed a simplified kinematic model of arm and hand that could give us the necessary estimation of some of the most affected

joints by RA. Those simplified models were extracted from the whole models of the human arm and hand. In the proposed approach, the diagnosis of RA relies on a system that measures the capabilities of movement of a subject and allows a direct comparison between those measurements and similar parameters extracted from healthy subjects. For this project, ten healthy volunteers and thirteen patients participated. The quantitative assessment was made possible through a series of videos of ten predefined hand and arm movements that were presented in chapter 4. The ten movements of hands and arms were defined such that the joints most affected by RA can be evaluated. One of the goals of our proposed solution is to remain simple as much as possible in order to enlarge its accessibility for a low cost. The use of a single camera is part of this preoccupation of developing a simple platform that is easy to use.

For each participant, ten different videos were processed: four videos of the left hand, four videos of the right hand and two videos of the arms. For each of the videos, it was possible to find and quantify human motion capability in various forms: based on SAD, based on joint angles estimation and based on matching blocks (section 4.4, 4.5 and 4.6). That quantification allowed the estimation of the relative level of severity of the illness based on classification criteria that was set using the participants' results and their standard deviation. Criteria of classification of severity were established, and tables were generated to classify the levels of severity in function of the measurements extracted from the processed videos. Some results of our proposed solutions were compared to existing solutions to evaluate our solution's accuracy. For each of the three methods used in our proposed solution, a table of classification of each participant in terms of the level of severity was established. In chapter 5, the results obtained from our proposed solution were compared to the previous solution based on infrared images and to the rheumatologist's evaluation. The second method (based on joints angles estimation) and the third method (based on matching blocks) of the proposed solution were identified as the most reliable compared to the rheumatologist and the infrared system results.

This research project as well as adding a new tool to the process of classification of RA level of severity opens the way of using digital images in diagnosing and monitoring process of the illness. As the introduction of the use of infrared images was an important step in accessibility of diagnosis process, this study adds another step by using digital images. The use of a low level of image processing techniques in this project and the results obtained from them, gives promising results while using more advanced techniques.

The quantitative assessment of human hands and arms mobility could be also an excellent tool to monitor RA over the long term. From one visit to another, one can compare the patients' mobility capabilities to measure their evolution and determine whether the treatment helps or not. The level of severity that can be measured from one visit to another is an important parameter for treatment prescriptions and to monitor how the patient reacts to the treatment over a long monitoring period.

An important aspect of our proposed solution based on human mobility capabilities is its accessibility. The proposed technology is built from one standard digital camera, and can therefore easily be made available in numerous hospitals or medical clinics for much lower cost than sophisticated MRI equipment, and even HRUS devices. Today, digital color cameras are accessible to all and make the examination cost affordable to a vast majority of patients, which is not the case with the MRI and HRUS used currently to diagnose and monitor RA properly. The technologies of MRI and HRUS currently used in medical centres remain very expensive and are less accessible because of their limited availability. This situation results in lengthy waiting lists, which delay the diagnosis of RA. Often, patients wait for several months before being given access to the tests. The delay of diagnosis lets the patient suffer from the disease and the destruction of joint cartilage progress. When, finally, the disease is diagnosed, it is in its critical phase and needs more care to avoid invalidity. With our proposed solution, the possibility of early diagnosis of RA is available for more patients and the possibility of early treatment and delaying invalidity is open. This approach that uses the motion

capabilities of human hands and arms combined with the previously developed infrared system offers an alternative technology that can be fully automated, therefore reducing the impact of interaction between the system and the user, minimizing the need for additional training to read and understand the results, and contributing to improve early diagnosis and long-term monitoring of RA.

6.2 Contributions

The specific contributions of this research are:

i) An examination of the potential of motion capture imaging technologies to perform quantitative evaluation of human gesture in medical context.
ii) The introduction of simplified kinematic mapping with a combination of human hands and arms image processing algorithms to determine the motion estimation of those body parts of the subject from a single camera view.
iii) A simplified vision-based estimator of the relative level of severity of RA that monitors the effects of the disease by classifying the extent of motion capabilities of the subject in a predefined number of categories, in accordance with a medical expert's appreciation.
iv) A table of classification based on the magnitude of motion vectors of hands and arms movement. From the table of classification, one can determine the level of severity of each subject from the results of straightforward imaging tests.
v) A study of classification levels in 3 categories and in 6 categories and comparison of the relative level of RA to that of an expert rheumatologist's evaluation.

This research combined with infrared-based imaging systems proposed in [3] and [4] could eventually contribute to early diagnosis and treatment of RA. By extension, it can be used also to monitor some other joint diseases because it can estimate the level of motion capabilities.

6.3 Future work

Many extensions to this research are still possible. Future work can be oriented in further developing the proposed tool, as well as integrating it within a general framework for diagnosing and monitoring RA with the infrared based approach developed by other researchers in our group. The future work could be oriented towards implementation and performance improvement of the existing tool, and could include:

i) An extension to a larger set of joints affected by RA to select which joints are best to use. This extension to all affected joints can make the proposed approach more reliable in its estimations. Extending the study to include all affected joints, such as toes and knees, could help to perform a medical evaluation that is based on the complete human body motion capabilities.

ii) Further implementation is needed to make this tool faster than it is now. The use of live video in the actual system would be a proper suitable extension. That could aid the rheumatologist in obtaining results in real time.

iii) This research could be used to monitor other joints debilitating diseases.

iv) It also can be used as a tool in telemedicine and could be tested in further research. From the video of a patient far away, the rheumatologist can define proper treatment. The long-term monitoring of a patient who has no access to hospitals could be supported by such a tool.

v) For better confirmation of the results of this present research, systematic MRI tests on a same group of patients would provide a gold standard for verifying our technique.

vi) Integration of this framework with infrared-based imaging systems proposed in [3] and [4] could eventually help to provide a more reliable diagnostic and monitoring system for RA. The possibility of having results from both multi-spectral imaging processes as well as achieving proper classification could serve as a confirmation tool for a rheumatologist in the process of diagnosing and

monitoring RA.

vii) The use of more advanced imaging technologies, such as Kinect sensors, that are well adapted for real-time acquisition and tracking of movement with depth perception also offers a direction of exploration with high potential for benefits in refining the movement capabilities measurements and accuracy.

Bibliography

[1] S. Bériault, Multi-camera system design, calibration and 3D reconstruction for markerless motion capture, Master thesis, University of Ottawa, 2008.

[2] A. Ghazisaeidi, Estimating human limb motion from video sequences with anatomical knowledge, Master thesis, Carleton University, 2011.

[3] C. Adéa, Severity of illness measures of rheumatoid arthritis using thermal infrared imaging, Master thesis, Carleton University, 2009.

[4] A. Ogungbemile , Classification of level of severity of rheumatoid arthritis using machine learning (Decision Tree), Master thesis, Carleton University, 2011.

[5] H. Zhou, T. S. Huang, "Tracking articulated hand motion with Eigen dynamics analysis," Proc. ICCV03, Nice, France, October 2003, pages 1102-1109.

[6] C.-C. Chang, W.-H. Tsai, "Model-based analysis of hand gestures from single images without using marked gloves or attaching marks on hands," in Proc. of Fourth Asian Conf. on Computer Vision, vol. 2, 2000, pages 923-930.

[7] E. Ueda, Y. Matsumoto, M. Imai, T. Ogasawara, "Hand pose estimation using multi-viewpoint silhouette images", Intelligent Robots and Systems, Proceedings IEEE/RSJ International Conference on, vol.4, 2001, pages 1989 - 1996.

[8] I. Albrecht, J. Haber, H. Seidel, "Construction and animation of anatomically based human hand models", Proc. of ACM SIGGRAPH/Eurographics SCA, 2003, pages 26-27.

[9] J. Lin, Y. Wu, T. S. Huang, "Capturing human hand motion in image sequences," in Proc. of IEEE WMVC, 2002, pages 99-104.

[10] Y. Wu, J. Lin, T. S. Huang, "Analyzing and capturing articulated hand motion in Image Sequences", IEEE Trans. PAMI, Vol. 27, No. 12, December 2005.

[11] J. Lin, Y. Wu, T.S. Huang, "Modeling the constraints of human hand motion", IEEE Conferences, Workshop on Human Motion, 2000, pages 121 - 126.

[12] K. Oka, Y. Sato, H. Koike, “Real-time fingertip tracking and gesture recognition," IEEE Transactions on Computer Graphics and Applications, vol. 22, Nov/Dec 2002, pages 64-71.

[13] K. Oka, Y. Sato, H. Koike, “Real-time tracking of multiple fingertips and gesture recognition for augmented desk interface systems," in Proc. of the IEEE Int'l Conf. Automatic Face and Gesture Recognition, 2002, pages 429-434.

[14] G. Johansson, “Visual motion perception”, Scientific American, volume 232, No. 6, 1975, pages 75–88.

[15] D. G. Lowe, “Local feature view clustering for 3D object recognition”, IEEE Conference on Computer Vision and Pattern Recognition, Kauai, Hawaii, December 2001, pages 682-688.

[16] M. Kato, Y. W. Chen, G. Xu, “Articulated hand tracking by PCA-ICA approach,” IEEE Proc. FG06, 2006, pages 329-334.

[17] A. Calin, *Diagnosis and management of rheumatoid arthritis*, Menlo Park, California: Addison-Wesley Pub. Co., Medical/Nursing Division, 1983.

[18] J. Theodosakis, B. Adderley, B. Fox, *Maximizing the arthritis cure*, St. Martin’s Press, New York, 1998.

[19] J. Theodosakis, B. Adderley, B. Fox, *The arthritis cure*, St. Martin’s Press, New York, 1997.

[20] J. Kellgren, “Diagnostic criteria for population studies”, Bulletin of Rheumatic Disease, volume 13, 1962, pages 291-292.

[21] E. B. Gary, S. Firestein, G. S. Pan, *Rheumatoid Arthritis*, Oxford University Press, 2nd Edition, 2006, page 31.

[22] E. D. Harris, Jr, *Rheumatoid Arthritis*, Philadelphia: Saunders, 1997.

[23] F. Arnett, S. Edworthy, D. Bloch, D. McShane, J. Fries, N. Cooper, L. Healey, S. Kaplan, M. Liang, H. Luthra, “The American Rheumatism Association 1987 revised criteria for the calcification of Rheumatoid Arthritis”, American Rheumatism Association, Atlanta, 1998, pages 31-315.

[24] D. Aletaha, T. Neogi, A. J. Silman, "2010 Rheumatoid arthritis classification criteria", *Journal of the American College of Rhematology*, vol. 62, No 9, September 2010, pages 2569-2581.

[25] S. Bouisset, E-J. Marey or when motion biomechanics emerged as a science. In A. Cappozzo, M. Marchetti, V. Tosi (Eds.), *Biolocomotion: A century of locomotion using moving pictures,* Rome: Promograph, 1992, pages 71–88.

[26] A. D. Young, "Wireless Real-time Motion Tracking System using Localized Orientation Estimation, PhD thesis, Institute of computing Systems Architecture, School of Informatics, University of Edinburgh, 2010.

[27] D. F. J. Perales, "Human motion analysis and synthesis using computer vision and graphics techniques: state of art and applications", Workshop on Centre of Computer Graphics and Data Visualisation, Czech Republic: University of West Bohemia, 2002.

[28] K. Dorfmuller, H. Wirth, "Real-time hand and head tracking for virtual environments using infrared beacons", In D. T. N. Magnenat-Thalmann, editor, Modelling and Motion Capture Techniques for Virtual Environments, volume 1537 of Lecture Notes in Artificial Intelligence, Springer Verlag, Heidelberg, 1998, pages 113–127.

[29] ART optical tracking system: http://www.art-tracking.com/technology/optical-tracking/, January 19, 2012.

[30] Vicon systems: http://www.vicon.com, January 19, 2012.

[31]AURORA tracking system: http://www.ndigital.com/medical/aurora.php, January, 19, 2012.

[32] The Polhemus LIBERTY tracking system: http://www.polhemus.com, January 19, 2012.

[33] MTx: 3DoF Orientation Tracker Datasheet. Xsens Motion Technologies : http:// www.xsens.com/en , June 19, 2012.

[34] MovenDatasheet.: http:// www.xsens.com/en/general, Xsens Motion Technologies, June 19, 2012.

[35] Animazoo IGS-190 inertial motion capture: http://www.inition.co.uk/3D-technologies/animazoo-igs-190-m, June 19, 2012.

[36] MEMS motion trackers:http://www.xsens.com/en/general/product-all, June 19, 2012.

[37] B. Rosenhahn, U. Kersting, L. He, A. Smith, T. Brox, R. Klette, H. P. Seidel, "A silhouette based human motion tracking system", Technical report 164, Centre for Imaging Technology and Robotics, University of Auckland, New Zealand, August 2005.

[38] S. Bériault, M. Côté, P. Payeur, "Volumetric modeling with multiple cameras for markerless motion capture in complex scenes", Proceedings of the IEEE International Instrumentation and Measurement Technology Conf., pages 359-364, Victoria, BC, May 2008.

[39] InertiaCube3 Datasheet. InterSense, Inc., http://www.intersense.com, April 5th, 2012.

[40] Inertia-Link Datasheet. MicroStrain, http://www.microstrain.com/inertial/Inertia-link, April 5th , 2012.

[41] Organic Motion: http://www.siggraph.org/s.2011/contact/organic-motion-o, January 20, 2012.

[42] H. Zhou, H. Hu, "Upper limb motion estimation from inertial measurements", International Journal of Information Technology, Volume 13, No. 1, 2007.

[43] E. R. Bachmann, R. B. McGhee, X. Yun, M. J. Zyda, "Inertial and magnetic posture tracking for inserting humans into networked virtual environments", In Proceedings of the ACM Symposium on Virtual Reality software and Technology, Banff, Canada, 2001, pages 9-16.

[44] J. Gall, C. Stoll, E. Aguiar, C. Theobalt, B. Rosenhahn, H.-P. Seide, "Motion capture using joint skeleton tracking and surface estimation", BIWI, ETH Zurich, MPI Informatik, Stanford University, Leibniz-Universitat Hannover, 1980.

[45] M. Frize, P. Payeur, J. Karsh, C. Herry, C. Adéa, I. Aleem, "Preliminary results of severity of illness measures of rheumatoid arthritis using infrared imaging", International Workshop on Medical Measurements and Applications, Cetraro, Italy, May 29-30, 2009, pages 187-192.

[46] B. Furht, J. Greenberg, R. Westwater, *Motion Estimation Algorithms for Video Compression*, Massachusetts: Kluwer Academic Publishers, Chapters 2 and 3, 1997.

[47] T. Koga, K. Iinuma, A. Hirano, Y. Iijima, T. Ishiguro, "Motion compensated interframe coding for video conferencing", in Proceedings of National Telecommunication Conference, Nov. 29–Dec. 3, 1981.

[48] J. R. Jain, A. K. Jain, "Displacement measurement and its application in interframe image coding," IEEE Trans. Commun., volume 29, Dec. 1981, pages 1799–1808.

[49] A. Barjatya, "Block matching algorithms for motion estimation", IEEE DIP 6620 spring final project paper, 2004.

[50] R. Li, B. Zeng, M. L. Liou, "A new three-step search algorithm for block motion estimation", IEEE Trans. Circuits And Systems For Video Technology, volume 4., No. 4, August 1994, pages 438-442.

[51] J. Lu, M. L. Liou, "A simple and efficient search algorithm for block-matching motion estimation", IEEE Trans. Circuits And Systems For Video Technology, volume 7, No. 2, April 1997, pages 429-433.

[52] L.-M. Po, W.-C. Ma, "A novel four-step search algorithm for fast block motion estimation", IEEE Trans. Circuits And Systems For Video Technology, volume 6, No. 3, June 1996, pages 313-317.

[53] S. Zhu, K.-K. Ma, "A new diamond search algorithm for fast block-matching motion estimation", IEEE Trans. Image Processing, volume 9, No. 2, February 2000, pages 287-290.

[54] C.-H. Cheung, L.-M. Po, "A novel small cross-diamond search algorithm for fast video coding and video conferencing applications", Processing IEEE ICIP, September 2002.

[55] C.-H. Cheung, L.-M. Po, "A novel cross-diamond search algorithm for fast block motion estimation", IEEE Trans. Circuits And Systems For Video Technology, volume 12, No. 12, December 2002, pages 1168-1177.

[56] C. W. Lam, L. M. Po, C. H. Cheung, "A new cross-diamond search algorithm for fast block matching motion estimation", Proceeding of 2003 IEEE International Conference on Neural Networks and Signal Processing, Nanjing, China, Dec. 2003, pages 1262-1265.

[57] Y. Nie, K.-K. Ma, "Adaptive rood pattern search for fast block-matching motion estimation", IEEE Trans. Image Processing, volume 11, No. 12, December 2002, pages 1442-1448.

[58] V. K. Ananthashayana, M.K. Pushpa, "Joint adaptive block matching search (JABMS) algorithm", World Academy of Science, Engineering and Technology 56, 2009.

[59] H. Zhao, X.-B. Yu, J.-H. Sun, C. Sun, H.-Z. Cong, "An enhanced adaptive rood pattern search algorigthm for fast block-matching motion estimation", Image and Signal Processing, CISP 08' congres, 2008.

[60] V. Pavlovic, R. Sharma, T. S. Huang, "Visual interpretation of hand gestures for human computer interaction: A review", IEEE Transactions on Pattern Analysis and Machine Intelligence, volume 19, July 1997, pages 677- 695.

[61] A. Aristidou, "Motion capture with constrained inverse kinematics for real-time hand tracking", in Proc. of the 4th International Symposium on communications, control and Signal Processing, Limassol, Cyprus, 3-5 March 2010.

[62] J. J. Craig, *Introduction to Robotics*, 2nd Edition, Addision-Wesley, 1989.

[63] S. Cobos, M. Ferre, M.A.S. Uran, J. Ortego, C. Pena, "Efficient human hand kinematics for manipulation tasks", in Proc. of the 2008 IEEE International

Conference on Intelligent Robots and Systems Acropolis Convention Center Nice, France, Sept, 22-26, 2008.

[64] A. Gams, J. Lenarcic, "Humanoid arm kinematic modeling and trajectory generation", in First IEEE/RAS-EMBS International Conference on Biomedical Robotics and Biomechatronics, PISA,Italy, 2006, pages 301-305.

[65] M.F. Chan, D.R. Giddings, C.S. Chandler, C. Crags, R.D. Plant, M.C. Day, "An experimentally confirmed statistical model on arm movement", Human Movement Science 22, volume 22, 2004, pages 631-648.

[66] J. Denavit, R.S. Hartenberg, "A kinematic notation for lower-pair mechanisms based on matrices," *ASME Journal of Applied Mechanics*, June 1955, pages 215-221.

[67] S. Vassiliadis, E.A. Hakkennes, J.S.S.M. Wong, G.G. Pechanek, "The sum-absolute-difference motion estimation accelerator" in Euromicro Conference, Proceedings. 24th, vol. 2, 25-27 Aug., 1998, pages 559-566.

[68] R.A. Hamzah, R.A. Rahim, Z.M. Noh, "Sum of absolute differences algorithm in stereo correspondence problem for stereo matching in computer vision application", Computer Science and Information Technology (ICCSIT), 2010 3rd IEEE International Conference, 2010, Vol. 1, Pages 652–657.

[69] MaxTRAQ software: http://www.innovision-systems.com/Products/MaxTraq2D.html, December, 26th, 2012.

[70] J. Lin, Y. Wu, T.S Huang, "Modeling the constraints of human hand motion", IEEE Conferences, Workshop on Human MotionProc, 2000, pages 121-126.

[71] N. Miyata, M. Kouch, M. Mochimaru, T. Kurihara, "Finger joint kinematics from MR images", in Proc. of IEEE Conf. on Intelligent Robots and Systems, 2005, pages 2750-2755.

[72] D. G. Lowe, "Object recognition from local scale-invariant features", *International Conference on Computer Vision,* Corfu, Greece, September 1999, pages 1150-1157.

[73] H. Zhou, H. Hu, N. Harris, J. Hammerton, "Aplications of wearable inertial sensors in estimation of upper limb movements", Journal of Biomedical Signal Processing and Control, volume 1, 2006, pages 22-32.

[74] L. K. Liu, E. Feig, "A block-based gradient descent search algorithm for block motion estimation in video coding", IEEE Trans. Circuits Syst. Video Technol., volume 6, Aug. 1996, pages 419–423.

[75] Y. Wang, Q. Guo, Y. Zhu, "Medical image segmentation based on deformable models and its applications", Springer, 2007, pages 209-260.

[76] A. Dawoud, M.S. Kamel, "Iterative multimodel subimage binarization for handwritten character segmentation", IEEE 13(9), 2004, pages 1223-1230.

[77] A. Ekik, M. Zribi, A.B. Hamida, M. Benjelloun,"An optimal unsupervised satellite image segmentation approach based on pearson system and k-Means clustering algorithm initialization", International Journal of Signal Processing, volume 5, No. 1, 2009.

[78] T. F. Chan, L. A. Vese, "Active contours without edges", IEEE 10(2), 2001, pages 266-277.

[79] J. J. Craig (Stanford University), *Introduction to Robotics, Mechanics and control*, Addison-Wesley publishing Company, Massachusetts, 1986.

[80] D. Lowe, "Object recognition from local scale-invariant features", Proceedings of the 7th International Conference on Computer Vision (ICCV'99), 1999, pages 1150-1157.

[81] M. Z. Al-Faiz, A. A. Ali, A. H. Miry, "Human arm inverse kinematic solution based geometric. Relations and optimization algorithm", International Journal of Computer Science and Security (IJCSS), Volume 1, Issue 3, 2011.

[82] D. G. Lowe, "Distinctive image features from scale-invariant keypoints", *International Journal of Computer Vision,* 60, 2, 2004, pages 91-110.

[83] L-K Liu, T.J. Watson, E. Feig, "A block-based gradient descent search algorithm for block motion estimation in video coding", Circuits and Systems for Video Technology, IEEE Transactions, Volume6, Issue 4, Aug. 1996, pages 419–422.

[84] J. Koga, K. Iiunuma, A. Hirani, Y. Iijima, T. Ishiguro, "Motion compensation interframe coding for video conferencing", Proceedings of the National Telecommunications Conference, 1981, pages G5.3.1-5.3.5.

[85] H.M. Schmidt, U. Lanz ; illustrations by G. Kohnle ; [translator: J. Grossman], *Surgical anatomy of the hand*, Stuttgart ; New York : Thieme, 2004.

[86] P.C. Taylor, *Rheumatoid arthritis in practice*, London: Royal Society of Medicine Press, 2007.

[87] P. Helliwell, *The foot and ankle in rheumatoid arthritis: a comprehensive guide*, Edinburgh: Churchill Livingstone/Elsevier, 2007.

[88] S. Weiss, N. Falkenstein, *Hand rehabilitation: a quick reference guide and review*, St. Louis: Elsevier Mosby, 2005.

[89] S. Lineker, H. Wood, editors, *Rheumatoid arthritis management protocol*, Toronto: Arthritis Society Consultation and Rehabilitation Service, 1998.

[90] A. Imai, N. Shimada, Y. Shirai, "3-D hand posture recognition by training contour variation," in Proc. of the Sixth IEEE Int. Conf. on Automatic Face and Gesture Recognition, 2004, pages 895-900.

[91] A. K. Jain, A. Ross, S. Pankanti, "A prototype hand geometry-based verification system," in Proc. of 2nd Int'l Conf. on Audio and Video-Based Biometric Person Authentication, 1999, pages 166-171.

[92] B. Stenger, P. R. S. Mendona, R. Cippola, "Model-based 3D tracking of an articulated hand," in Proc. IEEE Conf. on Computer Vision and Pattern Recognition, vol. 2, 2001, pages 310-315.

[93] C. Noelker, H. Ritter, "Visual recognition of continuous hand postures," IEEE Trans. Neural Networks, vol. 13, no. 4, 2002, pages 983-994.

[94] E. Uedat, Y. Matsumotott, M. Imait, T. Ogasawarat, “Hand pose estimation for vision-based human interface.”Robot and Human Interactive Communication, Proceedings. 10th IEEE International Workshop, 2001, pages 473–478.

[95] G. ElKoura, K. Singh, “Hendrix animating the human hand”, Proc. of ACM SIGGRAPH/Eurographics SCA, 2003, pages 110-119.

[96] J. Lee, T. Kunii, “Model-based analysis of hand posture," IEEE Computer Graphics and Applications, vol. 15, Sept. 1995, pages 77-86.

[97] M. Vebe, T. Bajd, “Assessment of human hand kinematics”, in Proc. of the 2006 IEEE International Conference on Robotics and Automation, Orlando, Florida, May 2006.

[98] A. Aristidou, “Motion capture with constrained inverse kinematics for real-time hand tracking”, in Proc. of the 4th International Symposium on communications, control and Signal Processing, Limassol, Cyprus, 3-5 March 2010.

[99] J. Freixenet, X. Munoz, D. Raba, J. Marti, X. Cufi, “Survey on image segmentation: region and boundary information integration”, Springer, 2002, pages 408-422.

[100] J. Lin, “Visual hand tracking and gesture analysis,” PhD thesis, Dept. of Electrical and Computer Eng., Univ. of Illinois at Urbana-Champaign, Urbana, 2004.

[101] F. Girard, F. Guillemin, J.L. Novella, I. Valckenaere, K. Krzanowska, F. Vitry, “Health-care use by rheumatoid arthritis patients compared with non-arthritic subjects”, Journal of Rheumatology vol. 41, 2002, pages 167-75.

[102] S.E. Gabriel, C.S. Crowson, M.E. Campion, W.M. O’Fallon, “Indirect and nonmedical costs among people with rheumatoid arthritis and osteoarthritis compared with nonarthritic controls”, Journal of Rheumatology vol. 24, 1997.

[103] R.B. Anderson, R.D. Needleman, R.A. Gatter, R.P. Andrews, J.A. Scarola, “Patient outcome following inpatient versus outpatient treatment of rheumatoid arthritis”, Journal of Rheumatology, vol. 15, 1988.

[104] L.-J. Luo, C. Zou, X.-Q. Gao, "A new prediction search algorithm for block motion estimation in video coding," IEEE Trans. Consumer Electron., vol. 43, Feb. 1997, pages 56–61.

[105] J.-B. Xu, L.-M. Po, C.-K. Cheng, "Adaptive motion tracking block matching algorithms for video coding," IEEE Trans. Circuits Syst. Video Technol., vol. 97, Oct. 1999, pages 1025–1029.

[106] C.-H. Hsieh, P.C. Lu, J.-S. Shyn, E.-H. Lu, "Motion estimation algorithm using interblock correlation," Electron Lett., vol. 26, no. 5, Mar. 1, 1990, pages 276–277.

[107] J. Chana, P. Agathoklis, "Adaptive motion estimating for efficient video compression," in Conf. Rec. 29th Asilomar Conf. Signals, Systems and Computers, vol. 1, 1996, pages 690–693.

[108] J.-C. Tsai, C.-H. Hsieh, S.-K. Weng, M.-F. Lai, "Block-matching motion estimating using correlation search algorithm," Signal Process.: Image Commun., vol. 13, 1998, pages 119–133.

[109] D.-W. Kim, J.-S. Choi, J.-T. Kim, "Adaptive motion estimation based on spatio–temporal correlation," Signal Process.: Image Commun., vol. 13, 1998, pages 161–170.

[110] S. Zafar, Y.-Q. Zhang, J.S. Baras, "Predictive block-matching estimation for TV coding—Part I: Inter-block prediction," IEEE Trans. Broadcast., vol. 37, Sept. 1991, pages 97–101.

[111] M. Bierling, "Displacement estimation by hierarchical block matching," Proc. SPIE, vol. 1001, 1988, pages 942–951.

[112] F. Dufaux, M. Kunt, "Multigrid block matching motion estimation with an adaptive local mesh refinement," Proc. SPIE, vol. 1818, 1992, pages 97–109.

[113] A. M.Tekalp, *Digital Video Processing*, Englewood Cliffs, NJ: Prentice-Hall, 1995.

[114] K. M. Uz, M. Vetterli, D. LeGall, "Interpolative multiresolution coding of advanced television with compatible subchannels," IEEE Trans. Circuits Syst. Video Technol., vol. 1, Mar. 1991, pages 86–99.

[115] J. Chalidabhongse, C.-C. Jay Kuo, "Fast motion vector estimation using multiresolution-spatio–temporal correlations," IEEE Trans. Circuits Syst. Video Technol., vol. 7, 1997, pages 477–488.

[116] B. Liu, A. Zaccarin, "New fast algorithms for the estimation of block motion vectors," IEEE Trans. Circuits Syst. Video Technol., vol. 3, no. 2, 1993, pages 148–157.

[117] Y. Yue, Z. Jian,W. Yiliang, L. Fengting, G. Chenghui, "A fast effective block motion estimation algorithm," in Proc. 4th Int. Conf. Signal Processing Proceedings, vol. 1, 1998, pages 827–830.

[118] S. Zhu, K.-K. Ma, "A new star search algorithm for fast blockmatching motion estimation," in Proc. Workshop on Very Low Bitrate Coding, Oct. 8–9, 1998, pages 173–176.

[119] W. Y. Au, O. C. Pang, J. Dai, "An efficient motion vector coding algorithm based on Adaptive predictor selection", Circuits and systems (ISCAS), Proceedings of 2010 IEEE, International Symposium on, August 2010.

[120] J. Lin, Y. Wu, T. S. Huang, "3D model-based hand tracking using stochastic direct search method," in Proc. of the Sixth IEEE Int. Conf. on Automatic Face and Gesture Recognition, 2004, pages 693-698.

[121] P. Fua, A. Gruen, N. D'Apuzzo, R.Plankers, "Markerless full body shape and motion capture from video sequences", in Proceedings of Symposium on Close Range Imaging, International Society for Photogrammetry and Remote Sensing, Corfu, Greece, 2002.

Appendices

Appendix A: Criteria of early diagnosis of Rheumatoid Arthritis

The diagnosis of RA is first based on clinical evaluation. For that reason, several classifications of adults' RA have been developed by the American Rheumatism Association (ARA). In 1956, the first "diagnostic criteria" were established by ARA. Those eleven criteria were revised in 1961 in Rome by the Council for International Organizations of Medical Sciences (CIOMS), and reduced to four criteria [20]. The third set of criteria was established in 1966 in New York during the third international symposium on population studies of rheumatic diseases. The four criteria of the third set were more precise than the previous ones. In 1987, the American College of Rheumatology (ACR) established new revised criteria for RA diagnosis which were closer to the New York criteria with seven different criteria (Table A.1). One of the most known classifications was published in 1998 [23]. In 2010, a new ACR set of criteria for RA classification was published [24], but kept the major criteria of the 1998 classification.

CRITERIA	DEFINITION
1. Morning stiffness	Morning stiffness in and around the joints lasting at least one hour before maximal improvement.
2. Arthritis of three or more joint areas	At least three joints areas simultaneously had a soft tissue swelling or fluid (not bony overgrowth alone) observed by a physician. The fourteen possible joint areas are (right or left): PIP, MCP, wrist, elbow, knee, ankle, and MTP joints.
3. Arthritis and hand joints	At least one joint area swollen as above in wrist, MCP, or PIP joint
4. Symmetric arthritis	Simultaneous involvement of the same joint areas (as in two) on both sides of the body (bilateral involvement of PIP, MCP, or MTP

	joints is acceptable without absolute symmetry).
5. Rheumatoid nodules	Subcutaneous nodules, over bony prominences or exterior surfaces or in juxtra-articular regions, observed by a physician.
6. Serum rheumatoid factor	Demonstration of abnormal amounts of serum ``rheumatoid factor`` by any method that has been positive in less than five percent of normal control subjects.
7. Radiographic changes	Radiographic changes typical of RA on PA hand and wrist x-rays, which must include erosions or unequivocal bony decalcification localized to or most marked adjacent to the involved joints (osteoarthritis changes alone do not qualify)

Table A.1: 2010 ACR criteria for classification of Rheumatoid Arthritis.

For classification purposes, a patient has RA if s/he has satisfied at least four of the seven criteria. For at least six weeks, criteria one through four must be present. From these seven criteria, there was established also a decision tree for RA classification (Fig. A.1).

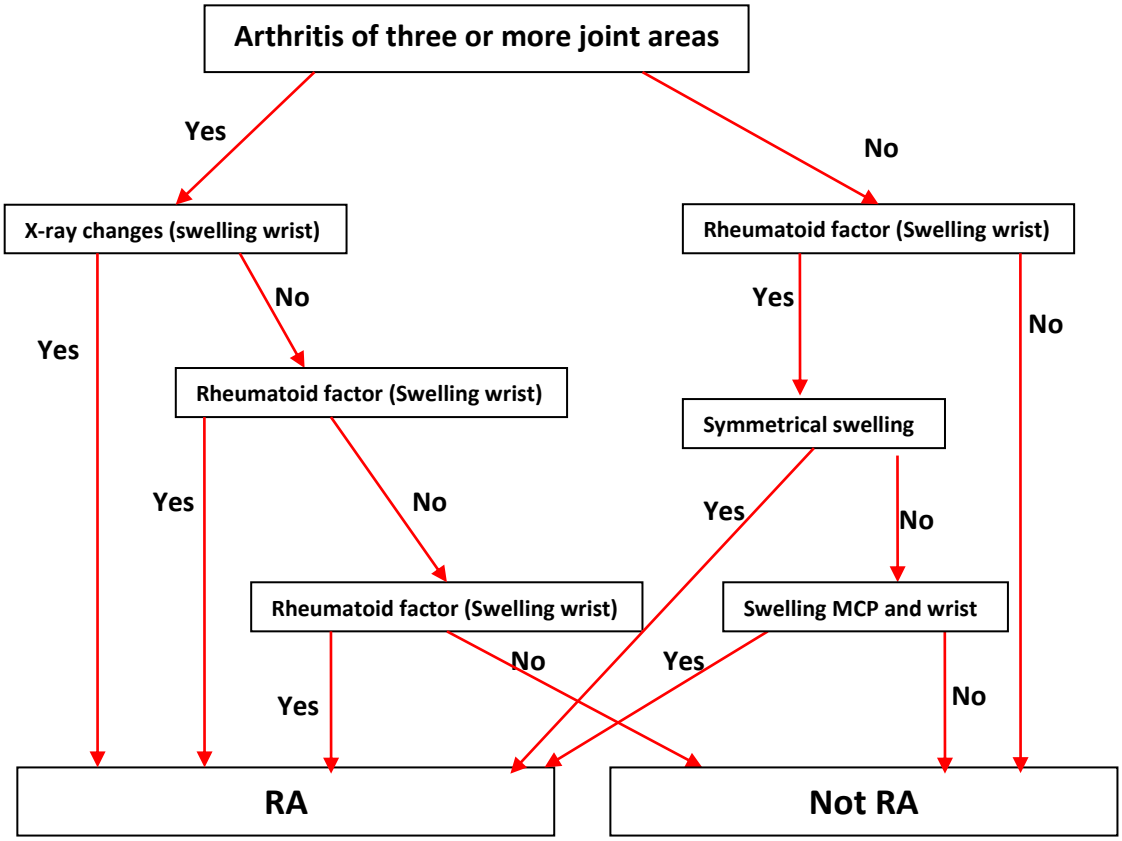

Fig. A.1: 1987 ACR decision tree for RA classification

Note that this decision tree was modified to add more precisions in 2010 rheumatoid arthritis classification criteria [24] but did not change anything in terms of the conclusion whether the subject has RA or not.

Appendix B: Denavit-Hartenberg convention

In 1955, Denavit and Hartenberg published their technique which has become the standard way of modeling the motion of robots. In their paper in the ASME Journal of Applied Mechanics [66], they proposed a model of representation that can define robot links and joints in a very simple way. This model can be used for any configuration of the robot, regardless its sequence or complexity. To define the position and orientation of the end-effector of the robot, some parameters need to be defined in a table (D-H parameters table) such that the forward and inverse kinematics can be specified. The definition of the position and orientation needs to be specified in the table by the number of DoF of all the joints. All joints are represented by a z-axis (Fig. 3.7) in the direction of rotation as followed by the right-hand rule for rotations. The rotation about the z-axis is the joint variable θ_i. The length of the link along the z-axis (the distance on the z-axis between the two successive common normals or joints offset) is represented by d_i. The angle between two successive z-axes (called also joint twist) is α_i. Finally, l_i represents the length of each common normal (the length of the link). In general, as shown in the D-H parameter table, only θ_i and d_i are joints variables. The rules to define those variables are:

i) Z_i is the axis of the i^{th} joint (in one direction or the other)

ii) X_i is the axis that is perpendicular both to Z_{i-1} and Z_i in a direction going from the first to the second one. If Z_{i-1} and Z_i intersect, the right-hand rule is used to set the direction of X_i.

iii) The distance between Z_i and Z_{i+1}, is denoted l_i. If Z_i and Z_{i+1} intersect, then $l_i = 0$.

iv) The Z_i coordinate of the intersection between the X_{i+1} axis and the Z_i axis is denoted d_i. This corresponds to the distance between X_i and X_{i+1}.

v) The angle between Z_i and Z_{i+1} is denoted α_i. It is measured with respect to the positive direction of the X_{i+1} axis (right-hand rule).

vi) The angle between X_i and X_{i+1} is denoted θ_i. It is measured with respect to the positive direction of the Z_i axis (right-hand rule).

The parameters l_i, d_i, α_i, and θ_i are known as the Denavit-Hartenberg parameters (D-H parameters). Each set of those parameters describes the architecture of one degree of freedom of the joint.

The general expression of an A_i matrix is that of an homogeneous transformation matrix that defines the relationship between two successive reference frames. In order to move from a given frame to the next frame, one must combine a sequence of elementary transformations to obtain the A_i matrix as follows:

$$A_i = Rot_{zi,\theta i}Trans_{zi,di}Trans_{xi+1,li}Rot_{xi+1,\alpha i} = \begin{matrix} cos\theta_i & -sin\theta_i cos\alpha_i & sin\theta_i sin\alpha_i & l_i cos\theta_i \\ sin\theta_i & cos\theta_i cos\alpha_i & -cos\theta_i sin\alpha_i & l_i sin\theta_i \\ 0 & sin\alpha_i & cos\alpha_i & d_i \\ 0 & 0 & 0 & 1 \end{matrix}$$

Where i (i = 1, 2, 3,…n) is the joint number.

For n DoFs, the transformation matrix is expressed as:

$$Q_{effector/base} = A_1 A_2 \dots A_n$$

Appendix C (French version) : Protocole de Recherche

Protocole de Recherche

Titre du projet de recherche: Détermination du Polyarthrite rhumatoïde (Rheumatoid Arthritis) à partir des images digitales.

Chercheurs / enquêteurs:

Nom: Boniface MBOUZAO
Institution de la Faculté, département: Université d'Ottawa, Faculté de Génie, Département de génie biomédical.

Nom: Monique FRIZE
Institution de la Faculté, département: Université d'Ottawa, Faculté de Génie.

Nom: Pierre PAYEUR
Institution de la Faculté, département: Université d'Ottawa, Faculté de Génie.

Plus de 300 000 canadiens, 2,1 millions d'américains et 260 000 français ont été diagnostiqués ces dernières années avec le Polyarthrite rhumatoïde (Rheumatoid Arthritis). De ce nombre de patient, il a été constaté que près de 50% ont eu un handicap sérieux dû à la maladie.

La méthode que l'on utilise aujourd'hui pour diagnostiquer la maladie est basée sur une évaluation médicale, l'histoire médicale du patient et les tests de laboratoire. Le diagnostique actuel est basée sur les résultats des tests du MRI (Magnetic Resonance Imaging) et du HRUS (High Resolution Ultra Sound) qui sont des examens très coûteux, peu accessibles de par les listes d'attente et la disponibilité limitée de ces appareils dans les hôpitaux. Il est ainsi indispensable de trouver une autre alternative aussi performante que ces dernières mais moins coûteuse et plus accessible.

Le but de cette recherche est de pouvoir aider les médecins à diagnostiquer plus rapidement le Polyarthrite rhumatoïde en utilisant une technique plus accessible et moins coûteuse. Il s'agit d'utiliser les vidéos des articulations les plus touchées par la maladie dans leur position de flexion et de courbure et pouvoir comparer leur capacité de mouvement d'une

personne saine à faire les mêmes mouvements. L'hypothèse qui soutient cette recherche est que l'utilisation des vidéos prises grâce aux caméras digitales peut conduire à évaluer la capacité de mouvement d'un sujet et pouvoir donner au médecin les informations pour évaluer si ce dernier est atteint de l'arthrite ou non. Ceci sachant que l'arthrite a pour principal effet de réduire la mobilité du patient en détruisant le cartilage de certaines articulations humaines.

Il s'agit de prendre les images avec l'appareil digital des patients qui sont en attente de l'examen au MRI ou HRUS pour un diagnostic. Le but est de baser un diagnostic sur les vidéos digitales prises et de le comparer à celui obtenu après les résultats du MRI ou HRUS. Il s'agira de prendre les vidéos des mains particulièrement les joins de la main et les articulations du bras. Après que chaque sujet ait accepté et signé le protocole de participation à la recherche que lui a soigneusement présenté le médecin ou le chercheur. On demandera ainsi au sujet de ne pas faire des exercices physiques intenses au moins 4 heures avant la séance, d'enlever tout vêtements recouvrant les mains et les bras lors de la prise des vidéos et ne pas porter de bagues, colliers et bracelets pendant la session.

Les avantages de la recherche sont multiples pour la société en général. La recherche pourrait ne pas directement bénéficier aux patients et volontaires de la recherche mais est hautement bénéfique pour la société et les futurs patients. Grâce à cette recherche, on pourrait trouver un moyen plus efficace, moins coûteux, plus accessible à tous de pouvoir diagnostiquer le Polyarthrite rhumatoïde et dans un délai raisonnable pour des soins appropriés.

Appendix C (English version): Research Protocol

RESEARCH PROTOCOL

Research project title: Quantitative Evaluation of Human Gesture with Passive Vision Monitoring

Researchers/investigators:

Name: Boniface MBOUZAO
Institution, Faculty, Department: University of Ottawa, Faculty of Engineering, Department of biomedical Engineering.

Name: Monique FRIZE
Institution, Faculty, Department: University of Ottawa, Faculty of Engineering.

Name: Pierre PAYEUR
Institution, Faculty, Department: University of Ottawa, Faculty of Engineering.

More than 300,000 Canadians, 2.1 million Americans and 260,000 French were diagnosed in recent years with Rheumatoid Arthritis (RA). Of these patients, it was found that nearly 50% had a serious disability due to illness.

The method used today to diagnose the disease is based on a medical assessment, the patient's medical history and laboratory tests. The laboratory tests are essentially MRI (Magnetic Resonance Imaging) and HRUS (High-Resolution Ultra-Sound) examinations which are very expensive, not accessible because of both lengthily waiting lists and the limited availability of these devices in hospitals. It is thus necessary to find an alternative solution as good as these previous ones but cheaper and more accessible.

The purpose of this research is to help rheumatologists to diagnose rheumatoid arthritis more quickly using a technique that is more accessible and cheaper. It's about

using the videos of the joints most affected by the disease in their position of bending and curvature and to compare the patient ability of movement to a healthy person performing the same movements. The assumption under this research is that the processing of videos taken with digital camera can help to find the motion capabilities of a subject and to give to the rheumatologist the necessary information to find out whether the patient is suffering from RA or not. In fact, the external manifestation of RA is the reduction of mobility of the patient by destroying the cartilage of certain human joints.

It is about taking pictures with the digital camera of patients who are waiting for the MRI or HRUS examination for diagnosis. The aim of this research is to base a diagnosis on processing digital videos and compare the results obtained from videos to the MRI or HRUS based diagnosis. The videos of hands and arm joints will be taken for this purpose. After each subject has accepted and signed the protocol of participation to this research that will be carefully presented by the rheumatologist or one of the researchers, it will be asked to the patient to not do intense physical exercise at least 4 hours before the meeting, to remove all clothing covering the hands and arms when taking videos and to not wear rings, necklaces and bracelets during the session.

The benefits of this research are manifold for society in general. The research may not directly benefit patients and volunteers of the research but is highly beneficial to society and future patients. Through this research, we could find a more efficient, less costly, more accessible to everyone, to be able to diagnose rheumatoid arthritis and in a reasonable time for appropriate care.

Appendix D (French version) : Lettre d'information

Lettre d'information

Titre du projet de recherche: Détermination du Polyarthrite rhumatoïde (Rheumatoid Arthritis) à partir des vidéos digitales.

Chercheurs / enquêteurs:

Nom: Boniface MBOUZAO
Institution de la Faculté, département: Université d'Ottawa, Faculté de Génie, Département de génie biomédical.

Nom: Monique FRIZE
Institution de la Faculté, département: Université d'Ottawa, Faculté de Génie.

Nom: Pierre PAYEUR
Institution de la Faculté, département: Université d'Ottawa, Faculté de Génie.

Vous êtes invités à participer à une expérience dans le cadre d'une recherche pour le diagnostic du Polyarthrite rhumatoïde (Rheumatoid Arthritis). Cette lettre vous donne des informations relatives au sujet de l'expérience. Les chercheurs sont prêts à répondre à vos questions concernant la recherche et l'expérience à laquelle ils vous invitent à prendre part comme participant.

S'il-vous-plaît vous êtes prié de lire cette lettre d'information attentivement et de poser des questions sur ce que vous ne comprenez pas sur cette expérience avant de décider de participer ou non à cette expérience.

Votre participation est totalement volontaire et vous pouvez refuser d'y participer. Vous pouvez prendre cette lettre et signer à domicile le formulaire de consentement et prendre le temps de réfléchir avant de prendre votre décision.

Quel est l'objectif de cette expérience?

Le but de cette étude est d'évaluer la valeur diagnostique potentielle de l'imagerie digitale pour les patients du Polyarthrite rhumatoïde (Rheumatoid Arthritis). Le projet se concentre sur les vidéos des articulations. Pour cela il faudra passer une séance de prise de vidéos de certaines parties du corps particulièrement les articulations de la main et du bras en mouvement.

Préparation:

• Le sujet ne doit pas s'adonner à un exercice sportif intense pendant 24 heures avant la session.

• Des dispositifs d'immobilisation pour bras et la main ne doivent pas être portés pendant 2 heures avant la session.

• Le sujet ne doit pas porter n'importe quel type de bijoux sur le poignet ou les doigts pendant la session.

•Le sujet ne devrait pas faire aucun exercice physique pendant 2 heures avant la session.

Pendant le test :

Vous aurez à enlever tout vêtement qui recouvre vos bras et vos mains pour permettre une bonne prise de la vidéo.

Il vous sera demandé d'effectuer quelques tâches physiques.

1. Vous allez étendre et plier les articulations de votre bras de manière rapide pendant 15 à 20 secondes.

2. Vous allez également devoir faire le même geste (étendre les articulations du bras et les refermer) de manière lente pendant également 15 à 20 secondes.

3. Vous allez tordre chaque main le plus que vous pouvez pour une minute où jusqu'à ce que la douleur ou l'inconfort apparaît dans vos doigts.

La session générale est prévue pour durer environ 40 minutes. Cette séance aura lieu à l'Université d'Ottawa dans le laboratoire VIVA.

Quels sont les avantages pour moi ou pour d'autres?

Vous ne pourrez peut être pas obtenir des avantages immédiats de cette expérience, mais ce test est totalement non-invasif et sans risque. Cette expérience a la potentialité d'aider toute la société dans la mesure où elle va pouvoir aider à trouver une meilleure méthode peu coûteuse et accessible à tous pour détecter chez un patient le Polyarthrite rhumatoïde (Rheumatoid Arthritis).

Quels sont les risques que je prends ?

Certains des tests physiques peuvent être légèrement douloureux ou inconfortables, surtout si vous présentez des symptômes de tâches répétitives ou de blessures. Il n'y a pas de risque prévu ou des malaises liés à l'imagerie digitale.

Qu'en est-il de l'anonymat et la confidentialité de mes données?

Votre identité restera confidentielle et l'anonymat sera préservé. Seul un numéro d'identification sera conservé avec vos données. La correspondance entre le numéro d'identification et des informations confidentielles ne sera disponible que pour un chercheur et toutes les informations confidentielles seront détruites à la fin de cette étude.

Serai-je payé?

Non, c'est une expérience aidant la société en générale et demande de votre part une solidarité avec les patients potentiels qui bénéficieraient de cette recherche.

Comment puis-je arrêter ma participation à cette expérience?

Vous pouvez vous retirer de cette étude en tout temps et refuser de répondre aux questions. Si vous décidez de vous retirer, toutes les données recueillies sur vous seront détruites. En outre il y a plusieurs raisons qui peuvent vous amener à arrêter votre participation: le test ne vous convient pas ou le chercheur cesse l'expérience, ou d'autres raisons liées à des problèmes inattendus.

Qui puis-je appeler si j'ai des questions?

Si vous avez des questions avant, pendant et après l'expérience lorsque vous participez, s'il vous plaît contactez Boniface MBOUZAO.

Ce projet a été examiné et a reçu l'approbation éthique du Comité d'éthique de recherche de l'Université d'Ottawa. Si vous avez des questions concernant vos droits en tant que sujet de recherche, vous pouvez communiquer avec le président du comité éthique de l'Université d'Ottawa, le Professeur Howard Alper (vice-recteur à la recherche).

Appendix D (English version): Information Letter

INFORMATION LETTER

Research project title: Quantitative Evaluation of Human Gesture with Passive Vision Monitoring

Researchers/investigators:

Name: Boniface MBOUZAO
Institution, Faculty, Department: University of Ottawa, Faculty of Engineering, Department of biomedical Engineering.

Name: Monique FRIZE
Institution, Faculty, Department: University of Ottawa, Faculty of Engineering.

Name: Pierre PAYEUR
Institution, Faculty, Department: University of Ottawa, Faculty of Engineering.

You are invited to participate in an experiment as part of research for the diagnosis of Rheumatoid Arthritis (RA). This letter gives information on the subject of experience. Researchers are ready to answer your questions about the research and the experience to which they invite you to participate as a volunteer.

You are advised to read this information letter carefully and ask questions about what you do not understand before deciding whether to participate in this experiment.

Your participation is completely voluntary and you can refuse to participate. You can take this letter home and sign the consent form and take time to reflect before making your decision.

What is the purpose of this experiment?

The purpose of this study is to evaluate the diagnostic potential of digital imaging for

patients of Rheumatoid Arthritis. The project focuses on the videos of the joints. This will require passing a session of taking videos of parts of the body especially the joints of the hand and arm movement.

Preparation:

• The subject does not engage in an intense athletic exercise for 24 hours before the session.
• Some immobilizers arm and hand should not be worn for two hours before the session.
• The subject should not wear any type of jewelry on the wrist or fingers during the session.
• The subject should not do any physical exercise for 2 hours before the session.

During the test:

You will have to remove any clothing that covers your arms and hands to allow a good grip of the video.

You will be asked to perform some physical tasks.

1. You will extend and bend the joints of your arms fast for 15 to 20 seconds.
2. You will also have to make the same gesture (extending the joints of the arms and close), slowly during from 15 to 20 seconds.
3. You will twist each hand as much as you can for a minute until the pain or discomfort appears in your fingers. The General Session is scheduled to last about 40 minutes. This session will be held at the University of Ottawa in the VIVA laboratory.

What are the benefits for me or for others?

You may be unable to obtain immediate benefits from this experience, but this test uses only passive sensing technologies and is safe. This experience has the potential to help all society. It will be able to help find a better inexpensive and accessible examination of a patient for Rheumatoid Arthritis.

What are the risks I take?

Some physical tests may be slightly painful or uncomfortable, especially if you have symptoms of repetitive or injury. There is no anticipated risk or discomfort associated with

digital imaging.

What about the anonymity and privacy of my data?

Your identity will remain confidential and anonymity will be preserved. Only an identification number will be kept with your data. The correspondence between the identification number and confidential information will only be available for a researcher and all confidential information will be destroyed at the end of the study.

I get paid?

No, it's an experience helping society in general and your request solidarity with potential patients who would benefit from this research.

How can I stop my participation in this experience?

You may withdraw from this study at any time and refuse to answer questions. If you decide to withdraw, all data collected will be destroyed. In addition there are several reasons that can cause you to stop your participation: the test does not suit you or the researcher stops the experience or other reasons related to unexpected problems.

Who can I call if I have any questions?

If you have any questions during the test experiment when you are participating, please contact Boniface MBOUZAO.

This project was reviewed and received ethics clearance by the University of Ottawa Research Ethics Committee. If you have any questions about your rights as a research subject, you may contact: Prof. Howard Alper, Chair, University of Ottawa Research Ethics Committee.

Appendix E (French version): Formulaire de consentement

Formulaire de consentement

Titre du projet de recherche: Détermination du Polyarthrite rhumatoïde (Rheumatoid Arthritis) à partir des vidéos et images digitales.

Chercheurs / enquêteurs:

Nom: Boniface MBOUZAO
Institution de la Faculté, département: Université d'Ottawa, Faculté de Génie, Département de génie biomédical.

Nom: Monique FRIZE
Institution de la Faculté, département: Université d'Ottawa, Faculté de Génie.

Nom: Pierre PAYEUR
Institution de la Faculté, département: Université d'Ottawa, Faculté de Génie.

Ne pas signer ce formulaire de consentement, sauf si vous avez eu la chance de poser des questions et vous avez reçu des réponses satisfaisantes à toutes vos questions ou bien vous accepter tout ce qui est mentionné dans ce formulaire.

Moi, _____ a été invités par Boniface MBOUZAO et ses associés de recherche du Département de génie biomédical, Université d'Ottawa, ON, à participer à un projet de recherche.

J'ai eu l'occasion de poser des questions. Mes questions ont toutes été répondues de façon satisfaisante. Je comprends que je peux poser d'autres questions à tout moment.

J'ai été informé que le but de cette étude est d'évaluer la valeur diagnostique potentielle de l'imagerie digitale pour les patients du Polyarthrite rhumatoïde (Rheumatoid Arthritis). Je comprends que ce projet se concentre sur la prise des vidéos des articulations, spécialement au niveau de la main et du bras.

Je suis conscient que je vais devoir passer par une séance de vidéo de certaines parties de mon corps particulièrement les joints de la main et du bras.

Je comprends que je peux refuser de répondre à toute question ou refuser d'effectuer des essais, à tout moment.

Je comprends que je devrai suivre les instructions suivantes avant la session de vidéos digitales afin d'assurer une imagerie exacte:

• Le sujet ne pas s'adonner à un exercice sportif intense pendant 24 heures avant la session.

• Des dispositifs d'immobilisation pour bras et la main ne doivent pas être portés pendant 2 heures avant la session.

• Le sujet ne doit pas porter n'importe quel type de bijoux sur le poignet ou les doigts pendant la session.

•Le sujet ne devrait pas faire aucun exercice physique pendant 2 heures avant la session.

Je vais devoir enlever tout vêtement qui est sur mon bras et ma main. Je vais pour la première vidéo ouvrir largement ma main et le refermer dans un mouvement rapide pendant 15 à 20 secondes.

Il me sera demandé d'effectuer quelques tâches physiques.

1. Je vais étendre et plier les articulations de mon bras de manière rapide pendant 15 à 20 secondes.

2. Je vais également devoir faire le même geste (étendre les articulations du bras et les refermer) de manière lente pendant également 15 à 20 secondes.

Si le chercheur note des lectures inhabituelles au cours de l'expérience, l'étude sera immédiatement arrêtée. Le chercheur n'est pas un médecin et ne peut pas faire un diagnostic médical. Je serai invité à communiquer avec mon médecin de famille. Le chercheur prendra contact avec mon médecin par écrit en expliquant pourquoi l'expérience a été arrêtée. Mais je ne retourne pas à l'étude ou d'entreprendre des expériences nouvelles, sans le consentement écrit de mon médecin.

La session générale est prévue pour durer environ 40 minutes. La séance aura lieu au Laboratoire VIVA situé à l'Université d'Ottawa sur King Edward.

Je comprends que certains des tests physiques peuvent être légèrement douloureux ou inconfortables, surtout si je présente des symptômes de tâches répétitives ou de blessures. Il n'y a pas de risques prévus ou de malaises liés à la partie de l'imagerie digitale.

Mon identité restera confidentielle et mon anonymat sera préservé. Seul un numéro d'identification sera conservé avec mes données. La correspondance entre le numéro d'identification et des informations confidentielles ne sera disponible que pour un chercheur et toutes les informations confidentielles seront détruites à la fin de cette étude.

Une copie de ce formulaire de consentement doit être conservée séparément de mes données. Les publications issues de ce projet ne pourront m'identifier en aucune façon. Seules les vidéos digitales de mes mains et de moi avec mes bras sont prises pour ce projet. Il n'existe aucun moyen de m'identifier à partir des résultats de traitement de ces vidéos. Seuls les résultats de traitement des vidéos anonymes pourront être rendu publics dans les publications.

Mes images seront stockées sur des supports enregistrables et protégées sur un ordinateur sécurisé. Les données des tests physiques seront stockées dans une base de données distincte que celle contenant les vidéos de la main. Mes données ne seront pas accessibles au public. Seuls les chercheurs impliqués dans le projet auront directement accès à mes données.

Mes données (vidéos de la main et vidéos des bras) seront conservées indéfiniment pour une réévaluation future, le suivi et la révision des résultats. Mes données pourraient également être partagées avec d'autres équipes au cas par cas. Toutes les demandes de partage seront évaluées avec soin. Mes données, si elles sont partagées, resteront anonymes et confidentielles.

J'accepte volontairement de participer à cette étude. Je peux me retirer de cette étude en tout temps et refuser de répondre aux questions. Si je décide de me retirer, toutes les données recueillies de moi seront détruites.

Si j'ai des questions concernant cette étude, la lettre d'information ou le formulaire de consentement, je peux contacter Boniface MBOUZAO.

Si j'ai des questions sur mes droits en tant que sujet de recherche, sur l'éthique, des préoccupations ou des plaintes, je peux communiquer avec le président du comité éthique de l’Université d’Ottawa, le Professeur Howard Alper (vice-recteur à la recherche).

Je comprends que je recevrai un exemplaire signé et daté du formulaire de consentement pour mes dossiers.

En signant ce formulaire, je n'ai renoncé à aucun de mes droits. Il indique simplement que j'ai accepté de participer à cette étude.

_____ _____

Signature du participant Date

_____ _____

Signature du chercheur Date

Appendix E (English version): Consent Form

INFORMED CONSENT FORM

Research project title: Quantitative Evaluation of Human Gesture with Passive Vision Monitoring

Researchers/investigators:

Name: Boniface MBOUZAO
Institution, Faculty, Department: University of Ottawa, Faculty of Engineering, Department of biomedical Engineering.

Name: Monique FRIZE
Institution, Faculty, Department: University of Ottawa, Faculty of Engineering.

Name: Pierre PAYEUR
Institution, Faculty, Department: University of Ottawa, Faculty of Engineering.

Do not sign this consent form unless you have had a chance to ask questions and have received satisfactory answers to all your questions or you do not have any questions and you totally agreed to all the conditions.

I, _____ have been invited by Boniface MBOUZAO and his research associates of the Department of biomedical Engineering, University of Ottawa, ON, to participate in a research project.

I have been given the opportunity to ask questions. My questions have all been answered satisfactorily. I understand that I can ask other questions at any time.

I have been informed that the purpose of this study is to assess the potential diagnostic value of digital imaging for Rheumatoid Arthritis patients. I understand that this project focuses on taking videos of articulation especially hands and limbs.

I understand that I can decline to answer any question or perform any tests, at any time.

I understand that I will have to follow the following instructions prior to the session to ensure accurate imaging:

• Subjects should not have intense exercise 24 hours prior the session.

• Immobilization devices for the limb and hand region should not be worn for 2 hours prior to the session.

• Subjects should not wear any type of jewelry on the wrist or fingers during the test.

• Subjects should not exercise for 2 hours prior to the session.

I will have to remove any piece of clothing that is on my limbs and hands. For the first video, open and close widely my hand (left and right hand) quickly as possible during 15 to 20 seconds.

I will be asked to perform some physical tasks.

I will bend and flex my limb's angles quickly during 15 to 20 seconds.

I will bend and flex my limb's angles slowly during 15 to 20 seconds.

If the researcher notes any unusual readings during the session of the experiment the study will be stopped immediately. The researcher is not a physician and cannot make a medical diagnosis. I will be asked to contact my family physician. The researcher will contact my physician in writing explaining why the experiment was stopped. I may not return to the study or undertake any further experiments without the written consent of my physician.

The overall session is expected to last approximately 40 minutes. The test session will take place at Ottawa University in VIVA laboratory in CBY Building.

I understand that some of the physical tests may be mildly painful or uncomfortable, especially if I show symptoms of repetitive strain injuries. There are no foreseen risks or discomforts with the test session.

My identity will remain confidential and my anonymity will be preserved. Only an identification number will be kept with my data. The correspondence between identification number and confidential information will only be available to one researcher and all confidential information will be destroyed at the end of this study.

A copy of this consent form will be kept separately from my data. Publications deriving from this project will not identify me in any way. Only videos of my hand and myself with limbs

gestures are taken for this project. There is no way to identify me from the results of the processing of my videos.

My videos will be stored on protected recordable media and on a secure computer. The data from my physical tests will be stored in a separate database than that containing the videos of my hands. My data will not be publicly accessible. Only the researchers involved in the project will have direct access to my data.

My data (hands and limbs videos) will be kept indefinitely for future reassessment, follow-up and review of the results. My data may also be shared with other research teams on a case by case basis. All sharing requests will be evaluated carefully. My data, if shared, will remain anonymous and confidential.

I voluntarily agree to participate in this study. I can withdraw from this study at any time and refuse to answer any questions. If I decide to withdraw, all the data collected from me will be destroyed.

If I have any questions about this study, the information letter or the consent form I can contact Boniface MBOUZAO.

If I have any questions about my rights as a research subject, about ethics concerns or complaints, I can contact the Ottawa University Research Ethics Committee Chair, Prof. Howard Alper.

I understand that I will receive a copy of the signed and dated consent form for my records.

By signing this form, I have not waived any of my rights. It simply indicates that I have agreed to participate in this study.

_____ _____

Signature of the participant Date

_____ _____

Signature of the researcher Date

Appendix F (French version): Affiche

Annonce

Des volontaires sont demandés comme participants

Saviez-vous que plus de 300 000 canadiens, 2,1 millions d'américains et 260 000 français ont été diagnostiqués ces dernières années avec le Polyarthrite rhumatoïde (Rheumatoid Arthritis). De ce nombre de patient, il a été constaté que près de 50% ont eu un handicap sérieux dû à la maladie.

Pour permettre une détection rapide au moyen d'une méthode peu coûteuse, passive et plus accessible, un groupe des chercheurs de l'université d'Ottawa sont en train de travailler pour arriver à cette solution. Ils ont besoin des volontaires pour participer à leur recherche et améliorer, voir sauver les patients qui vont être diagnostiqués avec cette maladie dans la génération future.

Grâce à cette recherche, on pourrait trouver un moyen plus efficace, moins coûteux, plus accessible à tous de pouvoir diagnostiquer le Polyarthrite rhumatoïde (Rheumatoid Arthritis) dans un délai raisonnable pour des soins appropriés.

Si vous désirez participer à cette recherche comme volontaire, vous êtes les bienvenus. Pour plus d'informations et votre demande de participation au projet de recherche, vous êtes priés de contacter :

Boniface MBOUZAO
Université d'Ottawa, Faculté de Génie,
Département de génie biomédical.

AppendixF (English version): Flyer

Announcement

Volunteers are needed

Did you know that over 300,000 Canadians, 2.1 million Americans and 260,000 French were diagnosed in recent years with Rheumatoid Arthritis? Of these patients, it was found that nearly 50% had a serious disability due to illness.

To allow rapid detection using an inexpensive, passive and more accessible method, a group of researchers at the University of Ottawa are working to reach that solution. They need volunteers to participate in their research and improve or even save patients that will be diagnosed with the disease in the next generation.

Through this research, we could find a solution that is more efficient, less costly, and accessible to everyone to be able to diagnose Rheumatoid Arthritis within a reasonable time for appropriate care.

If you wish to participate in this research as a volunteer, you are welcome. For more information and your request to participate in the research project, you should contact:

Boniface MBOUZAO
University of Ottawa, Faculty of Engineering,
Department of biomedical Engineering.

Appendix G: Implementation of SAD using Simulink

Implementation of SAD using Simulink

To make the computation of SAD quicker in Matlab, the use of Simulink was preferred to implementing the computation directly into Matlab.

The computation of SAD itself is a sub-system of the whole motion energy estimation system (Fig. G.1). SAD incorporates functions such as generating data for motion energy and threshold display, and comparing motion energy against threshold.

The system checks that the two frames have the same size (number of rows and number of columns) and then creates a table of the same size. The system computes from the two frames the difference of the intensity between corresponding pixels. This is the part that we named "Difference" in Fig. G.1.

Then, the absolute value of the difference between the two pixels is put in the corresponding cell of the table created. This is the part of the implementation called "Absolute value" (Fig. G.1). At the end of the process, it generates a table of the same size as the frame with the absolute difference value of each pixel in the corresponding cell of the table. Then a table with one row but the same number of columns as the previous one is created, its cells containing the result of the sum of each column of the first table. This is the rule of the block called Column Sum in Fig. G.1. The block called Row Sum will add all the values ranged in the new table of one Row which is the final value of SAD.

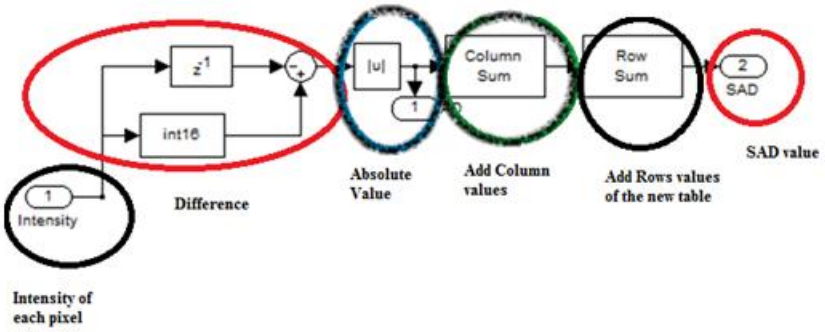

Fig. G.1: Computational process of SAD using Simulink blocks.

Composition of sub-system

The motion estimation requires a sub-system that provides the acquisition of the hand or arm video when the patient participant or volunteer is bending and stretching the hand and arm. A special image acquisition and image display is required as shown in Fig. G.2.

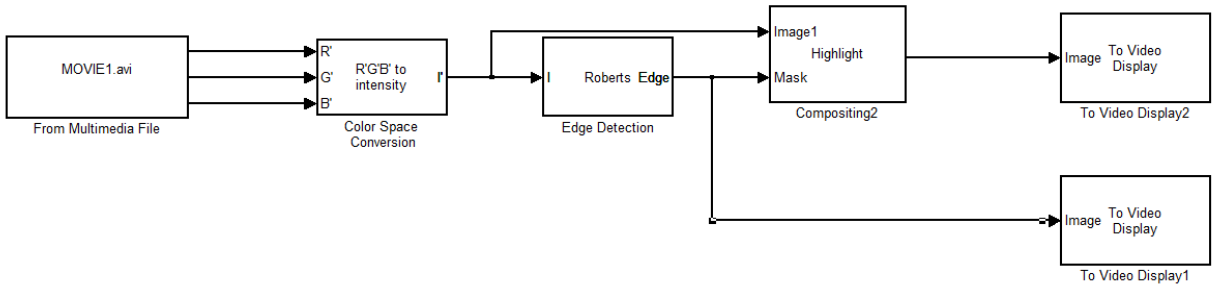

Fig. G.2: Video acquisition sub-system.

The input of this stage is the intensity of the video and a threshold value of $2.9xe^{6}$, which corresponds to the largest difference intensity value that we found while processing volunteers' video. The purpose of this threshold is to show how much

higher the value of SAD of the patient participant is, in comparison with a normal subject as explained in section 4.4. Then the sub-system looks like this:

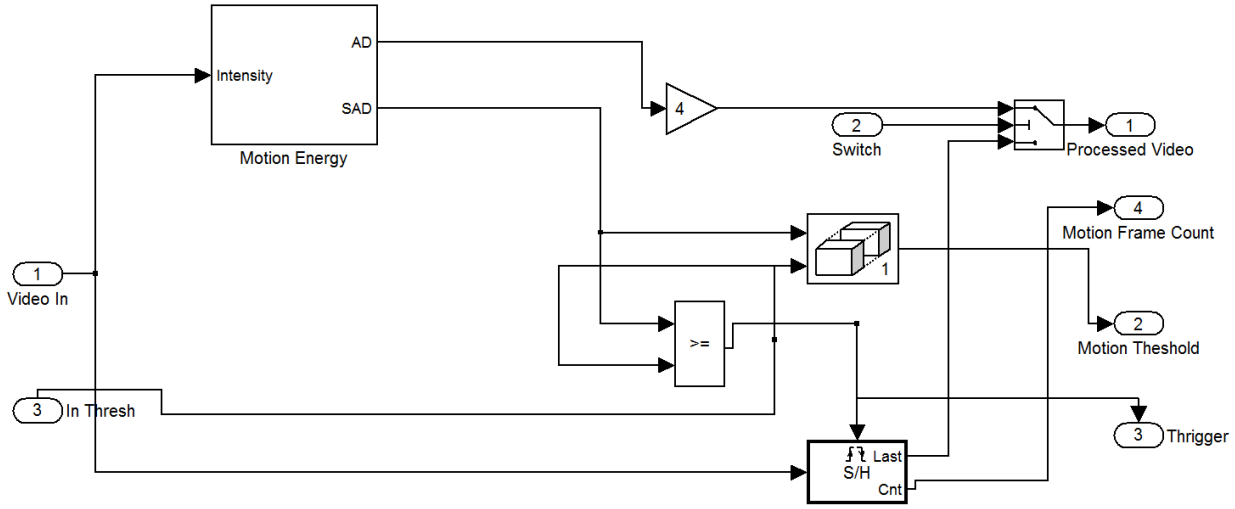

Fig. G.3: Sub-system (motion energy estimation) using SAD and Threshold.

The System

The final system shown in Fig. G.4 is the combination of the two previous sub-systems (motion energy sub-system and image acquisition sub-system) to estimate and represent the SAD values in a graph as a function of time corresponding to each frame of the video sequence. The interpretation of the graph is discussed along with the interpretation of results in chapter 5 of the thesis.

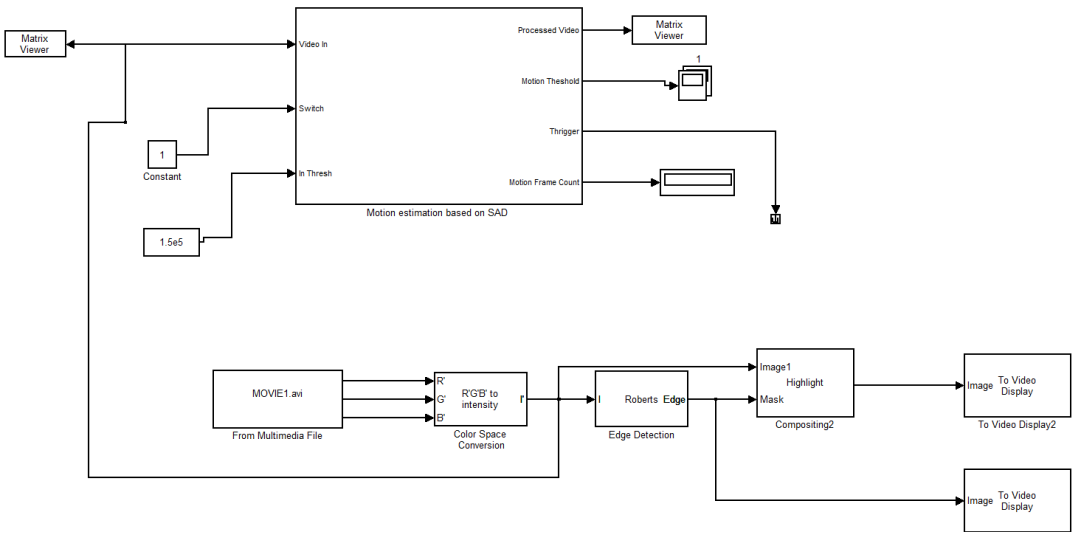

Fig. G.4: Complete SAD based motion estimation system.

Absolute Difference Image

The motion within the camera field of view is estimated by computing the difference between successive video frames. For this research, we used a 38 frames per second as the frame rate. Therefore, within one second, we obtained 37 absolute difference images. The value of SAD that we used for classification of severity of RA is the summation of the pixel intensities from the absolute difference image obtained from the difference between the present frame and the previous one. As such, the SAD estimate can be plotted in a graph over time (Fig. G.5). Generally speaking, greater the SAD value we obtain, the more motion is likely to have occurred between two successive frames. But the classification follows the rule explained in section 4.4 where in fact the difference between the largest and the smallest values of SAD is greater when the level of severity of RA is also higher.

Output of the system

The similarity that is established between any two consecutive frames has to be compared with the threshold by means of a relational comparator (Fig. G.3). In the final

display scope, the graphic represents the motion estimate for each video frame (Fig. G.5). The graph is, in fact, the summation of pixel in the absolute difference image for each video frame over time. The representation of each pixel ranges from 0 to 255 and the result obtained from the difference of pixel are multiplied by $2.9xe^6$ to have significant number. In the presentation of the result we choose $2.9xe^6$. Therefore we will have more significant numbers and our computations will be easier. The interpretation and classification of the graphical result is explained in detail in section 4.4.

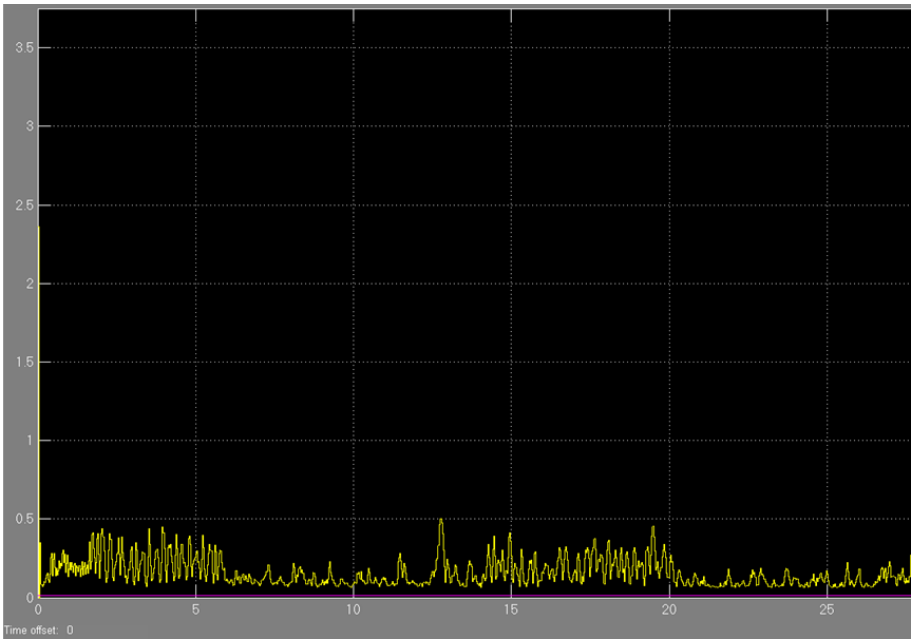

Fig. G.5: Graphical result of SAD based motion estimation through Simulink where the X axis represents the time in seconds and the Y axis the SAD values.

Appendix H: Description of Graphical User Interface

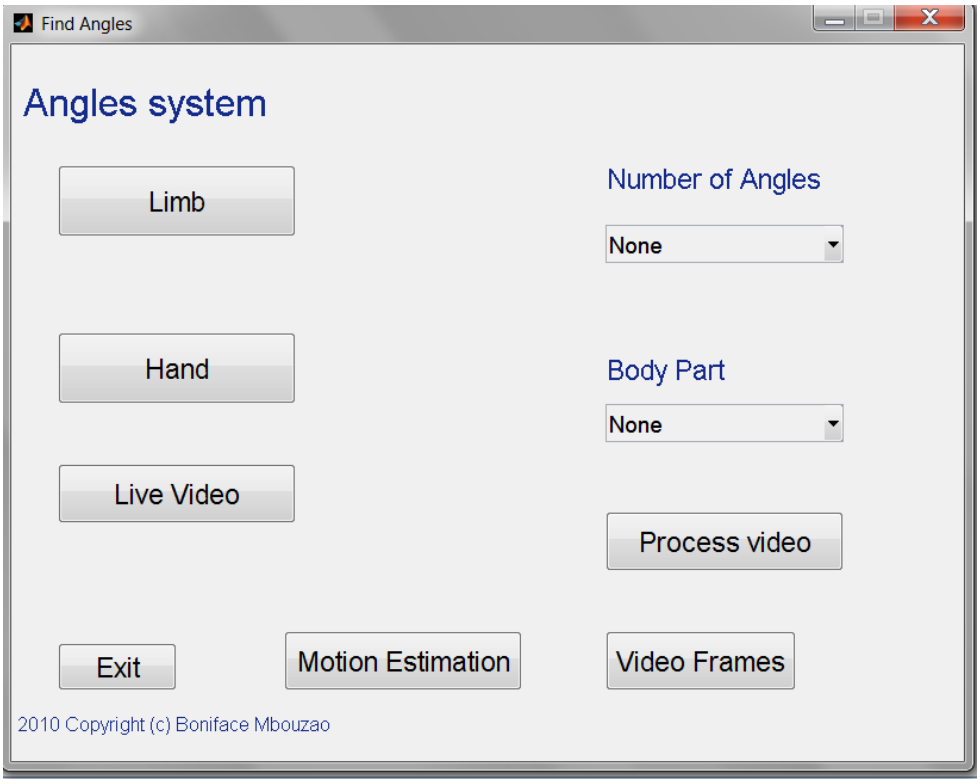

Fig. H.1: First user interface page of the system.

To start the system, the user needs to have all the videos as described in section 4.3 of the subject or patient recorded already in AVI format. It is one of those videos that the user will choose for the image processing through the Graphical User Interface (GUI).

H.1. ”Limb” button

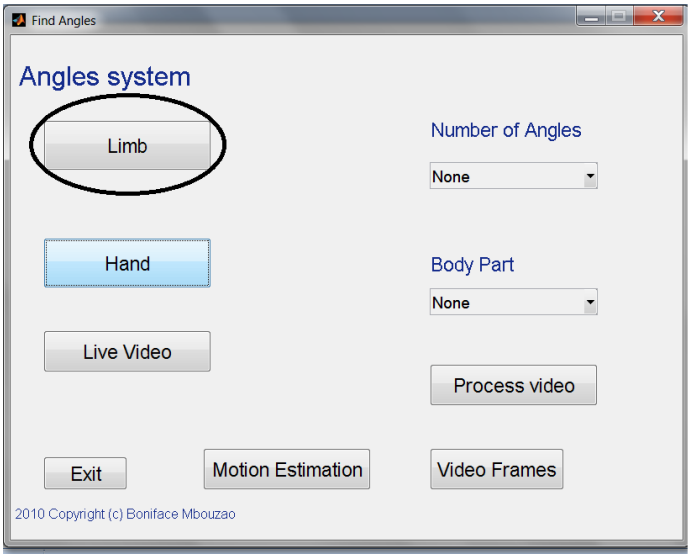

Fig. H.2: ”Limb” button.

The “Limb” button helps the user to process the limb images and to obtain the values of the two limbs’ joint angles. To do that, the user presses the “Limb” button and chooses the proper image of the subject in the position of a maximum bending of the limbs’ joints.

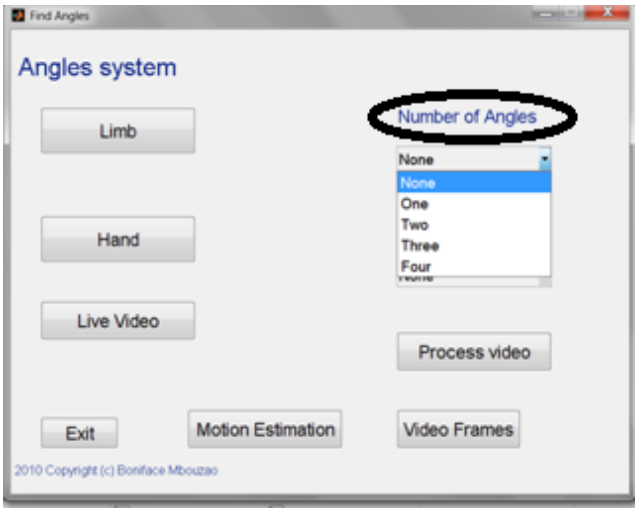

Fig. H.3: Number of angles selection.

The user has also the capability to control the number of angles that he/she wants to find in the image (Fig. H.3). As in this study the number of the angles is known in advance, this option is not really used. This option could help for further implementation when more joint angular values are needed.

H.2. "Hand" button

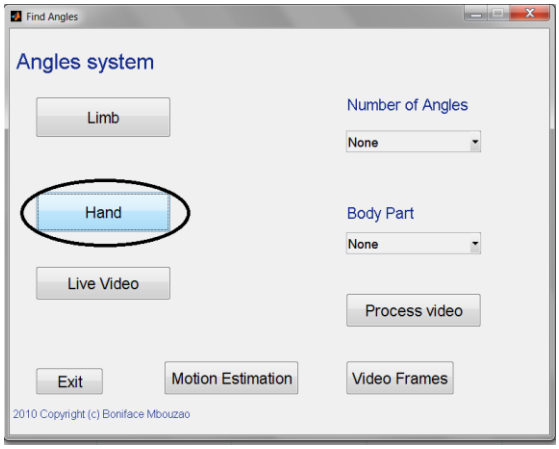

Fig. H.4: "Hand" button.

The "Hand" button helps the user to determine the three angle values for each finger of the hand. When the user selects the "Hand" button, the system asks to choose the proper image of the hand (Fig. H.4).

The system finally provides to the user, through a pop up, the values of the three angles of the chosen finger (Fig. H.5).

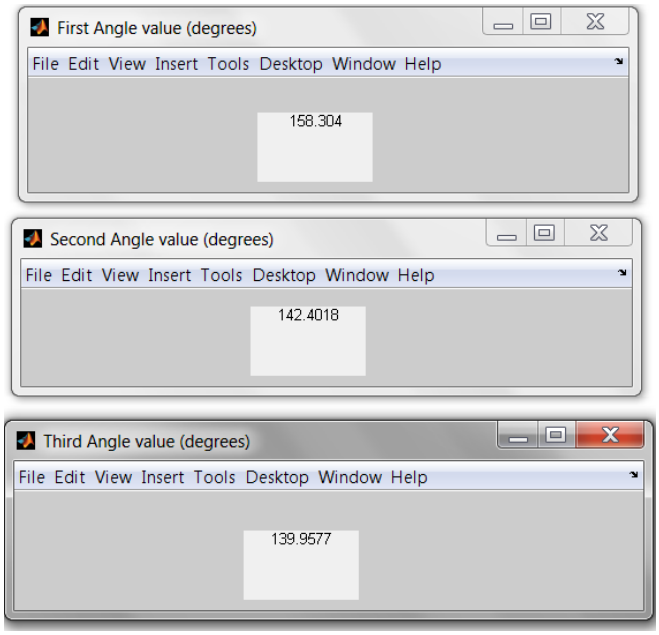

Fig. H.5: Results of finger's joint angles.

In addition, the user has the possibility to choose which part of the body one wants to measure the motion capability on (Fig. H.6).

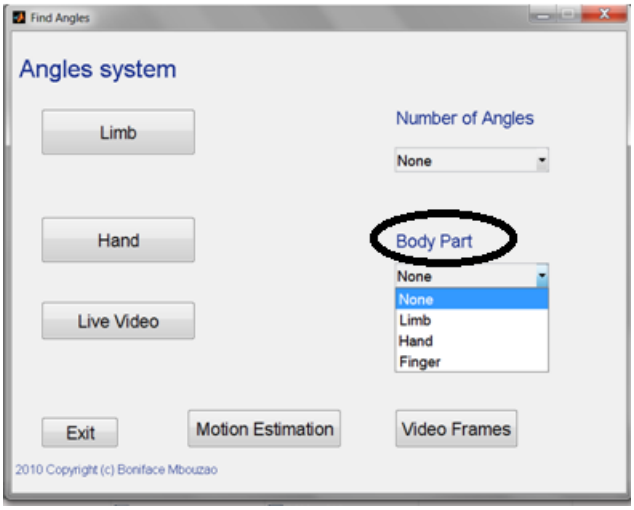

Fig. H.6: Body part specification.

H.3. “Live Video” button

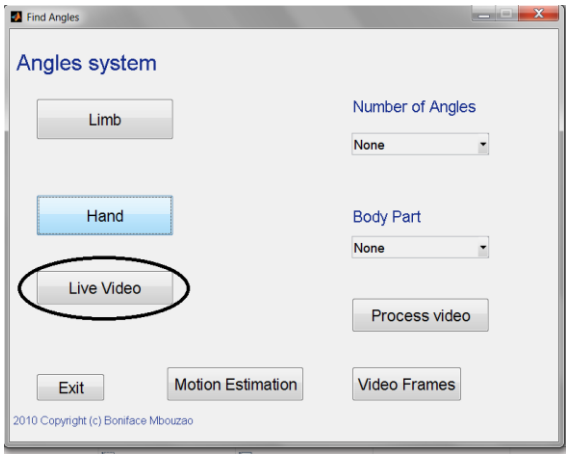

Fig. H.7: “Live Video” button.

This button helps the user to record a video if needed from the user interface. When the user presses this button, the system finds a camera connected to the computer and then turns the camera on and is able to record the video. The user can then record or stop recording a live video at any time. This tool could be used in the future for live processing when the system will be fast enough to process live videos.

H.4. “Motion Estimation” button

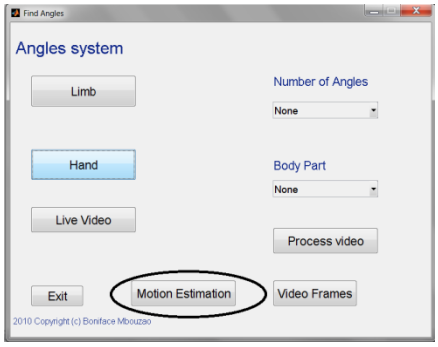

Fig. H.8: ”Motion Estimation” button.

This button helps to process the hand or limb video taken from the subject or patient stretching and bending the joints. The user has just to select the video that one wants to find the motion vector for.

H.5. "Process video" button

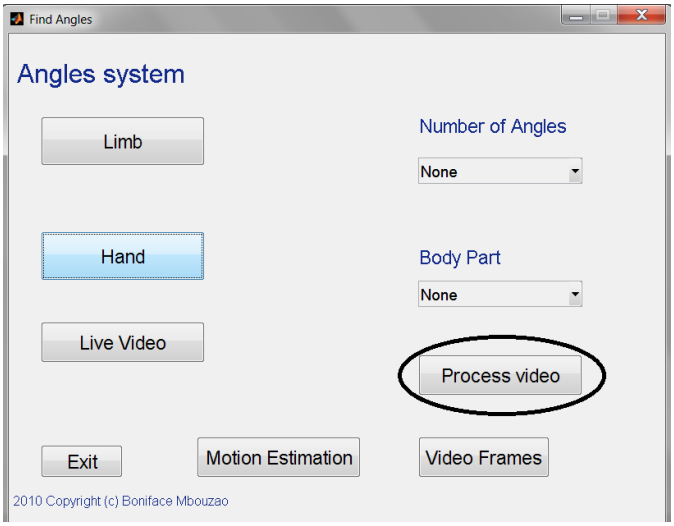

Fig. H.9: "Process video" button.

"Process video" button gives the opportunity to the user to have a version of the video with skeleton pose estimation. The user can play the new black and white video with the skeleton pose to see the movement of skeleton during stretching and bending joints. This application of the system could be used for further implementation to find the angles of joints in live videos.

H.5. “Video Frames” button

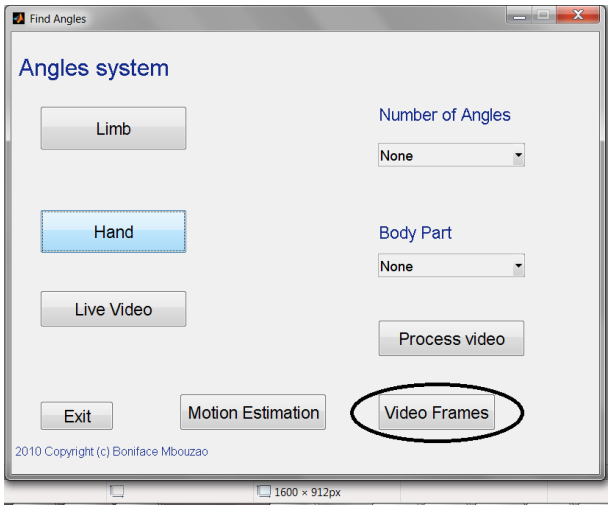

Fig. H.10: “Video Frames” button.

This button helps the user to cut any video in sequence of image frames. This is especially needed when the user wants to find the motion vector only over a part of the video.

H.6. “Exit” button

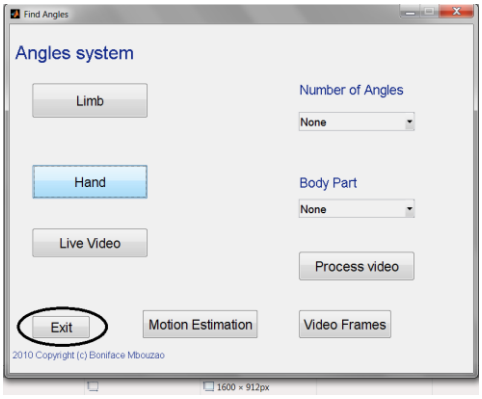

Fig. H.11: “Exit” button.

This button is to leave the application at any time of the process. When the user presses the “Exit” button, all the running applications of the system will stop and close properly.

Appendix I: Microbes and bacteria responsible of RA

Two types of microbes are most often discussed as potential etiological agents in RA. There are more viruses than bacteria. The following table summarizes the viruses and bacteria often shown as RA agents [23].

Viruses	**Bacteria**
Adenoviruses	Mycobacteria
Cytomegalovirus	Mycoplasmae
Epstein-Barr virus	Proteus mirabilis
Human T cell leukemia virus type 1	Clostridium perfringens
Parvovirus B19	
Rubella virus	

Table I.1: Viruses and bacteria agents in RA.